Johnston-Ogston effects in analytical ultracentrifugation (AUC) simulations of two model systems based on polystyrene beads that are polydisperse with respect to specific gravity

Introduction

This work qualitatively describes the results from analytical ultracentrifugation (AUC) simulations of two model aqueous systems based on polystyrene (PS) beads that are polydisperse with respect to specific gravity. These systems were contrived to exhibit Johnston-Ogston effects in those simulations.

The method of simulation is an implementation of an integral, finite-element solution to the continuity equation for AUC. The method is built on that which Claverie, Dreux and Cohen [1975] described in their solution to the Lamm equation, but differs in several respects. To correctly implement their concentration dependence, the transport coefficients are defined as spatially-independent parameters. To correctly evaluate the concentration-dependent transport coefficients at the time to be evaluated, the concentrations are calculated iteratively. By such an evaluation of the concentration-dependent transport coefficients at both the time already evaluated and the time being evaluated, the accuracy of each new set of concentrations is maximised. Computational artefacts are reduced by first calculating all concentrations in one order, then recalculating all concentrations in the opposite order, and averaging the results. Simpler results of integration are obtained by using one-half the square of the radial position, rather than the radial position, as the spatial parameter of the continuity equation. Additionally, a simple coupled-flow equation has been implemented.

For each model system, nonzero values of all coupled-flow coefficients are used in six cases, and nonzero values of just the self-to-self coupled-flow coefficients are used in one case. Details regarding the method of AUC simulation are found in an earlier work (Moody, 2011). The apparent sedimentation coefficient, s^*, and its distribution function, $g(s^*)$, can yield quantitative information about the model systems. With and without the addition of noise, the simulation results shown here have been subjected to $g(s^*)$ analysis in two other works (Moody, 2011 and 2014), the earlier of which focuses on the development of the $g(s^*)$ method, and the most recent

of which both develops that method further and applies it to test the distinguishability of four mixtures of the PS-bead systems at three significantly different times. In the latter work, replicate data sets were created by the addition of systematic and random noise to a common set of simulated AUC data for each mixture at each time. Across treatment groups, each of which comprised the replicates that pertain to a single mixture, the implicit solvent composition was identical, the initial concentrations of comparable solutes were as much alike as possible, the simulated AUC data were recorded at identical radial positions at identical times, and the signal-to-mass ratios were identical for comparable materials. For each mixture, the simulated AUC method was identical with respect to parameters that depend on temperature, rotor speed and data collection. For each replicate, a common observation, the weight-average apparent sedimentation coefficient within 5 Svedberg $< |s^*| <$ 10.625 Svedberg, was obtained by $g(s^*)$ analysis. At each time chosen for analysis, the population mean of the observations within one treatment group was compared to that within every other treatment group. To quantify the statistical significance of a difference between any two treatment groups, a Bonferroni-adjusted *t*-test (2-tailed) was applied to pair-wise comparisons of the population means from different treatment groups at each time. Confidence intervals about the population means were determined and graphed to illustrate selected results.

Common features of the two model systems

The model solute particles of two similar systems are based on the 30 nm diameter ($\pm$ 1 nm) product (part number 3030A) of the Thermo Scientific 3000 Series Nanosphere Size Standards, the composition of which may include polystyrene (PS) and polystyrene divinylbenzene (PSDVB). Thermo Scientific gives the most precise density of these particles as 1.05 g/ml, but an early investigation (Sharp and Beard, 1950) by AUC determined a slightly more precise value of 1.053 g/ml for larger (approximately 253 nm diameter) but materially similar particles, and the later value of the density is used (with its significant digits extended by two) as a reference here in all relevant calculations. (See Table 1 and *The implicit solvent component of the model systems*.)

Unlike the real particles on which they are based, the particles of each monomeric model species are treated as completely identical with respect to size, shape and atom-for-atom composition.

Each monomeric model species is distinguishable by its density, by which is meant the mass of one of its particles in a vacuum divided by the volume of that particle in a vacuum, and the ratio of that density to the density of water (at specified conditions of pressure and temperature) is the specific gravity of the particle.

One model particle ($k = 27$, Table 1) is given a density equal to the reference value of $\rho_{PS} = 1.05300$ g/ml. All other model particles ($k < 27$, Table 1) are given higher densities, but none so great as to be higher than that which could be achieved by substitutions of ^1H with deuterium. The solvent is modelled as an aqueous buffer with sufficient D_2O to render its density, ρ_0, equal to the density, ρ_k, of one model particle ($k = 14$, Table 1). Of the 26 model particles for which $\rho_k \neq \rho_0$ ($k \neq 14$, Table 1), ρ_0 is less than ρ_k for half ($k < 14$), and ρ_0 is greater than ρ_k for the rest ($k > 14$). The solvent is treated as being incompressible, as is each solute species.

The sum of the concentrations of 3 solute species, H ($k = 1$), L ($k = 27$) and LH ($k = 14$), equals 99% of the total solute concentration, c. Each of the other 24 solute species ($2 \leq k \leq 13$ and $15 \leq k \leq 26$) is present at 1/24 of 1% of c. Species LH is modelled as a heterodimer formed from 1 monomer of species H plus 1 monomer of species L. In the absence of concentration gradients, the molarity of species LH is half that of species L or H, while species L and H are equimolar.

In the limit as c approaches zero, species H has the most positive sedimentation coefficient, species L has the most negative sedimentation coefficient, and species LH has a sedimentation coefficient of 0 s. The transport parameters of the model particles (Table 1) and their concentration dependence (Equations 14 to 18) are such that each of the low-concentration solutes exhibits Johnston-Ogston effects in AUC simulations.

Distinguishing characteristics of the two model systems

In the first model system, H is a two-species component, L is a two-species component, HL is the second species of both two-species components, and all other solute species are single-species components. Components H and L give rise to species HL via mass-action association in the first system. In the second system, every species, including H, L and HL, is a single-species component. The two model systems are constructed to ensure that, in the absence of concentration gradients,

the concentration of a given species in one system will be equal to the concentration of that species in the other system.

name	index k	c_k (mg/ml) at t = 0	ρ_k (g/ml)	$\bar{v}_k^0 = \frac{1}{\rho_k}$ (ml/g)	M_k (g/mol)	σ_k^0 (cm^{-2}) at 60,000 RPM	s_k^0 (Svedberg)
H	1	33.891892	1.11150	0.89969	9,462,869	403.343	9.324
	2	0.041667	1.11075	0.90029	9,456,483	393.001	9.084
	3	0.041667	1.11000	0.90090	9,450,098	382.659	8.845
	4	0.041667	1.10925	0.90151	9,443,713	372.316	8.606
	5	0.041667	1.10850	0.90212	9,437,328	361.974	8.367
	6	0.041667	1.10775	0.90273	9,430,943	351.632	8.128
	7	0.041667	1.10700	0.90334	9,424,557	341.290	7.889
	8	0.041667	1.10625	0.90395	9,418,172	330.948	7.650
	9	0.041667	1.10550	0.90457	9,411,787	320.606	7.411
	10	0.041667	1.10475	0.90518	9,405,402	310.264	7.172
	11	0.041667	1.10400	0.90580	9,399,017	299.922	6.933
	12	0.041667	1.10325	0.90641	9,392,631	289.579	6.694
	13	0.041667	1.10250	0.90703	9,386,246	279.237	6.455
LH	14	33.000000	1.08225	0.92400	18,427,691	0	0
	15	0.041667	1.06200	0.94162	9,041,445	-279.237	-6.455
	16	0.041667	1.06125	0.94229	9,035,060	-289.579	-6.694
	17	0.041667	1.06050	0.94295	9,028,675	-299.922	-6.933
	18	0.041667	1.05975	0.94362	9,022,290	-310.264	-7.172
	19	0.041667	1.05900	0.94429	9,015,904	-320.606	-7.411
	20	0.041667	1.05825	0.94496	9,009,519	-330.948	-7.651
	21	0.041667	1.05750	0.94563	9,003,134	-341.290	-7.889
	22	0.041667	1.05675	0.94630	8,996,749	-351.632	-8.128
	23	0.041667	1.05600	0.94697	8,990,364	-361.974	-8.367
	24	0.041667	1.05525	0.94764	8,983,978	-372.316	-8.606
	25	0.041667	1.05450	0.94832	8,977,593	-382.659	-8.845
	26	0.041667	1.05375	0.94899	8,971,208	-393.001	-9.084
L	27	32.108108	1.05300	0.94967	8,964,823	-403.343	-9.324

Table 1. The major distinguishing characteristics of the model solute particles. The species index, *k*, ranges from 1 to $n = 27$. All particles other than species 14 are modelled as spheres with an anhydrous diameter of 30 nm. Species 14 (*LH*) is modelled as a dimer of species *L* and *H*. At

20.00°C, ρ_0, the density of the hypothetical buffer, is equal to ρ_{14}, the density of species 14. The density of species k is equal to ρ_k, which is given by $\rho_k = \rho_n + [(n-1)(3-\alpha_k) + 1 - k]\Delta\rho$, where $\Delta\rho = 0.00075$ g/ml is an increment of the density, $\alpha_{k<14} = 0$, $\alpha_{k=14} = 1$ and $\alpha_{k>14} = 2$. The inverse of ρ_k is equated to $\bar{v}_k^0$, the partial specific volume of species k in the zero-concentration limit. Thus, $\lim_{c\to 0} \bar{v}_k = \bar{v}_k^0 = \frac{1}{\rho_k}$, where $\bar{v}_k$ is the partial specific volume of species k. Equation 6 describes M_k, the molar mass of species k. Equation 8 describes σ_k^0, the reduced molar mass of species k at 60,000 RPM in the limit as c approaches 0. Equations 13 and 19 describe s_k^0, the sedimentation coefficient of species k in the limit as c approaches 0.

Construction of the model systems

For each species, k, the density, ρ_k, was calculated as described in Table 1. For each species, k, the partial specific volume, $\bar{v}_k$, in the limit as c approaches zero is denoted as $\bar{v}_k^0$, which is treated as equal to $1/\rho_k$ (Table 1).

The upper value of ρ_k was constrained by the limits of what might be achievable through substitution with heavy, but stable, isotopes. The individual values of ρ_k were constrained by the aim of obtaining model particles that exhibit both positive and negative values of s°_k, the sedimentation coefficient in the limit as c approaches zero, such that, with one exception, 6 Svedberg $< |s_k^0| <$ 10 Svedberg. The exception is species 14, for which $s_{k=14}^0 = 0$. The resulting values of s_k^0 are shown in Table 1. As necessitated to ensure that $s^\circ_{14} = 0$, the model solvent (treated as identical to the buffer) is given a density, ρ_0, that is equal to ρ_{14}. Thus, species 14 (*LH*) would be neutrally buoyant in a system composed solely of that species and the solvent. The calculations of s_k^0 and related coefficients, plus the determination of the solvent characteristics on which those calculations partially depend, are described below. (See *The implicit solvent component of the model systems* and *Calculations of coefficients*.)

The total number of solute species is given by $n = 27$, and the total mass concentration of all solute species is equal to

$$c = \sum_{k=1}^{n=27} c_k \,,$$

(1)

where c_k is the mass concentration of species k. For $1 < k < 14$ and $14 < k < 27$, $c_k =$ (0.001 g/ml)/(n - 3). The other three species, $k = 1$ (H), $k = 14$ (LH) and $k = 27$ (L), are present in excess, with their concentrations chosen to yield $c_{H,LH,L} = c_H + c_{LH} + c_L = 0.099$ g/ml. Thus, $c =$ 0.1 g/ml, of which species 1, 14 and 27 account for 99%.

The initial concentrations of species 1, 14 and 27 were subject to the constraint that $c_H/M_H = 2(c_{LH}/M_{LH}) = c_L/M_L = m_{ref}$, where m_{ref} is a common reference concentration in mole/ml, and where $M_H = M_1$, $M_{LH} = M_{14}$ and $M_L = M_{27}$. The initial concentrations of species 1, 14 and 27 were also subject to the constraint that $c_{LH}/c_L c_H = K_a$ in the first system, where, treating all activity coefficients as equal to 1, K_a is the equilibrium constant of the mass-action association, $L + H \rightleftharpoons LH$, in which 1 monomer of species 1 (H) and 1 monomer of species 27 (L) form 1 heterodimer of species 14 (LH). Thus, $M_{LH} = M_L + M_H$,

$$K_a = \frac{c_{LH}}{c_L c_H} = \frac{c_{H,LH,L} - c_L - c_H}{c_L c_H} = \frac{c_{H,LH,L} - m_{ref}(M_L + M_H)}{{m_{ref}}^2 M_L M_H} \,,$$

(2)

and

$$K_a = \frac{c_{LH}}{c_L c_H} = \frac{\frac{m_{ref}}{2}(M_L + M_H)}{{m_{ref}}^2 M_L M_H} = \frac{(M_L + M_H)}{2 m_{ref} M_L M_H} \,.$$

(3)

Equating the right-hand sides of the preceding 2 equations and solving for m_{ref} yields

$$m_{ref} = \frac{2}{3}\frac{c_{H,LH,L}}{(M_L + M_H)} \,.$$

(4)

The values of $c_{H,LH,L}$, M_L and M_H used here yield m_{ref} = 3.582E-9 mol/ml, from which K_a = 30.325 ml/g is obtained via Equation 2 or 3. The initial concentrations of species 1, 27 and 14 in either system are then determined, respectively, by $c_H = m_{ref}M_H$, $c_L = m_{ref}M_L$ and $c_{LH} = (m_{ref}M_{LH})/2$.

The model, mass-action association linking species 1, 27 and 14 in the first system is given a forward rate constant of k_{for} = 30,000 [ml/g]/s. The reverse rate constant, k_{rev}, is equal to k_{for}/K_a = 989.277 s. Consequently, the equilibration of this reaction is effectively instantaneous on the scale of the maximum time increment (3 s) used in the AUC simulation of this system. (See *Simulation parameters, including limits on* Δt*, iterations per* Δt*, equilibrations per* Δt*,* D_k *and* σ_k.) For the second system, in which all species are single-species components, there is no K_a that applies to species 1, 27 and 14 because both k_{for} and k_{rev} are effectively equal to zero. Hence, the description of K_a as undefined in reference to the second system.

The relevant work by Sharp and Beard (1950) provides evidence that real particles of the sort modelled here tend to behave as single-species components, even at fairly high (20 mg/ml) concentrations, at least in aqueous solutions having an ionic strength of approximately 0.15 M, and a nearly neutral pH. In both of the model systems described here, species 2 to 13 and species 15 to 26, being defined as single-species components, can be said to lack characteristics that would cause them to participate in any mass-action associations. Given the (admittedly imaginary) material similarities between all the solute particles, this implies that a subtle (and also imaginary) modification of species 1 and species 27 causes them to participate in a mass-action association in the first system. Thus, the model system in which all solutes are single-species components is the more realistic of the two.

Realistic or not, the two model systems differ solely with respect to whether the solute species that is neutrally buoyant (relative to the solvent) can dissociate to solute species that are not neutrally buoyant (relative to the solvent). Of interest was whether this particular difference between the two model systems gives rise to readily distinguishable results.

The implicit solvent component of the model systems

In AUC, it is common practice to treat the buffer as the implicit solvent component of the system, and this convention is applied to the model systems examined here. The model buffer of the model systems was required to meet three criteria: First, it must be an aqueous buffer that is similar in composition to that which Sharp and Beard (1950) successfully employed in their AUC experiments with PS beads; second, at 20.00°C (293.15 K), its density, ρ_0, must be equal $\rho_{14} =$ 1.08225 g/ml; and third, the sought-after solvent density must be achievable by substituting some portion of the H_2O with D_2O.

The model, aqueous buffer so chosen consists of 71.23% D_2O, 0.15 M NaCl, 20 mM NH_4HCO_3 and pH 7.0 at 20.00°C, where the amount of D_2O is given in volume-percent. At 20.00°C, the calculated density, ρ_0, of this buffer equals the desired value of 1.08225 g/ml. (The density of the buffer at 20.00°C would be 1.00594 g/ml at 0% D_2O.) The calculated viscosity, η_0, of this buffer at 20.00°C is 0.010196 poise. These density and viscosity calculations were performed using the Sedimentation Interpretation Program, Sednterp (Laue et al., 1992), version 1.09. (Sednterp is available at http://www.rasmb.bbri.org/software/, the Analytical Ultracentrifugation Software Archive of the Reversible Associations in Structural and Molecular Biology (RASMB) website.) The reference density of an unmodified PS/PSDVB bead, $\rho_{PS} = 1.05300$ g/ml, was padded with zeroes to match the significant digits of the values returned by Sednterp.

Calculations of coefficients

All of the model monomers are spherical and have the same anhydrous radius, R_k, of 15 nm. The radius of each hydrated monomeric particle is modelled as being equal to $h_k R_k$, where $h_k =$ 1/0.65 for each species. Due to their identical size, shape and hydration, the diffusion coefficient, D_k, of each monomeric species is identical. (As will be shown, the diffusion coefficient is independent of the density.)

The diffusion coefficient in the limit as c approaches zero is approximated as

$$\lim_{c\to 0} D_k = D_k^0 = \left(\frac{k_B T}{6\pi\eta_0 h_k R_k}\right),$$

(5)

where k_B is the Boltzmann constant and T is the absolute temperature.

Using $h_k = 1/0.65$, $T = 293.15$ K and $\eta_0 = 0.010196$ poise, a value of $D_k^0 = 9.126\text{E-}8$ cm^2/s was obtained for each monomer.

For each species that consists of spherical particles, its molar mass is given by

$$M_k = N_A \rho_k \frac{4\pi}{3} R_k^3 ,$$

(6)

where N_A is Avogadro's number. Solving this equation for R_k yields

$$R_k = \left(\frac{3}{4\pi} \frac{M_k}{N_A \rho_k} \right)^{\frac{1}{3}} ,$$

(7)

which is the anhydrous radius of a spherical particle of molar mass M_k and density ρ_k.

For a nonspherical particle of molar mass M_k, density ρ_k, hydration h_k and zero-c diffusion coefficient D_k^0, Equation 7 is not generally valid, but the effective anhydrous radius (the anhydrous radius of an equivalent sphere) of such a particle is obtained by solving Equation 5 for R_k. Nevertheless, the heterodimer, species 14 (LH), is modelled as a nonspherical particle for which, by chance, Equation 7 does yield the effective anhydrous radius required to obtain D_k^0 by Equation 5. That is, in the exceptional case of species LH, the value of R_k obtained by Equation 7 is the same as that obtained by solving Equation 5 for R_k.

For species LH, the density is fixed at $\rho_{LH} = \rho_0$, and the molar mass is constrained to $M_{LH} = M_L + M_H$. Its effective anhydrous radius, R_{LH}, is modelled as being equal to that given by Equation 7. Using $M_{LH} = M_L + M_H$ (see Table 1) and $\rho_{LH} = \rho_0 = 1.08225$ g/ml in Equation 7, a value of $R_{LH} = 18.899$ nm is obtained. The effective radius of the hydrated heterodimer is modelled as equal to $h_{LH} R_{LH}$, where $h_{LH} = 1/0.65 = h_k$ of all the other solute species. For the heterodimer, then, at $T = 293.15$ K and with $\eta_0 = 0.010196$ poise, $D_{LH}^0 = 7.243\text{E-}8$ cm^2/s.

The reduced-molar-mass coefficient of species k is denoted as σ_k, and its value in the limit as c approaches zero is given by

$$\lim_{c\to 0}\sigma_k = \sigma_k^0 = \frac{M_k(1-\bar{v}_k^0\rho_0)\omega^2}{RT},$$

(8)

where $(1-\bar{v}_k^0\rho_0)$ is the density increment of the system as it affects the transport of component k in the zero-concentration limit, and ω is the angular velocity of the centrifuge rotor. The angular velocity is equal to

$$\omega = 2\pi\left(\frac{\text{RPM}}{60\ \frac{\text{s}}{\text{min}}}\right),$$

(9)

where RPM is the rotor speed in rotations per minute. For the model system described here, all relevant calculations are based on a rotor speed of 60,000 RPM.

Concentration dependence of D_k and σ_k

For each species, *k*, the concentration-dependent equations describing the reduced-molar-mass coefficient, σ_k, and the diffusion coefficient, D_k, are

$$\sigma_k = \frac{\frac{M_k}{c_k}\sum_{q=1}^{n}\frac{c_q}{M_q}X_{k,q}^{\sigma}X_{k,q}^{D}\sigma_q^0 D_q^0\left(\frac{1+\sum_{a=1}^{n}p_{q,a}c_a}{1+\sum_{a=1}^{n}h_{q,a}c_a}\right)}{D_k} = \frac{\frac{M_k}{c_k}\sum_{q=1}^{n}\frac{c_q}{M_q}X_{k,q}^{s}\sigma_q^0 D_q^0\left(\frac{1+\sum_{a=1}^{n}p_{q,a}c_a}{1+\sum_{a=1}^{n}h_{q,a}c_a}\right)}{D_k}$$

(10)

and

$$D_k = \frac{M_k}{\frac{\Delta c_k}{\Delta\xi}}\sum_{q=1}^{n}\frac{\frac{\Delta c_q}{\Delta\xi}}{M_q}X_{k,q}^{D}D_q^0\left(\frac{1+\sum_{a=1}^{n}y_{q,a}c_a}{1+\sum_{a=1}^{n}h_{q,a}c_a}\right),$$

(11)

respectively, where $X_{k,q}^{\sigma}$ (Table 2) is a constant that couples the effects of gravitational forces on species q to σ_k, $X_{k,q}^{D}$ (Table 2) is a constant that couples the diffusion of species q to D_k, $\frac{\Delta c_k}{\Delta \xi}$ approximates $\left(\frac{\partial c_k}{\partial \xi}\right)_t$, $\frac{\Delta c_j}{\Delta \xi}$ approximates $\left(\frac{\partial c_k}{\partial \xi}\right)_t$, and $\xi = r^2/2$. Equations 10 and 12 are used to define the sedimentation coefficient of species k as

$$s_k = \frac{\sigma_k D_k}{\omega^2}.$$

(12)

Similarly, the sedimentation coefficient of species k in the limit as c approaches zero can be defined as

$$s_k^0 = \frac{\sigma_k^0 D_k^0}{\omega^2}.$$

(13)

The constant $X_{k,q}^{s}$, which appears in Equation 10, couples the effects of gravitational forces on species q to s_k (Equations 26 to 29). The parameters $p_{q,a}$, $y_{q,a}$ and $h_{q,a}$ are the second virial coefficients of the density increment, thermodynamic nonideality and viscosity, respectively. These coefficients are used to model the concentration-dependent effects of species a on the transport of species k. It can be shown (Moody, 2011) that, for a given pair of species, k and q, $X_{k,q}^{s}$ and $X_{k,q}^{D}$ are identical, and that $X_{k,q}^{\sigma}$ must therefore be equal to 1. As will be shown, however ($X_{k,q}^{\sigma}$, $X_{k,q}^{D}$ *and* $X_{k,q}^{s}$ *values*; and *AUC simulation of cases* -2, -1, 1 *and* 2, *for which* $X_{k,q\neq k}^{s} \neq 0$ *and* $X_{k,q\neq k}^{D} \neq 0$), it is useful to treat $X_{k,q}^{s}$ and $X_{k,q}^{D}$ as if they were independent parameters.

The species-q-applicable transport coefficient that links the concentration of species a to the viscosity of the system was calculated as

$$h_{q,a} = \frac{2.5}{\rho_a} = 2.5 \lim_{c \to 0} \bar{v}_a = 2.5 \bar{v}_a^0,$$

(14)

where the coefficient 2.5 is the value of the intrinsic viscosity that, according to theory, applies to spherical particles (Eisenberg & Crothers, 1979; van Holde, 1985 - Viscosity). The independence of $h_{q,a}$ from parameters of species k is due to the assumption that the presence of one species does not affect the relationship between the volume fraction of any other species and η, the viscosity of the solution. Hydration can be expected to render Equation 14 an underestimate of $h_{q,a}$, but no correction for hydration was applied to the values of $h_{q,a}$ used in the simulations described here.

The species-q-applicable transport coefficient that links the concentration of species a to the thermodynamic nonideality of the system was calculated as

$$y_{q,a} = \frac{4}{\rho_a} = 4 \lim_{c \to 0} \bar{v}_a = 4\bar{v}_a^0 \,,$$

(15)

which is based solely on the expected excluded-volume effect of a spherical solute with a partial specific volume of $\bar{v}_a$ (van Holde,1985 - Solutions of Macromolecules). Hydration could also be expected to render Equation 15 an underestimate of $y_{q,a}$, but no correction for hydration was applied to the values of $y_{q,a}$, either.

Although $h_{q,a}$ and $y_{q,a}$ explicitly depend on parameters of species a only, the index k is retained because, in general, these coefficients may explicitly depend on parameters of species k as well. For example, the right-hand sides of Equations 14 and 15 could be multiplied by h_a to account for hydration. (To highlight the density-increment effects mediated by the $p_{q,a}$ coefficients, $h_{q,a}$ and $y_{q,a}$ are deliberately minimised to the values expected for a system of anhydrous, spherical particles.) In any case, D_k^0, $h_{q,a}$ and $y_{q,a}$ are independent of the density of any species. Thus, D_k is also independent of the density of any species.

Provided that, as is the case for $q \neq 14$, $\left(1 - \bar{v}_q \rho_0\right) \neq 0$, the species-$q$-applicable transport coefficient that links the concentration of species a to the density increment of the system can be calculated as

$$p_{q \neq 14,a} = \frac{\bar{v}_a^0}{[\varphi_a]_{max}} \left[\frac{\left(1 - \bar{v}_q^0 \rho_a\right) - \left(1 - \bar{v}_q^0 \rho_0\right)}{\left(1 - \bar{v}_q^0 \rho_0\right)} \right] = \frac{-1}{\rho_a [\varphi_a]_{max}} \left[\frac{\rho_a - \rho_0}{\rho_q - \rho_0} \right],$$

(16)

where $\rho_a = 1/\bar{v}_a^0 = 1/\bar{v}_a$ in the limit as c approaches 0, $[\varphi_a]_{max}$ is the volume fraction of the system occupied by species a at its maximum concentration, $\left(1 - \bar{v}_q^0 \rho_0\right)$ would be the density increment of the system with respect to the component to which species q pertains if there were no other component present besides a solvent with a density equal to ρ_0, and $\left(1 - \bar{v}_q^0 \rho_a\right)$ would be the density increment of the system with respect to the component to which species q pertains if there were no other component present besides a solvent with a density equal to ρ_a. By definition, the maximum concentration of species a is equal to $\rho_a[\varphi_a]_{max} = [\varphi_a]_{max}/\bar{v}_a^0$. For all model species, $[\varphi_a]_{max}$ was given a value of 0.5.

In the case of $\sigma_q^0 = 0$ for one or more species, q, a modification of Equation 10,

$$\sigma_k = \frac{\frac{M_k}{c_k}\sum_{q=1}^{n}\frac{c_q}{M_q}X_{k,q}^{\sigma}X_{k,q}^{D}D_q^0\left(\frac{\sigma_q^0 + \sum_{a=1}^{n}(\sigma p)_{q,a}c_a}{1+\sum_{a=1}^{n}h_{q,a}c_a}\right)}{D_k} = \frac{\frac{M_k}{c_k}\sum_{q=1}^{n}\frac{c_q}{M_q}X_{k,q}^{s}D_q^0\left(\frac{\sigma_q^0 + \sum_{a=1}^{n}(\sigma p)_{q,a}c_a}{1+\sum_{a=1}^{n}h_{q,a}c_a}\right)}{D_k},$$

(17)

is used to calculate σ_k in terms of the set of $(\sigma p)_{q,a}$, each of which is the species-q-applicable transport coefficient that links the concentration of species a to the density increment of the system, and each of which is given by

$$(\sigma p)_{q,a} = \sigma_q^0 p_{q,a} = \frac{M_q\omega^2}{RT}\frac{\bar{v}_a^0}{[\varphi_a]_{max}}\left[\bar{v}_q^0(\rho_0 - \rho_a)\right] = \frac{\omega^2 M_q}{RT\rho_q}\left[\frac{\rho_0 - \rho_a}{\rho_a[\varphi_a]_{max}}\right].$$

(18)

For $[\rho_0 - \rho_a]\omega^2 \neq 0$, Equation 18 generally results in nonzero values of $((\sigma p)_{q,a}$, in which case, nonzero values of σ_k could occur even if σ_q^0 were equal to zero for nearly every species, q.

The dependence of s_k^0 on ρ_k - ρ_0

Given that h_k is the same for all species, R_k is the same for all species except species $k = 14$, and $\rho_{k=14} = \rho_0$, s_k^0 varies solely in proportion to ρ_k - ρ_0 from one species to another. First substituting the right-hand sides of Equations 5 and 8 for D_k^0 and σ_k^0, respectively, in Equation 13, then substituting the right-hand side of Equation 6 for M_k in the result, yields, upon substitution of R for k_B/N_A and $1/\rho_k$ for $\bar{v}_k^0$,

$$s_k^0 = \frac{2R_k^2(\rho_k - \rho_0)}{9\eta_0 h_k}.$$

(19)

Effects of ^{1}H-to-D substitutions on PS/PSDVB beads

As PS/PSDVB beads are composed entirely of carbon and hydrogen, deuterium is the only stable heavy isotope available for substitution. With the expectation that the PS/PSDVB beads have a C-to-H ratio of 1, achievable amounts of substitutions of ^{1}H with D would suffice to produce the particles described in Table 1, where species 1 to 13 have higher densities than the solvent, and thus have positive s_k^0 values in the 6 Svedberg to 10 Svedberg range, while species 15 to 27 have lower densities than the solvent, and thus have negative s_k^0 values in the -10 Svedberg to -6 Svedberg range.

Simulation parameters, including limits on Δt, iterations per Δt, equilibrations per Δt, D_k and σ_k

Each system was simulated in terms of the gravitational-potential-space parameter, $\xi = r^2/2$, where r is the radial position in the centrifuge. In terms of r, the meniscus position was set to 6 cm, and the base of the system was set to 7.2 cm. The number of spatial elements was set to 900. The spatial increment, $\Delta\xi$, was the same ($\Delta\xi = 8.8\text{E-}3$ cm^2) for all adjacent pairs of spatial elements.

Data sets were saved at 0.5-min increments until $t = 1$ min. Data sets were then saved at 2.5-min increments until $t = 126$ min. Lastly, data sets were saved at 30-min increments until $t = 26.1$ hr. For the purpose of data output, spatial data were saved in terms of radial position, $r = (2\xi)^{0.5}$.

Concentration data were saved in terms of g/ml for each individual species. Data were also saved in terms of g/ml for the sum of the concentrations of the three species, 1 (*H*), 14 (*LH*) and 27 (*L*), that chemically equilibrate in the first system, but exist as single-species components present at high concentrations in the second system. Additionally, the sum of the concentrations of species 2 to 13 plus 15 to 26 was multiplied by a signal factor of 1000 AU/[g/ml], and the data saved in terms of AU, where AU represents an arbitrary unit. In this instance, AU is numerically equivalent to the mg/ml scale.

For concentration-dependent systems, it has been found that liberally realistic limits on D_k and σ_k reduce the likelihood of artefacts and instabilities in regions of high concentrations. On that basis, the following limits were imposed on D_k and σ_k:

$$0.025D^\circ{}_k \leq D_k \leq 160D^\circ{}_k$$

(20)

for all D_k;

$$-50\sigma_k^0 \leq \sigma_k \leq 50\sigma_k^0$$

(21)

for $\sigma_k^0 > 0$;

$$50\sigma_k^0 \leq \sigma_k \leq -50\sigma_k^0$$

(22)

for $\sigma_k^0 < 0$; and

$$-5000\ cm^{-2} \leq \sigma_k \leq 5000\ cm^{-2}$$

(23)

for $\sigma_k^0 = 0$.

The time, t, at which AUC began was set to 0 s. The time increment, Δt (Equations B17, B34, B35, C28 and C73 to C76 of Moody, 2011), was given an upper limit, Δt_{max}, of 3 s. Such an upper limit is useful, because the simulation programme includes a mass-conservation algorithm that can increase Δt when the system appears to be stable. More importantly, the mass-conservation algorithm can also reduce Δt and return the system to the most recent stable time point in instances of computational instability. Without an upper limit on Δt, these opposing functions can lead to unproductive cycles of Δt changes. (See the mass-conservation and time-increment-adjustment algorithms in Section L of Moody, 2011.) To permit the mass-conservation algorithm to reduce Δt in all instances of instability that would introduce major inaccuracies in the data, the minimum time increment, Δt_{min}, was set to 0 s.

For the mass flow calculations, an upper limit of 8 iterations per time increment was imposed. (See the iterative application of the second approximate solution in Section J of Moody, 2011.) The acceptance criterion of convergence (Equation J6 of Moody, 2011), which, when met, stops further mass flow recalculations within a given Δt, was h/erg·s, where h is the cgs Planck constant.

For the reaction flow calculations, for all $t > 0$, a maximum of $N_{equil} = 2{,}500$ was imposed on the number of iterations allowed when recalculating a chemical equilibrium at a given spatial element. (See the reaction-flow algorithms in Section K of Moody, 2011.) For $t = 0$, a limit of $N_{equil} = 5{,}000$ was used. For the mass-action association of the first system, the criterion for adequate equilibration was

$$\zeta K_a \leq \frac{c_{LH}}{c_L c_H} \leq \frac{1}{\zeta} K_a$$

(24)

(from Equation K29 of Moody, 2011). At $t = 0$, $\zeta = 0.999$ was used. For all $t > 0$, $\zeta = 0.995$ was used.

The concentration-change factor used in the reaction flow calculations was

$$k_w = \frac{k_0}{k_0 + (w - w_0)}$$

(25)

(Equation K26 of Moody, 2011), where k_0 and w_0 are real numbers greater than zero, and w is the iteration index of the reaction-flow algorithm. (Thus, $1 \leq w \leq N_{equil}$.) For $t = 0$, w_0 was set to 1, while for $t > 0$, w_0 was set to 4. For all t, a value of $k_0 = 3$ was used.

Additional limits prevent reaction flow calculations from being done when the computational effort is especially high but the information that could be gained is very low. For the work presented here, if the concentration of one reactant species was greater than $(10^{-21}$ erg·s$)/h$ times the sum of the concentrations of the product species and the other reactant species, no effort was made to recalculate the chemical equilibrium. (See test-parameter α of Equations K42 and K43 of Moody, 2011.) If the concentration of each reactant species and the product species was less than $h(10^{21}$ g/ml$)/($erg·s$)$, any remaining product was converted to reactants, and no further reaction flow calculations were done. (See test-parameter β of Equations K44 to K46 of Moody, 2011.)

Notation

For various parameters, the notation used here identifies each species by a subscript, such as k or a specific number. As such, the parameters in Table 1, and Equations or Inequalities 1 to 25, display a component-based notation, such as that found in Section B of Moody, 2011. Though the correct notation would be the component-species sort found in Section C of that paper, that notation is more cumbersome, and is not especially useful here, where only one system has any multi-species components, and even there, they are outnumbered 12 to 1 by single-species components. Thus, in this paper, where it is pertinent, such distinctions are noted in the text, rather than in the subscripts.

$X_{k,q}^{\sigma}$, $X_{k,q}^{D}$ and $X_{k,q}^{S}$ values

As noted with respect to Equations 10 and 11, $X_{k,q}^{\sigma}$ is a constant that couples the effects of gravitational forces on species q to σ_k, and $X_{k,q}^{D}$ is a constant that couples the diffusion of species

q to D_k. The implementation of the transport equations employs $X_{k,q}^s$ and $X_{k,q}^D$, rather than $X_{k,q}^\sigma$ and $X_{k,q}^D$, however. (For a description of how $X_{k,q}^\sigma$, $X_{k,q}^s$ and $X_{k,q}^D$ are applied to simulations of coupled-flow transport in the analytical ultracentrifuge, see Section N (**A simple coupled-flow equation for AUC**) in Moody (2011)). From Equations 10 and 13, or Equations 17 and 13, it follows that

$$X_{k,q}^\sigma = \frac{X_{k,q}^s}{X_{k,q}^D},$$

(26)

where $X_{k,q}^s$ is a constant that couples the effects of gravitational forces on species q to s_k. Equation 26 is written with $X_{k,q}^s$ and $X_{k,q}^D$ on the right-hand side because $X_{k,q}^\sigma$ is the derived parameter. Provided that $X_{k,q}^D$ is not equal to zero, $X_{k,q}^\sigma$can be calculated using Equation 26. Where $X_{k,q}^D = 0$, $X_{k,q}^\sigma$ is undefined, except that the product, $X_{k,q}^\sigma X_{k,q}^D$, is nevertheless treated as being equal to $X_{k,q}^s$.

Using Equations 10 and 11 in Equation 12, and introducing the coefficient $s_{k,q}$, yields

$$s_k = \frac{\sigma_k D_k}{\omega^2} = \frac{M_k}{c_k}\sum_{q=1}^{n}\frac{c_q}{M_q}X_{k,q}^\sigma X_{k,q}^D\frac{\sigma_q^0 D_q^0}{\omega^2}\left(\frac{1+\sum_{a=1}^n p_{q,a}c_a}{1+\sum_{a=1}^n h_{q,a}c_a}\right) = \frac{M_k}{c_k}\sum_{q=1}^{n}\frac{c_q}{M_q}s_{k,q},$$

(27)

where

$$s_{k,q} = X_{k,q}^\sigma X_{k,q}^D\frac{\sigma_q^0 D_q^0}{\omega^2}\left(\frac{1+\sum_{a=1}^n p_{q,a}c_a}{1+\sum_{a=1}^n h_{q,a}c_a}\right) = X_{k,q}^s s_q^0\left(\frac{1+\sum_{a=1}^n p_{q,a}c_a}{1+\sum_{a=1}^n h_{q,a}c_a}\right)$$

(28)

is an approximation of the coupled-flow sedimentation coefficient linking the molar flow of solute component k to the conjugate molar force of solute component q. (See Equations 13 and 26.)

In the case of $s_q^0 = 0$ for one or more species, q, a modification of Equation 28,

$$s_{k,q} = X_{k,q}^s\left(\frac{s_q^0 + \sum_{a=1}^n (sp)_{q,a}c_a}{1+\sum_{a=1}^n h_{q,a}c_a}\right),$$

(29)

is used to calculate $s_{k,q}$ in terms of the set of $(sp)_{q,a}$, each of which is the species-q-applicable transport coefficient that links the concentration of species a to the density increment of the system, and each of which is given by

$$(sp)_{q,a} = s_q^0 p_{q,a} = \frac{2R_q^2}{9\eta_0 h_q}\left[\frac{\rho_0 - \rho_a}{\rho_a[\varphi_a]_{max}}\right],$$

(30)

where Equations 16 and 19 were used to express $p_{q,a}$ and s_q^0, respectively. (Compare Equations 28, 29 and 30 with Equations 10, 17 and 18, respectively.)

Introducing the coefficient $D_{k,q}$ in Equation 11 yields

$$D_k = \frac{M_k}{\frac{\Delta c_k}{\Delta\xi}}\sum_{q=1}^{n}\frac{\frac{\Delta c_q}{\Delta\xi}}{M_q}X_{k,q}^D D_q^0\left(\frac{1+\sum_{a=1}^n y_{q,a}c_a}{1+\sum_{a=1}^n h_{q,a}c_a}\right) = \frac{M_k}{\frac{\Delta c_k}{\Delta\xi}}\sum_{q=1}^{n}\frac{\frac{\Delta c_q}{\Delta\xi}}{M_q}D_{k,q},$$

(31)

where

$$D_{k,q} = X_{k,q}^D D_q^0\left(\frac{1+\sum_{a=1}^n y_{q,a}c_a}{1+\sum_{a=1}^n h_{q,a}c_a}\right)$$

(32)

is an approximation of the coupled-flow diffusion coefficient linking the molar flow of solute component k to the conjugate molar force of solute component q.

As mentioned previously, it can be shown (Moody, 2011) that, for a given pair of species, k and q, $X_{k,q}^s$ and $X_{k,q}^D$ are identical, and that $X_{k,q}^\sigma$ must therefore be equal to 1. First, however, $X_{k,q}^s$ and $X_{k,q}^D$ will be treated as if they were independent parameters. Treating them as such offers the advantage of allowing the coupled-flow effects on s_q to be evaluated separately from the coupled-flow effects on D_q. Furthermore, in this work, the finite-element approach applied to the simulation of AUC (Moody, 2011) appears to be unstable at $X_{k,q}^D$ values that are large enough to

have any effects distinguishable for those seen at $X_{k,q}^D$ values of zero. Thus, as in six of the cases described in Table 2, treating $X_{k,q}^s$ as independent of $X_{k,q}^D$, and limiting $X_{k,q}^D$ values to negligible magnitudes, allows the coupled-flow effects on s_q to be evaluated via results that are uncluttered by chaotic artefacts.

Table 2 shows the values of $X_{k,q\neq k}^\sigma$, $X_{k,q\neq k}^D$, $X_{k,q\neq k}^s$, $X_{k,k}^\sigma = X_{k,q=k}^\sigma$, $X_{k,k}^D = X_{k,q=k}^D$ and $X_{k,k}^s = X_{k,q=k}^s$ for the seven coupled-flow cases applied to each of the two model systems ($K_a = 30.325$ ml/g and K_a undefined) described above.

case	$X_{k,q\neq k}^\sigma$	$X_{k,q\neq k}^D$	$X_{k,q\neq k}^s$	$X_{k,k}^\sigma$	$X_{k,k}^D$	$X_{k,k}^s$	J-O Effect
-2	-1E+6	1E-10	-1E-4	1	1	1	case -2 > case 0
-1	-1E+6	-1E-10	1E-4	1	1	1	case -1 < case 0
0	$X_{k,q}^s/X_{k,q}^D$	0	0	1	1	1	comparison case
1a	1E+6	1E-10	1E-4	1	1	1	case 1a < case 0
1b	1	1E-4	1E-4	1	1	1	case 1b≅ case 1a
2a	1E+6	-1E-10	-1E-4	1	1	1	case 2a > case 0
2b	1	-1E-4	-1E-4	1	1	1	case 2b≅ case 2a

Table 2. The five coupled-flow cases applied to each of the two model systems ($K_a = 30.325$ ml/g and K_a undefined). The constant $X_{k,q}^\sigma$ couples the effects of gravitational forces on species q to σ_k (Equations 10 and 17). The constant $X_{k,q}^D$ couples the diffusion of species q to D_k (Equation 11, 31 and 32). Like $X_{k,q}^\sigma$, the constant $X_{k,q}^s$ couples the effects of gravitational forces on species q to s_k (Equations 26 to 29). For each model system, the Johnston-Ogston (J-O) effect observed for case 0 ($X_{k,q\neq k}^s = 0$ and $X_{k,q\neq k}^D = 0$) is used as a comparison against which to measure the other cases. Where $X_{k,q}^D = 0$, $X_{k,q}^\sigma$ is undefined (Equation 26), except that the product, $X_{k,q}^\sigma X_{k,q}^D$, is nevertheless treated as being equal to $X_{k,q}^s$. Hence, in case 0, the value of $X_{k,q\neq k}^\sigma$ is given as $X_{k,q}^s/X_{k,q}^D$.

It can be assumed that each $X_{k,k}^D$ is equal to 1 and each $X_{k,k}^s$ is equal to 1 in all cases, so that, by Equation 26, each $X_{k,k}^\sigma$ is also equal to 1 in all cases. As such, in case 0, Equation 11 reduces to

$$D_k = X_{k,k}^D D_k^0 \left(\frac{1+\sum_{k=1}^n y_{k,a}c_a}{1+\sum_{k=1}^n h_{k,a}c_a}\right) = D_k^0 \left(\frac{1+\sum_{k=1}^n y_{k,a}c_a}{1+\sum_{k=1}^n h_{k,a}c_a}\right)$$

(33)

by virtue of each $X_{k,q\neq k}^D$ being equal to zero, and, after substitution of the right-hand side of Equation 33 for D_k, Equation 10 reduces to

$$\sigma_k = X_{k,k}^{\sigma}\sigma_q^0\left(\frac{1+\sum_{a=1}^{n} p_{k,a}c_a}{1+\sum_{a=1}^{n} y_{k,a}c_a}\right) = \sigma_q^0\left(\frac{1+\sum_{a=1}^{n} p_{k,a}c_a}{1+\sum_{a=1}^{n} y_{k,a}c_a}\right)$$

(34)

by virtue of each $X_{k,q\neq k}^D$ and each $X_{k,q\neq k}^S$ being equal to zero. Likewise, in case 0, by virtue of each $X_{k,q\neq k}^D$ and each $X_{k,q\neq k}^S$ being equal to zero, Equation 17 reduces to

$$\sigma_k = X_{k,q}^{\sigma}\left(\frac{\sigma_q^0+\sum_{a=1}^{n}(\sigma p)_{q,a}c_a}{1+\sum_{k=1}^{n} y_{k,a}c_a}\right) = \frac{\sigma_k^0+\sum_{a=1}^{n}(\sigma p)_{k,a}c_a}{1+\sum_{k=1}^{n} y_{k,a}c_a}$$

(35)

after substitution of the right-hand side of Equation 33 for D_k. Equations 34 and 35 show that $h_{q,a}$ values exert no influence on σ_k values, provided that all $X_{k,q\neq k}^D$ and $X_{k,q\neq k}^S$ values are zero. As shown by the inability to eliminate the $(1+\sum_{a=1}^{n} h_{q,a}c_a)$ terms from σ_k (Equations 10 and 17) when not all $X_{k,q\neq k}^D$ and $X_{k,q\neq k}^S$ values are equal to zero, however, $h_{q,a}$ values can wield some influence on σ_k values, even at equilibrium, unless all $X_{k,q\neq k}^D$ and $X_{k,q\neq k}^S$ values are equal to zero. This residual influence of $h_{q,a}$ is a flaw of the approximation of σ_k by Equations 10 and 17, as the equation (Equation A23 of Moody, 2011) that defines σ_k is devoid of any viscosity-related terms such as $h_{q,a}$, which represents the component-q affecting viscosity coefficient of c_a (Equation 14).

The results of AUC simulations for the seven cases (Table 2) of the two model systems ($K_a =$ 30.325 ml/g and K_a undefined) are shown below. (Each data plot occupies most of a page.) Case 0, in which $X_{k,q\neq k}^S = 0$ and $X_{k,q\neq k}^D = 0$, is presented in the greatest detail.

Observations regarding the two model systems in case 0*, for which* $X_{k,q\neq k}^S = 0$ *and* $X_{k,q\neq k}^D = 0$

For the AUC simulation of case 0 ($X_{k,q\neq k}^S = 0$ and $X_{k,q\neq k}^D = 0$) in each model system ($K_a = 30.325$ ml/g and K_a undefined), the programme was compiled and run in debugger mode using Borland

C++ Builder 6.0 on a laptop PC with a 2.1 GHz CPU, 4 GB RAM and a 32-bit OS (Windows Vista). For case 0, in the both model systems, the implementation can exploit Equations 33, 34 and 35, rather than Equations 11, 10 and 17, respectively. Exploiting the former set of equations reduces the time taken to simulate either model system by approximately 34% for the first model system ($K_a = 30.325$ ml/g) and approximately 43% for the second model system (K_a undefined), as compared to the time taken when the latter set of equations is used to simulate the corresponding model system in case 0. The use of Equations 33, 34 and 35 yielded the times reported below for both model systems in case 0.

For case 0 ($X^S_{k,q\neq k} = 0$ and $X^D_{k,q\neq k} = 0$) in the first model system, in which species *H*, *L* and *HL* participate in a mass-action association with $K_a = 30.325$ ml/g, 2.76 min of AUC were simulated per minute of computation, on average, in the first 116 min of simulated AUC. Although it approached vanishingly small values wherever the concentration of *H* or *L* approached zero, the concentration of *LH* remained greater than zero throughout the system during the first 66 min of simulated AUC, for which 2.54 min of AUC were simulated per minute of computation, on average. After the first 68.5 min of simulated AUC, and during the next 47.5 min of simulated AUC, the concentration of *LH* was equal to zero throughout the system, and 3.17 min of AUC were simulated per minute of computation, on average.

For case 0 ($X^S_{k,q\neq k} = 0\ and\ X^D_{k,q\neq k} = 0$) in the second system, in which all species are single-species components, 3.63 min of AUC were simulated per minute of computation, on average, in the first 116 min of simulated AUC, during which, the time to compute 1 min of simulated AUC remained fairly constant.

For both systems, for the first 116 min of simulated AUC and well beyond, the observed Δt was equal to $\Delta t_{max} = 3$ s. Neither system exhibited instabilities.

A comparison of the low-concentration solute data for the two model systems (Figures 1, 6 and 7 for the $K_a = 30.325$ ml/g system versus Figures 8, 13 and 14 for the system with K_a undefined) does not reveal any obvious characteristics by which the data pertaining to one system can be distinguished from the data pertaining to the other. A comparison of the high-concentration solute data for the two model systems (Figures 2 to 5 for the $K_a = 30.325$ ml/g system versus Figures 9 to 12 for the system with K_a undefined) reveals many such characteristics. This shows the extent to which a more or less neutrally buoyant solute may leave little evidence of its

presence, unless it is detected directly. Some indirect evidence of its presence does exist in the results for species *H* and *L*, however (Figures 3 and 4, which are described in some detail following Figure 5 in the case of the $K_a = 30.325$ ml/g system; and Figures 10 and 11, which are described in some detail following Figure 12 in the case of the system with K_a undefined), and arguably, the two model systems are not terribly difficult to distinguish on the basis of those results.

In both systems, the low-concentration species exhibit Johnston-Ogston effects (Figures 1, 6 and 7 for the $K_a = 30.325$ ml/g system; and Figures 8, 13 and 14 for the system with K_a undefined) that result from each of those species having a significantly higher-magnitude sedimentation coefficient ($|s_k|$) behind the boundary of the high-concentration solute with which it approximately comigrates (species 2 to 13 being comigratory with species *H*, and species 15 to 26 being comigratory with species *L*) than it does ahead of that boundary, relative to the direction in which the boundary travels. In both of the systems described here, the Johnston-Ogston effects are primarily due to the concentration dependence of the density increment. (See Equations 8, 10, 16, 17 and 18.) The direction of the mass flow affects the intensity of Johnston-Ogston effects.

The volume of the sector-shaped system increases in proportion to ξ. Thus, the mass flow of a sedimenting species ($s_k > 0$) is in the direction of higher volume, and the mass flow of a floating species ($s_k < 0$) is in the direction of lower volume. Consequently, a sedimenting species is subject to a radial-dilution effect in which its concentration between its boundary and the pellet decreases with time such that $(\partial c_k/\partial t)_\xi < 0$ even in a region where $(\partial c_k/\partial \xi)_t = 0$. Likewise, a floating species is subject to a radial-concentration effect in which its concentration between its boundary and the supernatant increases with time such that $(\partial c_k/\partial t)_\xi > 0$ even in a region where $(\partial c_k/\partial \xi)_t = 0$. (For a neutrally buoyant species, in a region where both $(\partial c_k/\partial \xi)_t = 0$ and $s_k = 0$, $(\partial c_k/\partial t)_\xi = 0$.) As the Johnston-Ogston effects are concentration dependent, and as the geometry of the system produces radial-dilution or radial-concentration effects depending on the direction of mass flow, the Johnston-Ogston effects tend to continuously intensify with time for floating species, but eventually start to weaken with time for sedimenting species.

As the system with K_a undefined approaches equilibrium (Figures 15 and 16), the concentration of single-species component *LH* rises to a peak at either the pellet formed mainly by *H*, or the supernatant formed mainly by *L*. This effect may be an artefact of using severely truncated virial

expansions to describe the density increment, thermodynamic nonideality and viscosity of the system in regions where the concentrations of *LH*, *L* or *H* are extremely high. (See Equations 10 to 18.)

Results for case 0*, in which* $X^s_{k,q\neq k} = 0$ *and* $X^D_{k,q\neq k} = 0$, and $K_a = 30.325$ ml/g*, for which two of the components account for three of the species present in the system.*

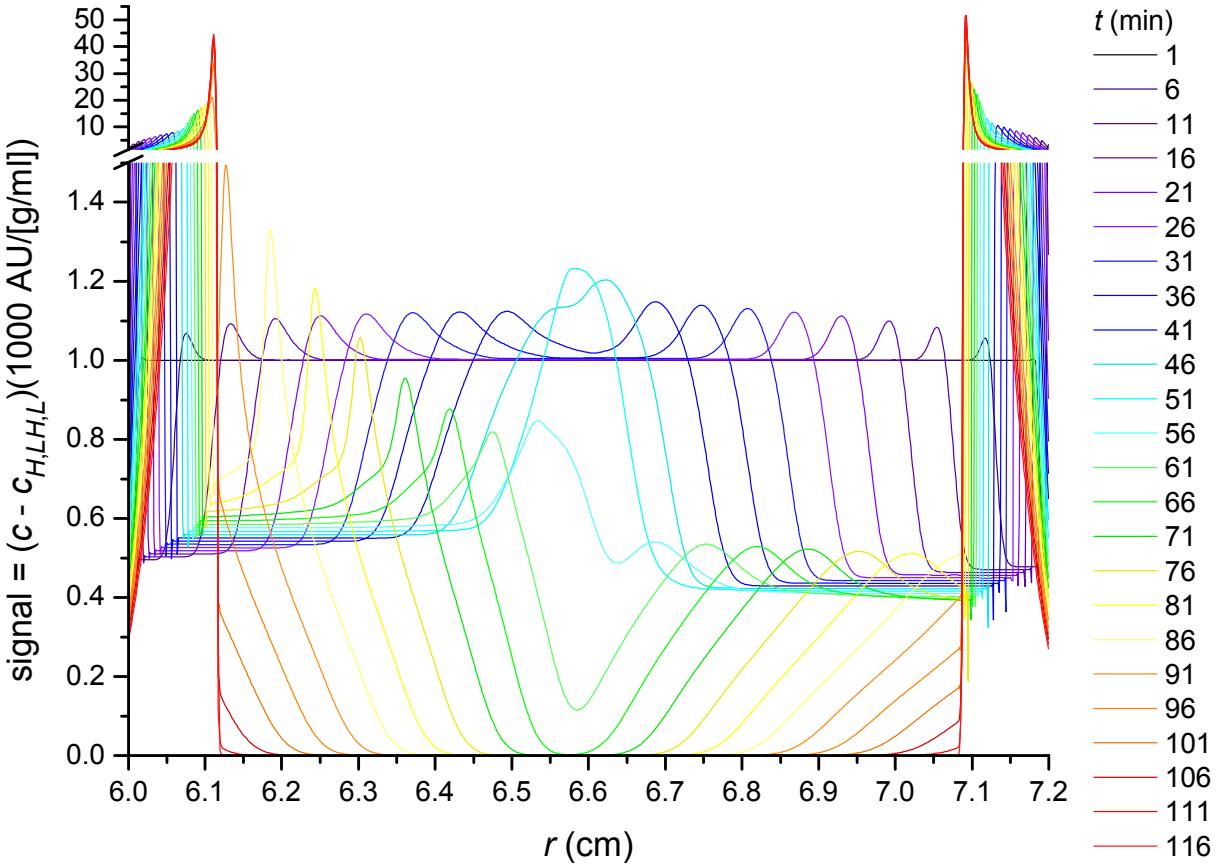

Figure 1, $K_a = 30.325$ ml/g, case 0 (Table 2, $X^s_{k,q\neq k} = 0$ and $X^D_{k,q\neq k} = 0$). (Compare with Figures 21, 22, 29 and 30.) The sum of the signals from all species except species 1 (*H*), 14 (*LH*) and 27 (*L*), given by $(c - c_{H,LH,L})$(1000 AU/[g/ml]), versus r (cm) for 1 min $\leq t \leq$ 116 min. High concentration data in the pellet and supernatant are shown on a compressed scale above the break in the AU-axis. Compare this figure with Figure 8, K_a undefined.

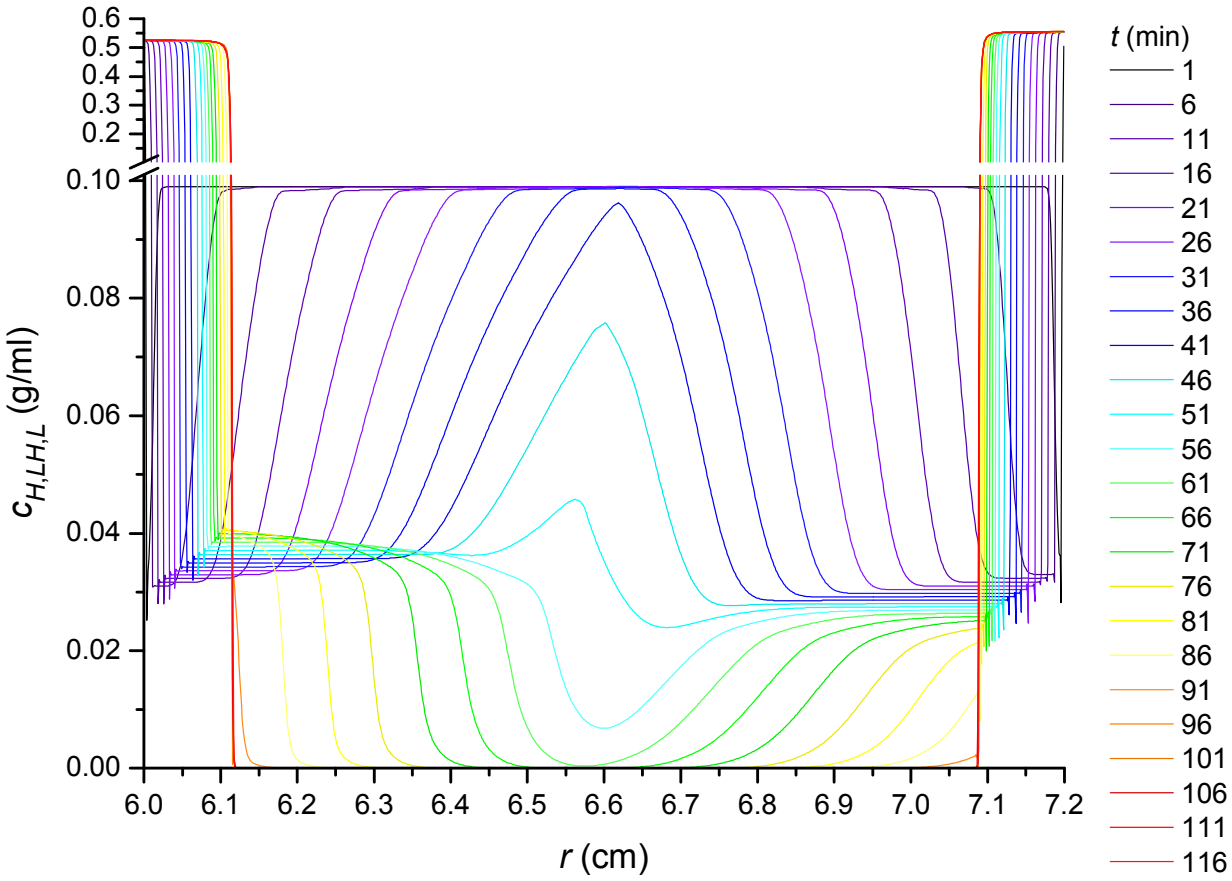

Figure 2, $K_a = 30.325$ ml/g, case 0 (Table 2, $X^s_{k,q\neq k} = 0$ and $X^D_{k,q\neq k} = 0$). The sum of the concentrations of species 1 (H), 14 (LH) and 27 (L), $c_{H,LH,L}$ (g/ml), versus r (cm) for 1 min $\leq t \leq$ 116 min. High concentration data in the pellet and supernatant are shown on a compressed scale above the break in the $c_{H,LH,L}$-axis. Compare this figure with Figure 9, K_a undefined.

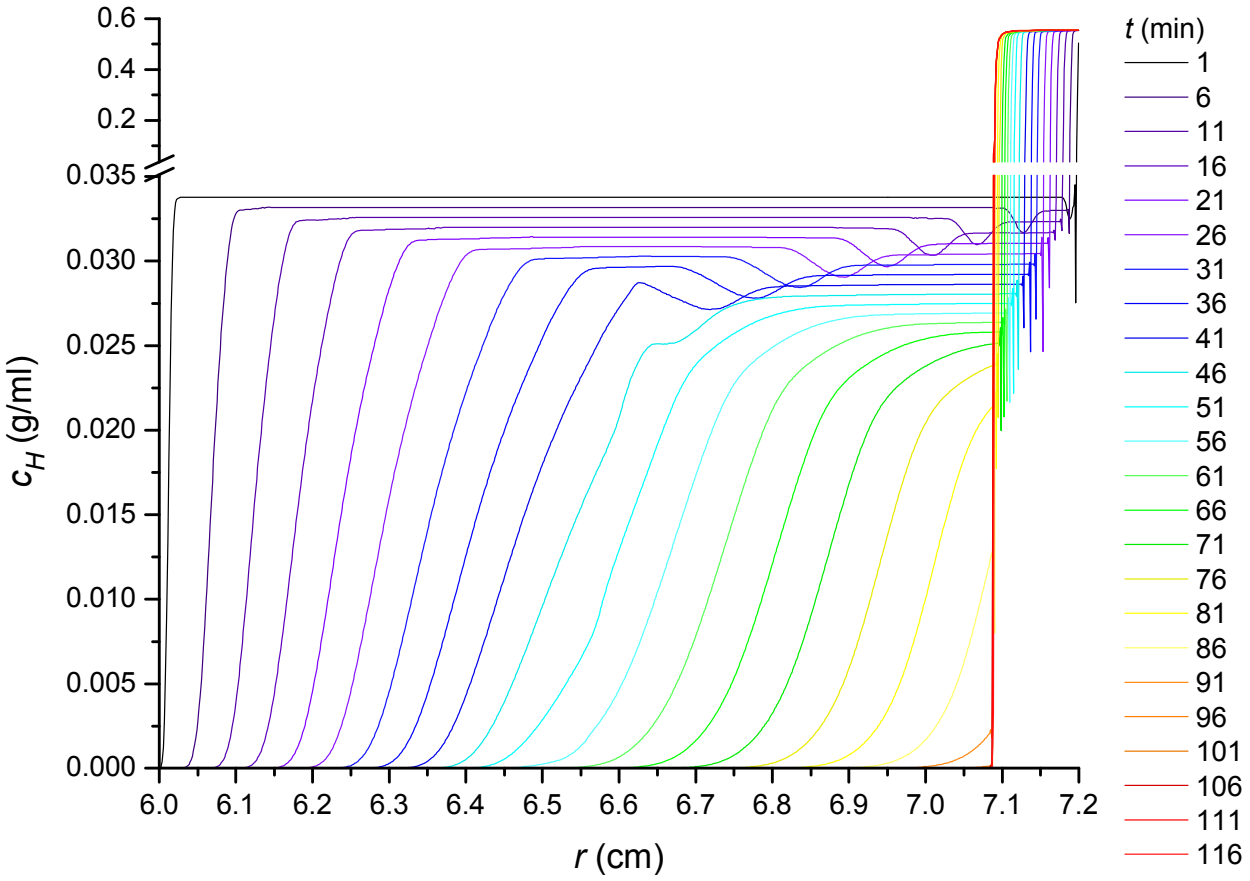

Figure 3, $K_a = 30.325$ ml/g, case 0 (Table 2, $X^s_{k,q\neq k} = 0$ and $X^D_{k,q\neq k} = 0$). The concentration of species 1 (H), c_H (g/ml), versus r (cm) for 1 min $\leq t \leq$ 116 min. High concentration data are found solely in the pellet, and are shown on a compressed scale above the break in the c_H-axis. There is no supernatant. Compare this figure with Figure 10, K_a undefined.

There are dips in the concentration gradients of species H (Figure 3, $K_a = 30.325$ ml/g) that align with the right-hand boundaries of species LH (Figure 5, $K_a = 30.325$ ml/g) at the corresponding times.

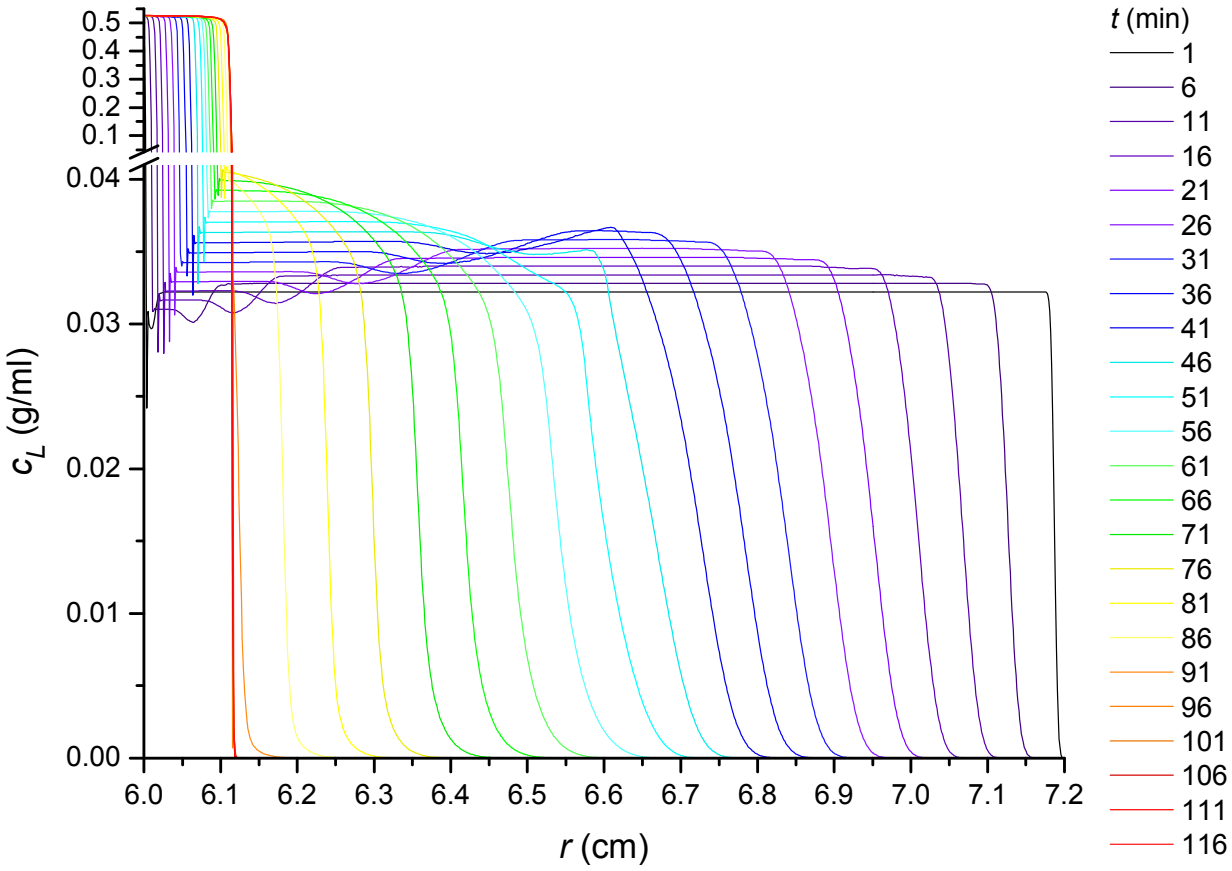

Figure 4, $K_a = 30.325$ ml/g, case 0 (Table 2, $X^S_{k,q\neq k} = 0$ and $X^D_{k,q\neq k} = 0$). The concentration of species 27 (L), c_L (g/ml), versus r (cm) for 1 min $\leq t \leq$ 116 min. High concentration data are found solely in the supernatant, and are shown on a compressed scale above the break in the c_L-axis. There is no pellet. Compare this figure with Figure 11, K_a undefined.

There are dips in the concentration gradients of species L (Figure 4, $K_a = 30.325$ ml/g) that align with the left-hand boundaries of species LH (Figure 5, $K_a = 30.325$ ml/g) at the corresponding times.

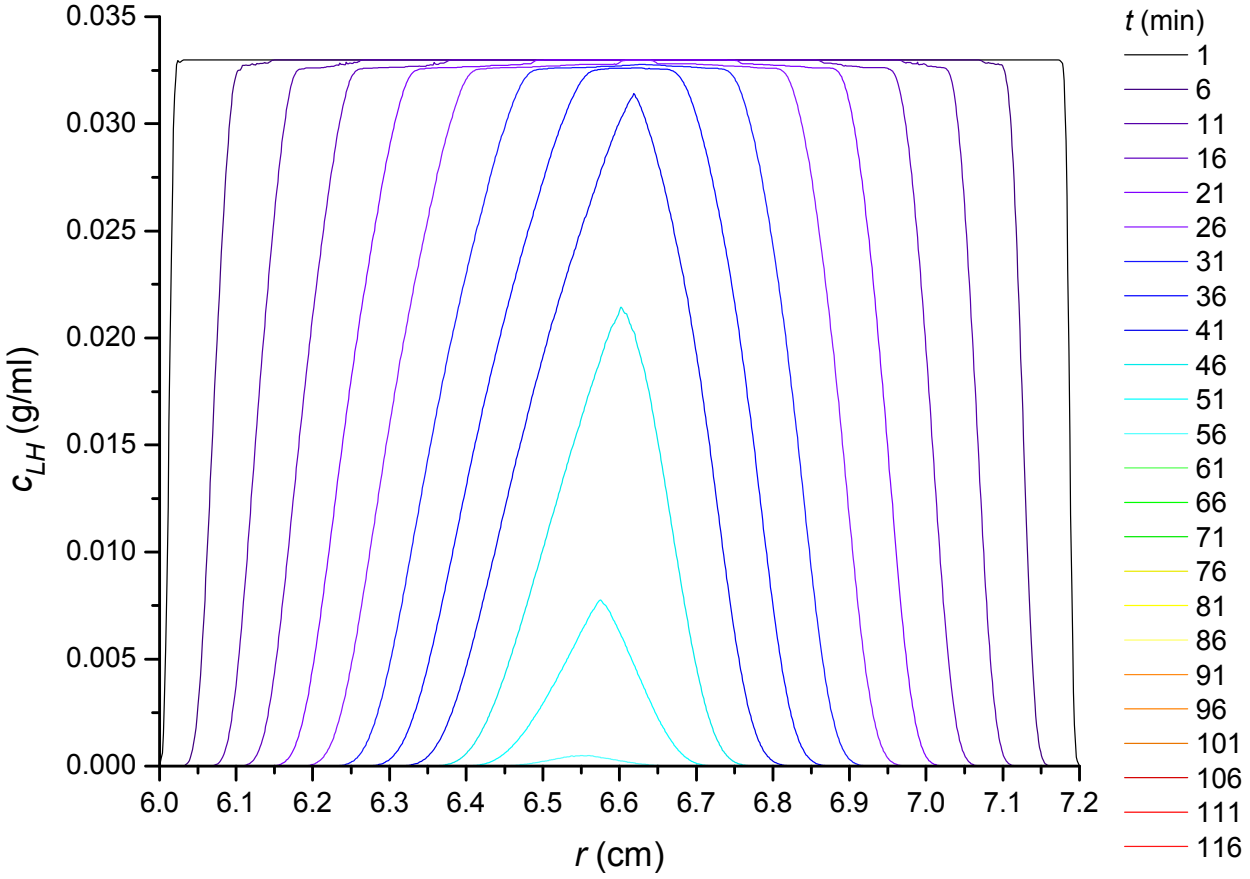

Figure 5, $K_a = 30.325$ ml/g, case 0 (Table 2, $X^s_{k,q\neq k} = 0$ and $X^D_{k,q\neq k} = 0$). The concentration of species 14 (LH), c_{LH} (g/ml), versus r (cm) for 1 min $\leq t \leq$ 116 min. There is neither a pellet nor a supernatant. Compare this figure with Figure 12, K_a undefined.

The depletion of species H from the meniscus outward and the depletion of species L from the base inward give rise, respectively, to the left-hand and right-hand boundaries of species LH. As the left-hand and right-hand boundaries of species LH move toward the centre of the system (Figure 5, $K_a = 30.325$ ml/g), LH dissociates to form the oppositely migrating species, H and L, causing the dips in the concentrations of those species seen in Figures 3 and 4 ($K_a = 30.325$ ml/g), respectively. The effect occurs even with all $(\sigma p)_{q,a}$, $p_{q,a}$, $y_{q,a}$ and $h_{q,a}$ set to zero, and all $c_k = 0$ for $1 < k < 14$ and $14 < k < 27$.

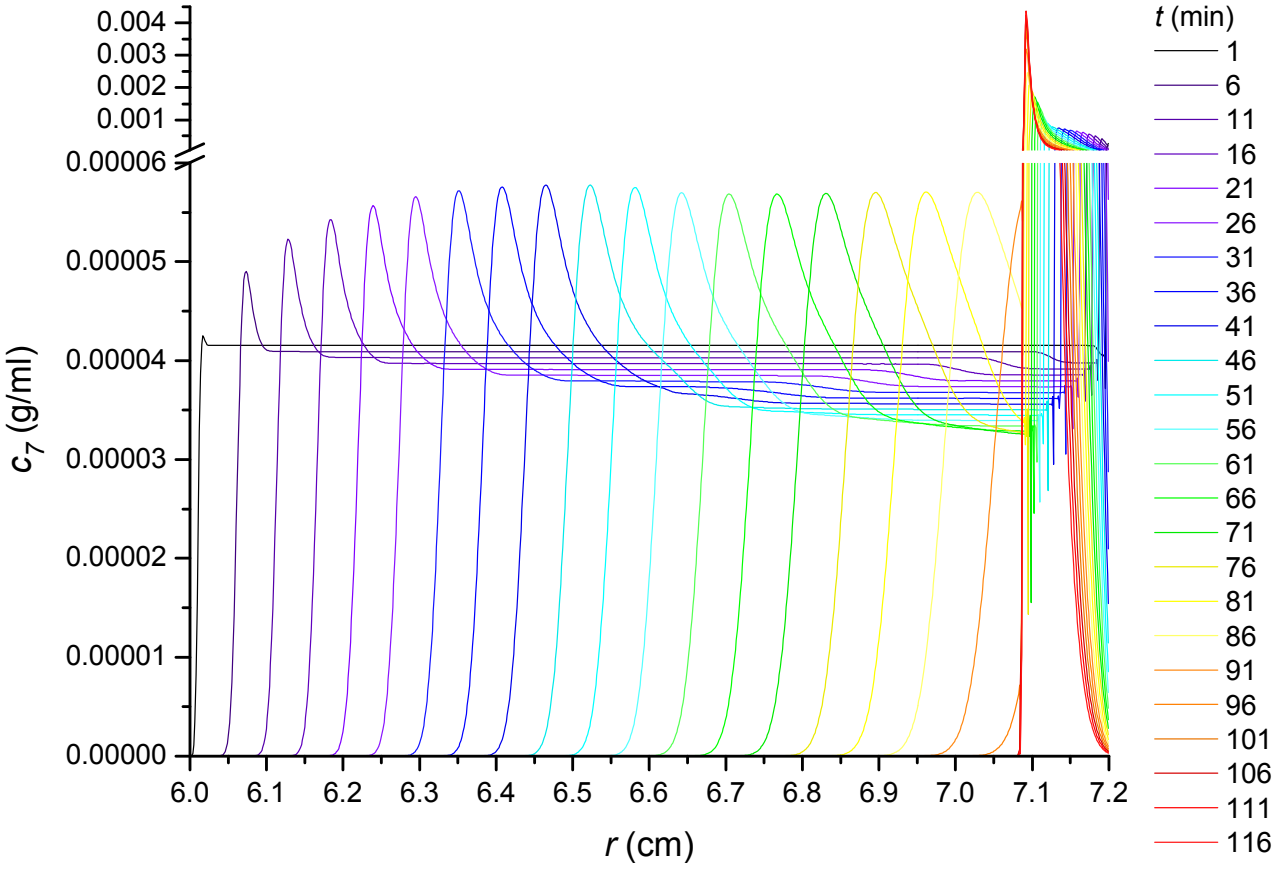

Figure 6, $K_a = 30.325$ ml/g, case 0 (Table 2, $X^s_{k,q\neq k} = 0$ and $X^D_{k,q\neq k} = 0$). (Compare with Figures 23 and 31.) The concentration of species 7, c_7 (g/ml), versus r (cm) for 1 min $\leq t \leq$ 116 min. High concentration data are found solely in the pellet, and are shown on a compressed scale above the break in the c_7-axis. There is no supernatant. The data for this species are representative of the data for species 2 through 13, for which $s_k^0 > 0$, and total c_k is small relative to total c. Compare this figure with Figure 13, K_a undefined.

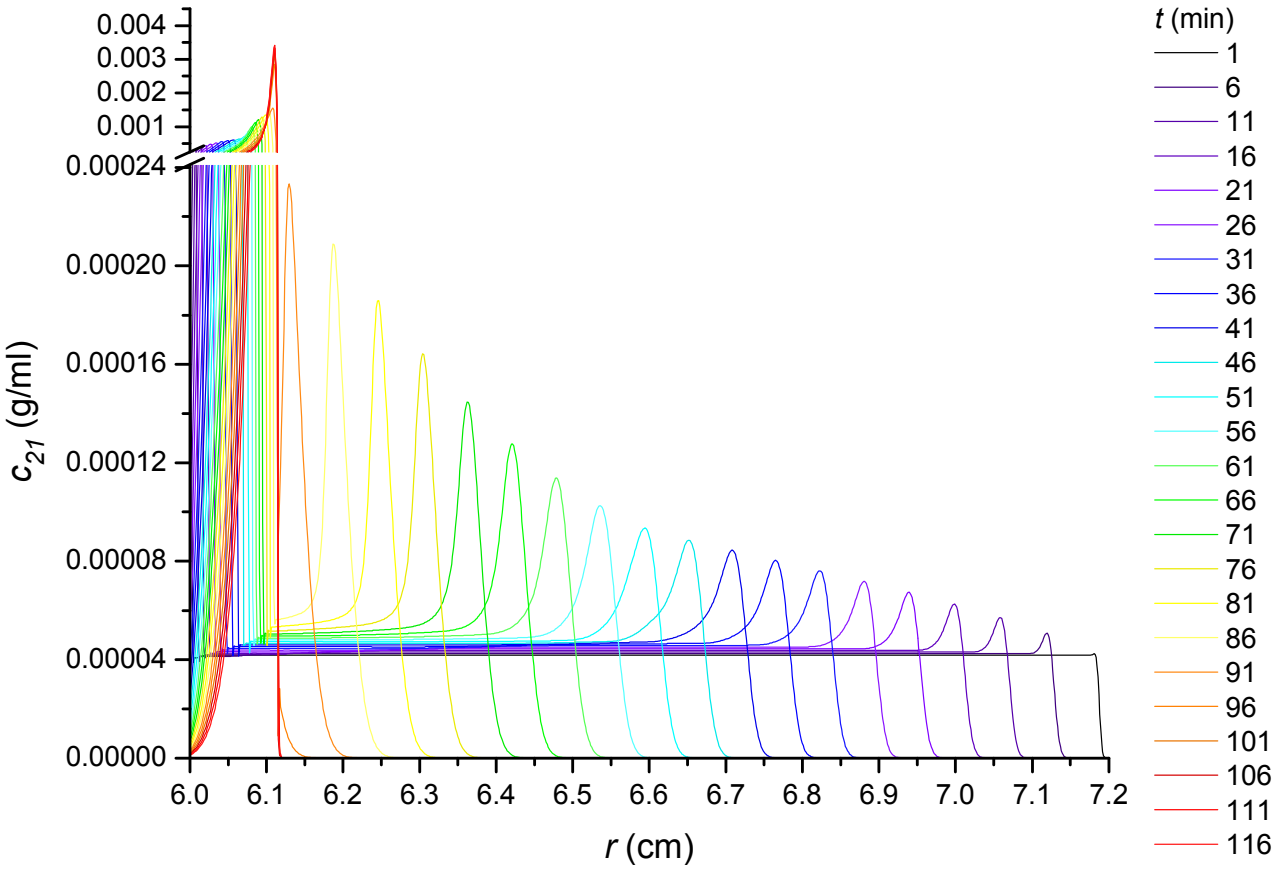

Figure 7, $K_a = 30.325$ ml/g, case 0 (Table 2, $X^s_{k,q\neq k} = 0$ and $X^D_{k,q\neq k} = 0$). (Compare with Figures 24 and 32.) The concentration of species 21, c_{21} (g/ml), versus r (cm) for 1 min $\leq t \leq$ 116 min. High concentration data are found solely in the supernatant, and are shown on a compressed scale above the break in the c_{21}-axis. There is no pellet. The data for this species are representative of the data for species 15 through 26, for which $s_k^0 < 0$, and total c_k is small relative to total c. Compare this figure with Figure 14, K_a undefined.

K_a undefined: All species are single-species components. Results for case 0*, in which* $X^s_{k,q\neq k} = 0$ *and* $X^D_{k,q\neq k} = 0$, and *K_a undefined, for which all species are single-species components.*

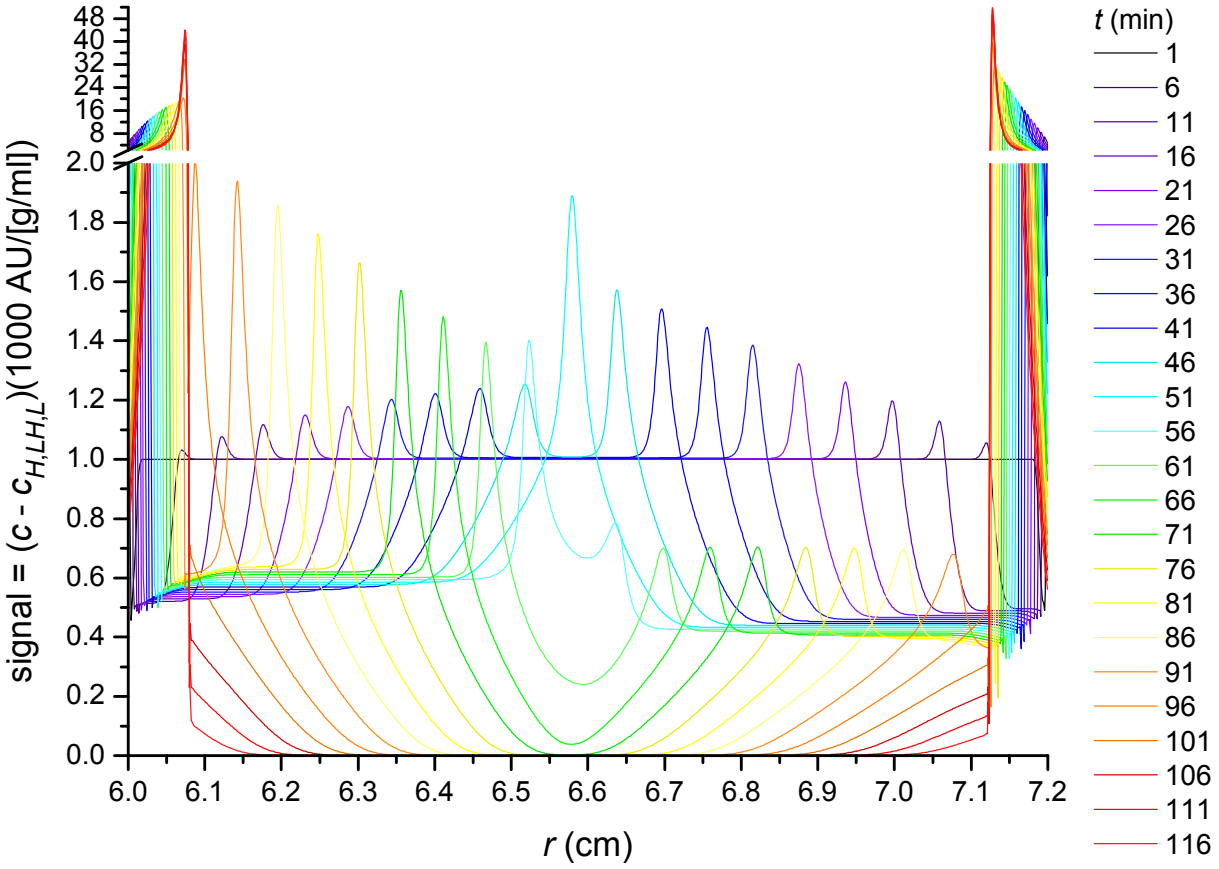

Figure 8, K_a undefined (all species are single-species components), case 0 (Table 2, $X^S_{k,q\neq k} = 0$ and $X^D_{k,q\neq k} = 0$). (Compare with Figures 17, 18, 25 and 26.) The sum of the signals from all species except species 1 (*H*), 14 (*LH*) and 27 (*L*), given by (c - $c_{H,LH,L}$)(1000 AU/[g/ml]), versus r (cm) for 1 min $\leq t \leq$ 116 min. High concentration data in the pellet and supernatant are shown on a compressed scale above the break in the AU-axis. Compare this figure with Figure 1, $K_a =$ 30.325 ml/g.

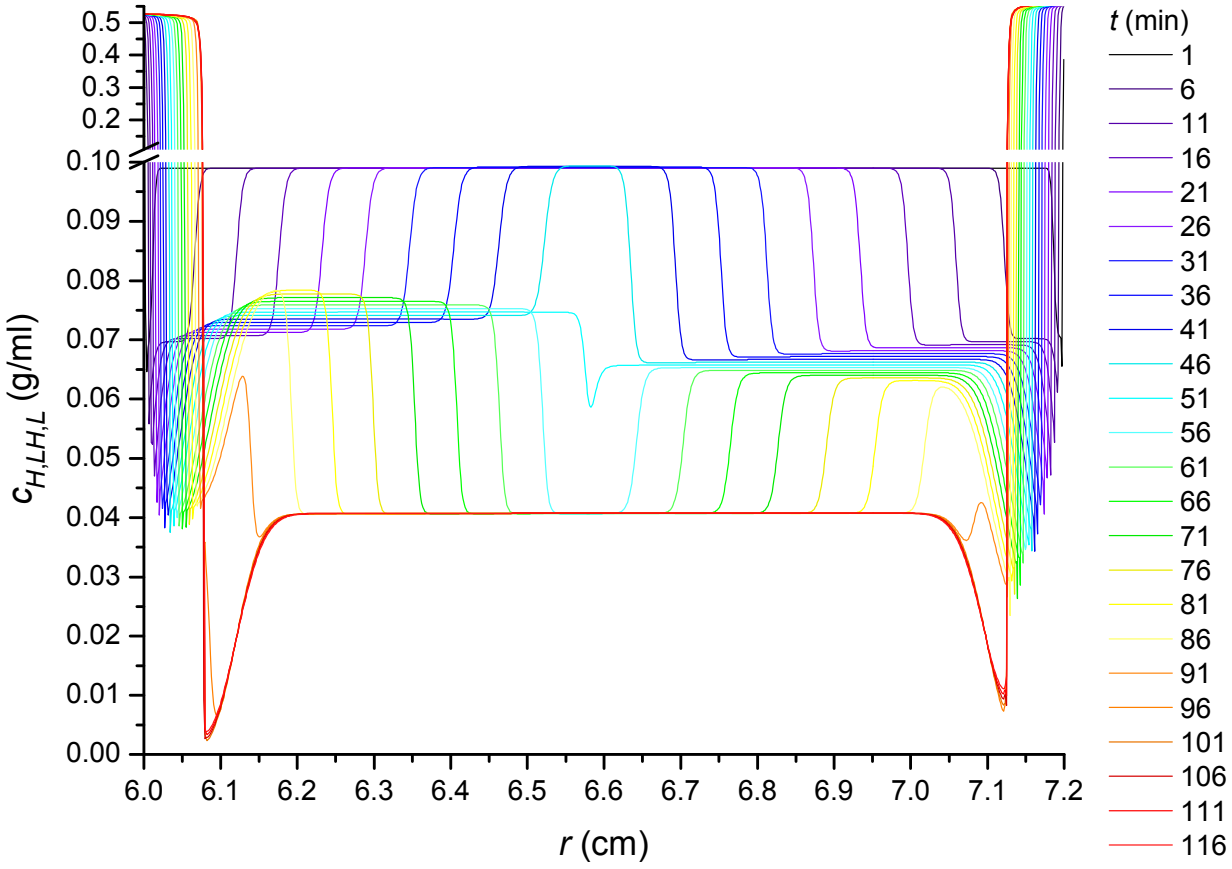

Figure 9, K_a undefined (all species are single-species components), case 0 (Table 2, $X^S_{k,q\neq k} = 0$ and $X^D_{k,q\neq k} = 0$). The sum of the concentrations of species 1 (H), 14 (LH) and 27 (L), $c_{H,LH,L}$ (g/ml), versus r (cm) for 1 min $\leq t \leq$ 116 min. High concentration data in the pellet and supernatant are shown on a compressed scale above the break in the $c_{H,LH,L}$-axis. Compare this figure with Figure 2, $K_a = 30.325$ ml/g.

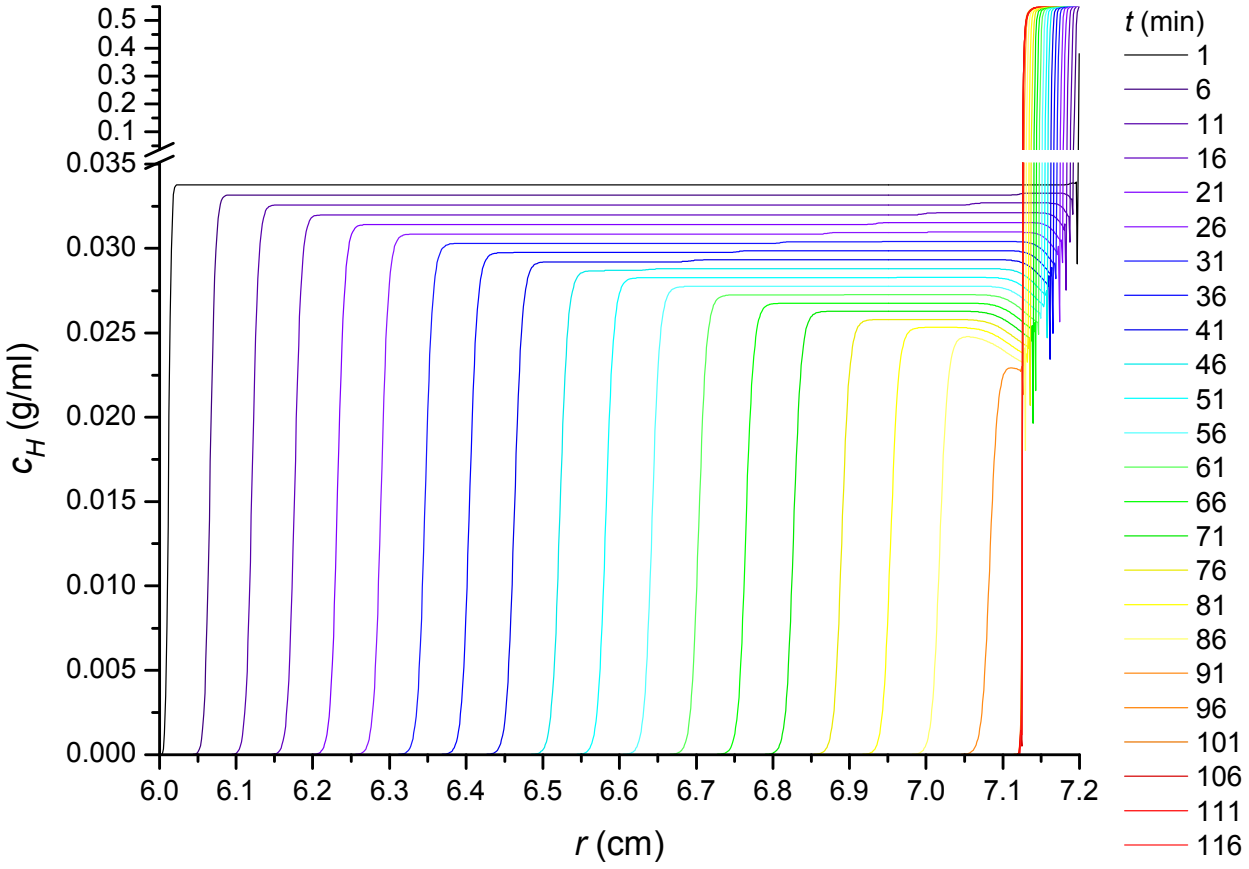

Figure 10, K_a undefined (all species are single-species components), case 0 (Table 2, $X^s_{k,q\neq k} = 0$ and $X^D_{k,q\neq k} = 0$). The concentration of species 1 (H), c_H (g/ml), versus r (cm) for 1 min $\leq t \leq$ 116 min. High concentration data are found solely in the pellet, and are shown on a compressed scale above the break in the c_H-axis. There is no supernatant. Compare this figure with Figure 3, $K_a =$ 30.325 ml/g.

The decreased concentration of H (Figure 10, K_a undefined) toward the pellet, which is most evident from $t =$ 21 min to $t =$ 86 min, is seen even with all $c_k = 0$ for $1 < k < 14$ and $14 < k < 27$. If all $(\sigma p)_{LH,a} = 0$, the effect is absent because c_{LH} does not redistribute with time. If all $h_{q,a} = 0$, the effect is absent because c_{LH} does not affect $s_{k\neq 14}$. The effect is weakened if all $y_{q,a} = 0$, even with all $(\sigma p)_{q,a}$, $p_{q,a}$ and all $h_{q,a}$ governed by Equations 18, 16 and 14, respectively.

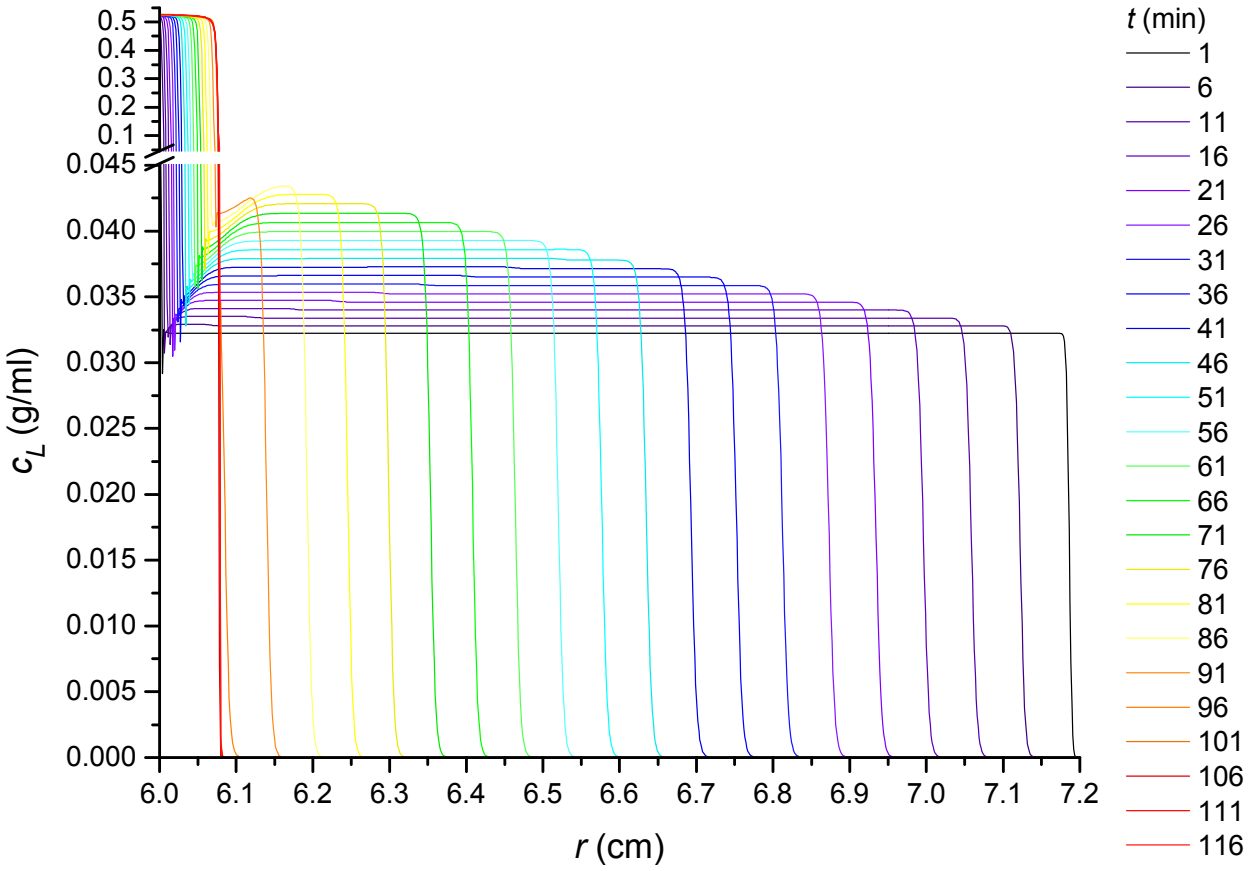

Figure 11, K_a undefined (all species are single-species components), case 0 (Table 2, $X^S_{k,q\neq k} = 0$ and $X^D_{k,q\neq k} = 0$). The concentration of species 27 (L), c_L (g/ml), versus r (cm) for 1 min $\leq t \leq$ 116 min. High concentration data are found solely in the supernatant, and are shown on a compressed scale above the break in the c_L-axis. There is no pellet. Compare this figure with Figure 4, $K_a = 30.325$ ml/g.

The decreased concentration of L (Figure 11, K_a undefined) toward the supernatant, which is most evident from $t = 31$ min to $t = 91$ min, is seen even with all $c_k = 0$ for $1 < k < 14$ and $14 < k < 27$. If all $(\sigma p)_{LH,a} = 0$, the effect is absent because c_{LH} does not redistribute with time. If all $h_{q,LH} = 0$, the effect is absent because c_{LH} does not affect $s_{k\neq 14}$. The effect is weakened if all $y_{q,a} = 0$, even with all $(\sigma p)_{q,a}$, $p_{q,a}$ and all $h_{q,a}$ given by Equations 18, 16 and 14, respectively.

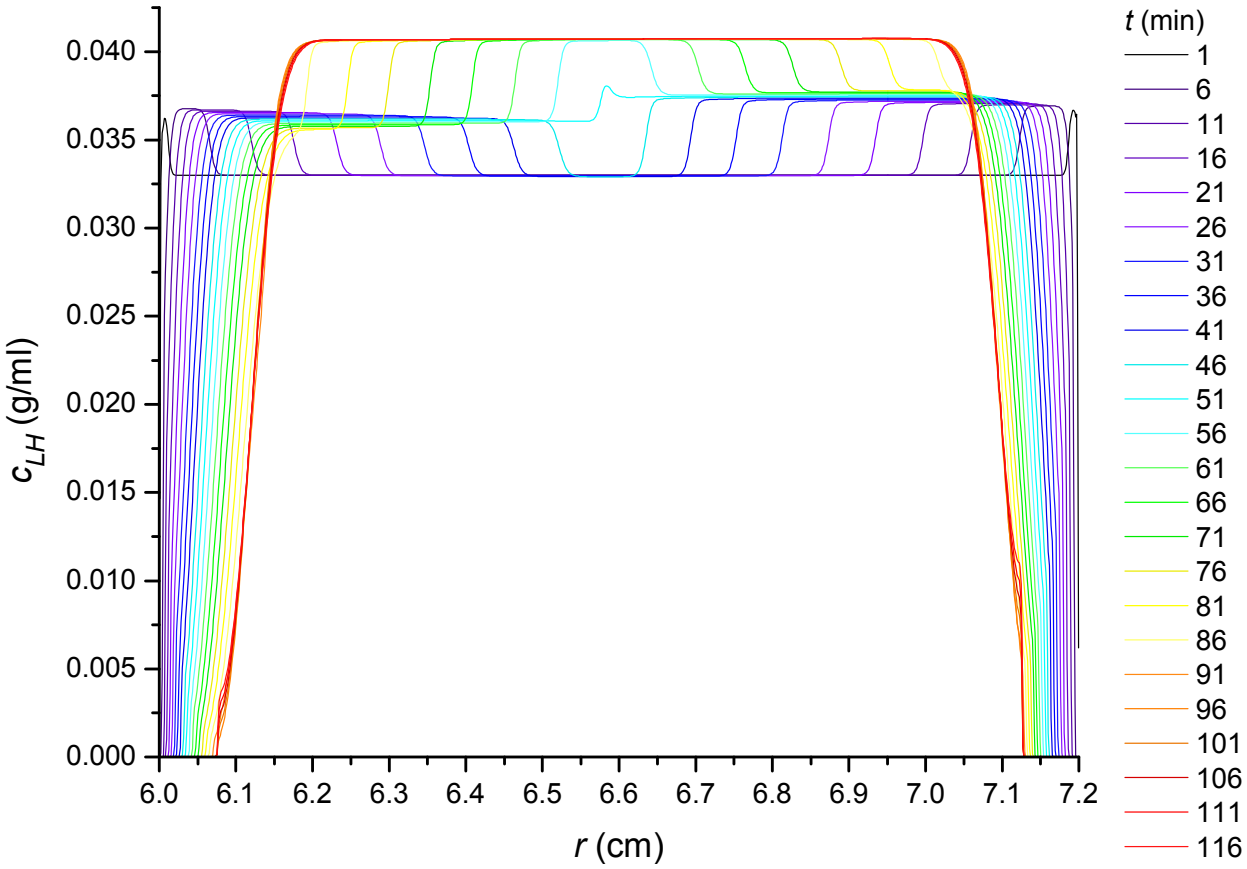

Figure 12, K_a undefined (all species are single-species components), case 0 (Table 2, $X^s_{k,q\neq k} = 0$ and $X^D_{k,q\neq k} = 0$). The concentration of species 14 (LH), c_{LH} (g/ml), versus r (cm) for 1 min $\leq t \leq$ 116 min. There is neither a pellet nor a supernatant. Compare this figure with Figure 5, $K_a =$ 30.325 ml/g.

Changes in c_{LH} (Figure 12, K_a undefined) are entirely driven by changes in the concentrations of the system's other solute species, particularly H (Figure 10, K_a undefined) and L (Figure 11, K_a undefined). As c_H increases, s_{LH} (the sedimentation coefficient of species 14) becomes more negative. As c_L increases, s_{LH} becomes more positive. Thus, where c_H accumulates in the pellet or c_L accumulates in the supernatant, c_{LH} decreases. (With respect to species LH, the effects of species 2 to 13 are similar to the effects of species H, and the effects of species 15 to 26 are similar to the effects of species L.)

Species LH has no effect on the density of the system because $p_{q,LH} = 0$ for all q. However, concentration gradients in other species produce density gradients, and those density gradients redistribute species LH. The resulting concentration gradients in species LH give rise to a radial dependence in the viscosity and thermodynamic nonideality of the system. Of these, only the radial dependence in the viscosity imparts a radial dependence to s_H and s_L. Where c_{LH} plummets toward the pellet and supernatant, the decrease in viscosity causes $|s_H|$ and $|s_L|$ to increase enough to cause the small decreases seen in c_H toward the pellet and c_L toward the supernatant (Figures 10 and 11, respectively). (With respect to species LH, the effects on species 2 to 13 are similar to the effects on species H, and the effects on species 15 to 26 are similar to the effects on species L.) A radial dependence in thermodynamic nonideality is also implicated, however, as the effect is weakened if all $y_{q,a}$ (Equation 11) are set to zero, even with all $(\sigma p)_{q,a}$, all $p_{q,a}$ and all $h_{q,a}$ governed by Equations 18, 16 and 14, respectively. (All $y_{q,14}$ and all $h_{q,a\neq14}$ can be set to zero without weakening the effect, however.) Setting all $(\sigma p)_{LH,a}$ equal to zero renders $s_{LH} = 0$ everywhere at all times, with the result that c_{LH} does not redistribute with time. Setting all $h_{q,LH}$ equal to zero renders $s_{k\neq14}$, including s_H and s_L, insensitive to c_{LH}. Thus, setting all $h_{q,LH}$ equal to zero, or setting all $(\sigma p)_{LH,a}$ equal to zero, eliminates the effect.

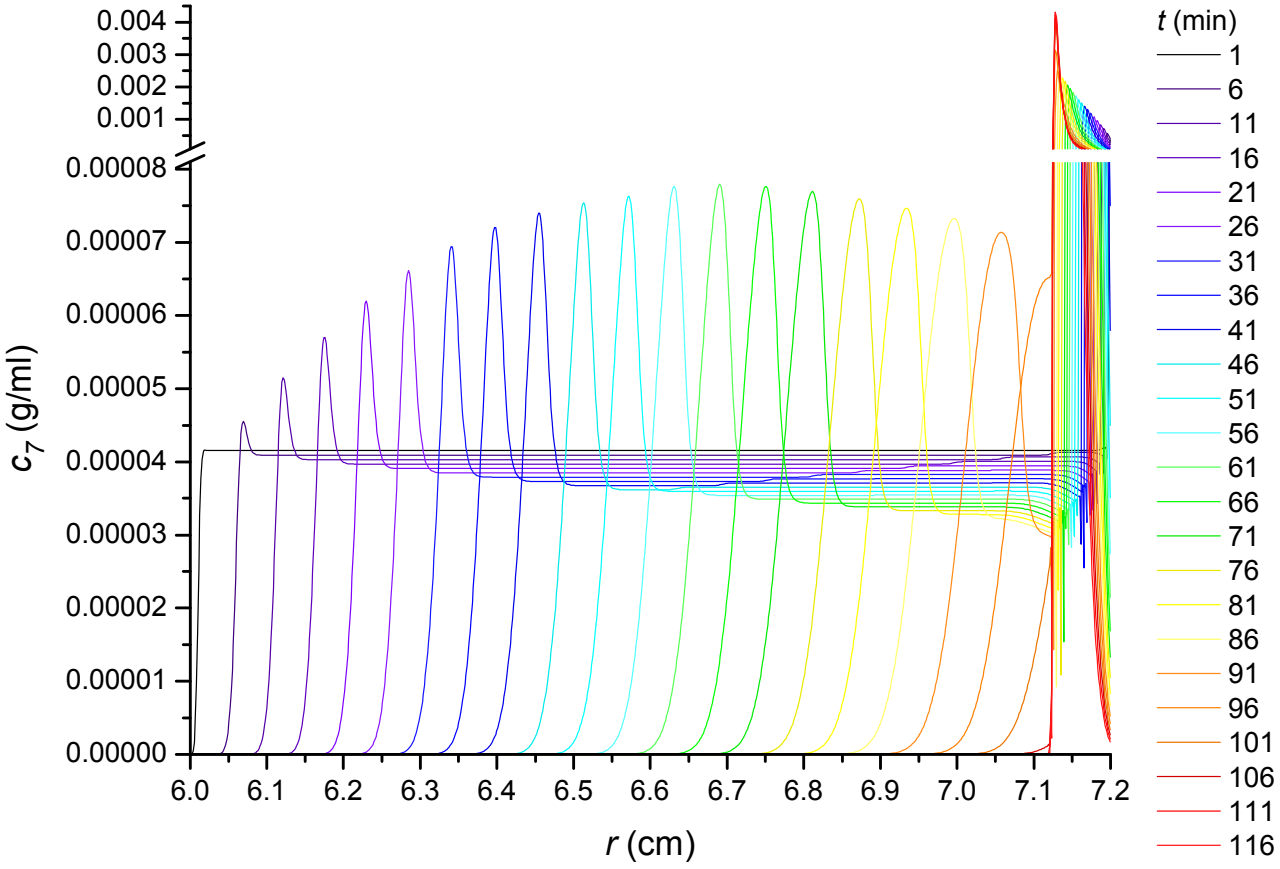

Figure 13, K_a undefined (all species are single-species components), case 0 (Table 2, $X^s_{k,q\neq k} = 0$ and $X^D_{k,q\neq k} = 0$). (Compare with Figures 19 and 27.) The concentration of species 7, c_7 (g/ml), versus r (cm) for 1 min $\leq t \leq$ 116 min. High concentration data are found solely in the pellet, and are shown on a compressed scale above the break in the c_7-axis. There is no supernatant. The data for this species are representative of the data for species 2 through 13, for which $s_k^0 > 0$, and total c_k is small relative to total c. Compare this figure with Figure 6, $K_a = 30.325$ ml/g.

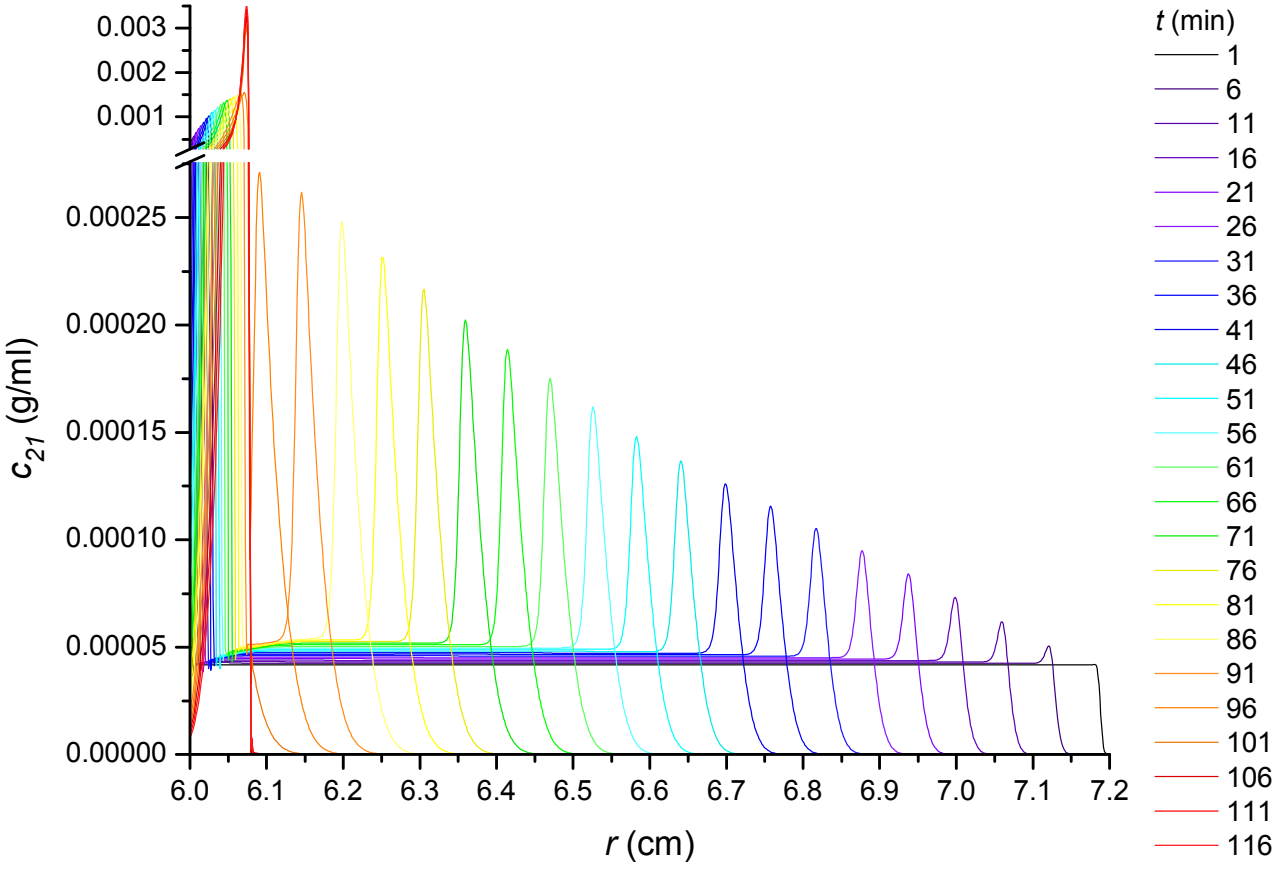

Figure 14, K_a undefined (all species are single-species components), case 0 (Table 2, $X^s_{k,q\neq k} = 0$ and $X^D_{k,q\neq k} = 0$). (Compare with Figures 20 and 28.) The concentration of species 21, c_{21} (g/ml), versus r (cm) for 1 min $\leq t \leq$ 116 min. High concentration data are found solely in the supernatant, and are shown on a compressed scale above the break in the c_{21}-axis. There is no pellet. The data for this species are representative of the data for species 15 through 26, for which $s^0_k < 0$, and total c_k is small relative to total c. Compare this figure with Figure 7, $K_a =$ 30.325 ml/g.

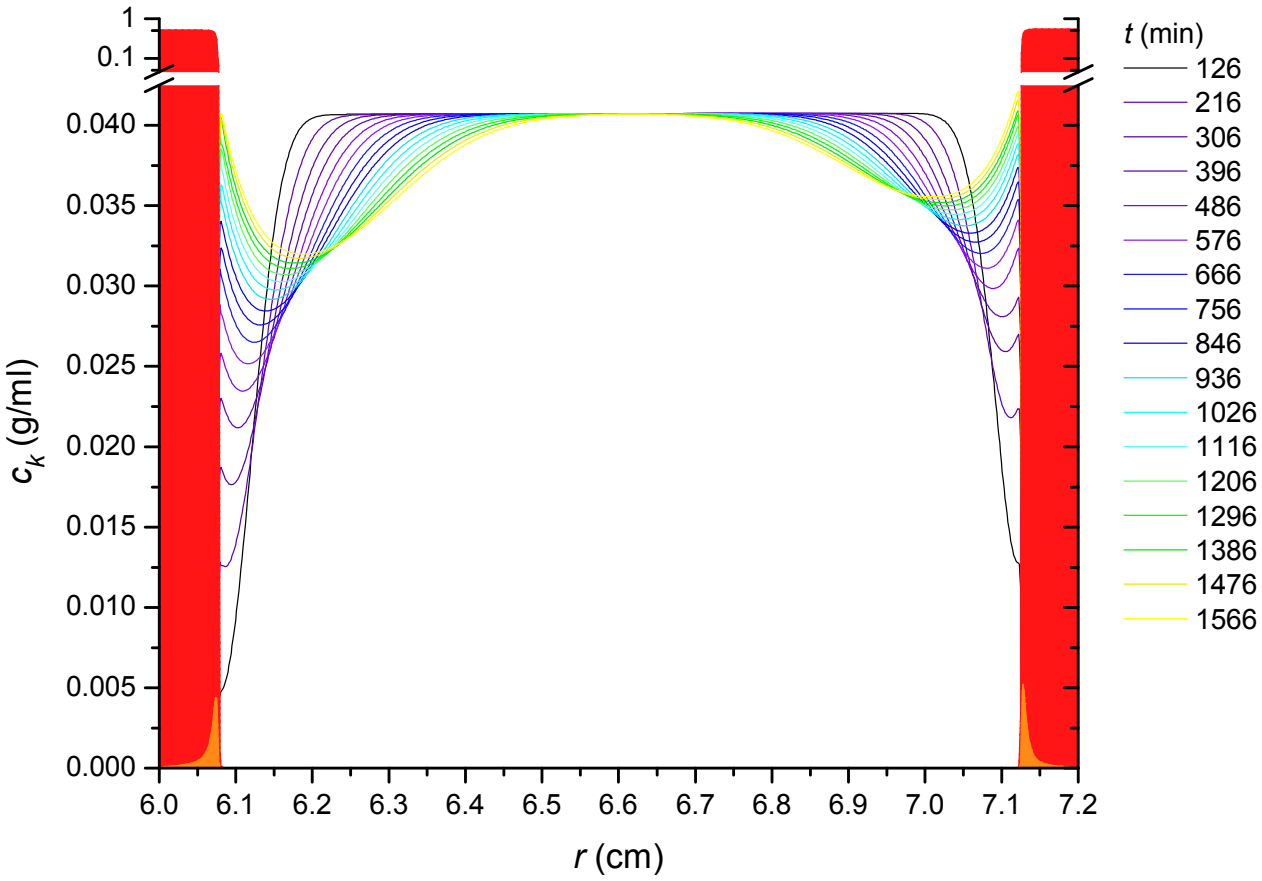

Figure 15, K_a undefined (all species are single-species components), case 0 (Table 2, $X^S_{k,q\neq k} = 0$ and $X^D_{k,q\neq k} = 0$). Concentration, c_k (g/ml), versus radial position, r (cm) during the medium-term approach to equilibrium. The various lines show the concentration of species 14 (*LH*) versus r from $t =$ 126 min to $t =$ 1566 min, in 90-min increments. The concentrations of species 1 (*H*, which forms most of the pellet) and species 27 (*L*, which forms most of the supernatant) at $t =$ 116 min are shown in solid red. The sum of the concentrations of species 2 to 13 (which form a small part of the pellet) and species 15 to 26 (which form a small part of the supernatant) at $t =$ 116 min are shown in solid orange. High concentration data in the pellet and supernatant and are shown on a logarithmic scale above the break in the c_k-axis. After $t =$ 116 min, no significant changes were seen in the concentration distribution of any species other than *LH*.

The density of species *LH* is such that it should neither sediment nor float in a solvent-*LH* system. Perturbations in the solution density by the mass transport of the other species from $t = 0$ to $t =$ 116 min (Figures 8 to 11, K_a undefined) caused species *LH* to redistribute in that period (Figure

12, K_a undefined), however. Figure 15 (for K_a undefined) shows the further re-distribution of species LH after species 1 to 13 have formed a nearly time-invariant pellet, and species 15 to 27 have formed a nearly time-invariant supernatant. As was the case prior to $t = 126$ min, the concentration of species LH is nearly zero in either the pellet or the supernatant at all times after $t = 126$ min.

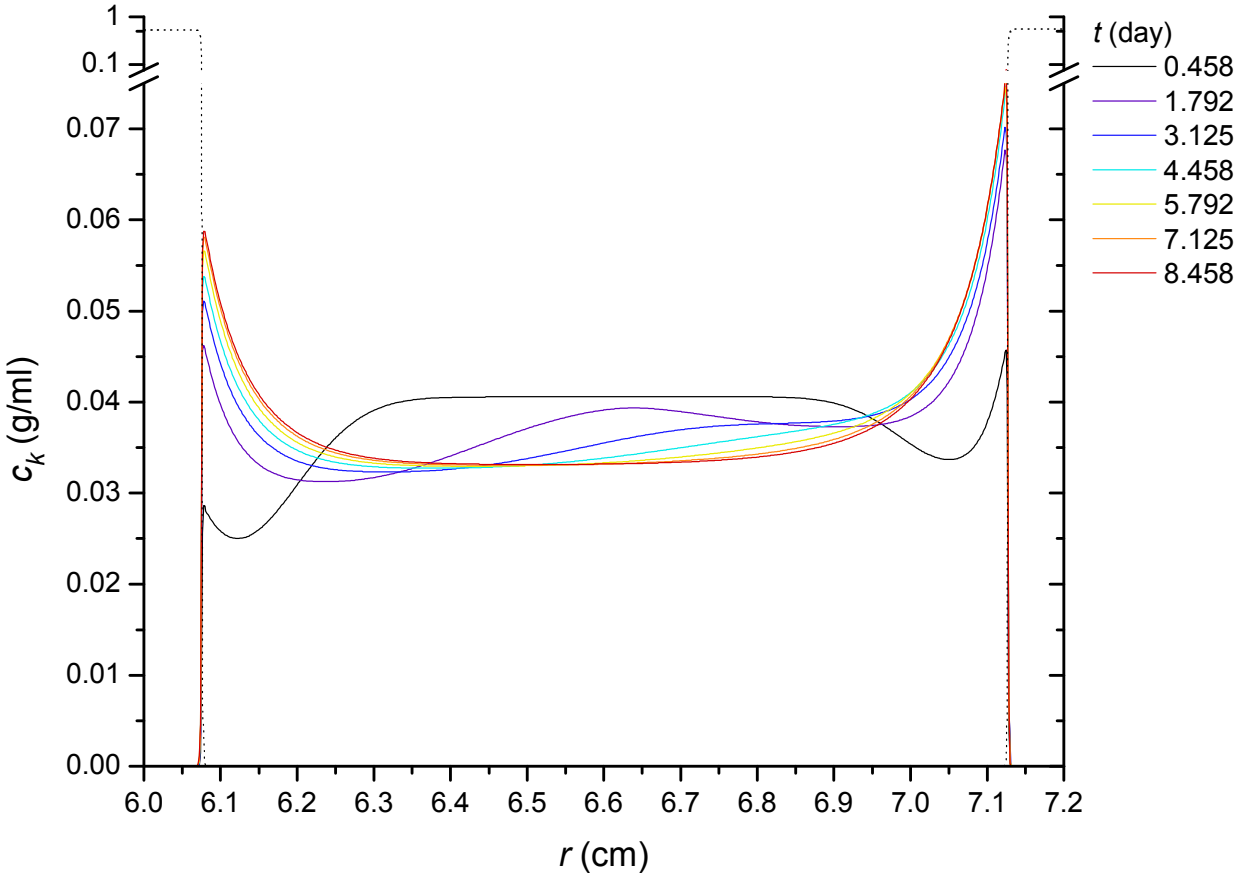

Figure 16, K_a undefined (all species are single-species components), case 0 (Table 2, $X^S_{k,q\neq k} = 0$ and $X^D_{k,q\neq k} = 0$). Concentration, c_k (g/ml), versus radial position, r (cm) during the long-term approach to equilibrium. The system differed from that of Figures 8 to 15 (for K_a undefined), in that the low-concentration species (2 to 13 and 15 to 26) were excluded. The solid lines show the concentration of species 14 (LH) versus r from $t = 0.458$ days to $t = 8.458$ days, in 1.333-day increments. The dotted black lines show the concentrations of species 1 (H, which forms the pellet) and species 27 (L, which forms the supernatant) at $t = 8.458$ days. High concentration

data in the pellet and supernatant and are shown on a logarithmic scale above the break in the c_k-axis.

As the system approaches equilibrium, the concentration of species LH does not approach a radially-independent value in the space between the supernatant and the pellet. Instead, at the boundary between the bulk of the solution occupied by species LH and either the pellet or the supernatant, the concentration of species LH rises to a peak. At either boundary, a large and steep gradient in the concentration of species LH drives mass transport of LH into the pellet or supernatant, while the solution density in either the pellet or the supernatant drives mass transport of LH out of those regions. A model that included third- and higher-order virial coefficients of the density increment, thermodynamic nonideality and viscosity might reduce or eliminate this effect, or even produce the opposite effect, wherein the concentration of LH would be lower at the supernatant and pellet boundaries than it would be toward the centre of the system.

For concentration-dependent systems, the inclusion of well-chosen third- and higher-order virial coefficients of the density increment, thermodynamic nonideality and viscosity might also reduce or eliminate the likelihood of artefacts and instabilities in regions of high concentrations, and thus obviate the need for artificially imposed limits (Equations 20 to 23) on D_k and σ_k.

AUC simulation of cases -2, -1, 1 *and* 2*, for which* $X_{k,q\neq k}^{S} \neq 0$ *and* $X_{k,q\neq k}^{D} \neq 0$

In what follows, cases 1a and 1b are referred to collectively as case 1, while cases 2a and 2b are referred to collectively as case 2. For the AUC simulation of cases -2, -1, 1 and 2 ($X_{k,q\neq k}^{S} \neq 0$ and $X_{k,q\neq k}^{D} \neq 0$) in each model system ($K_a = 30.325$ ml/g and K_a undefined), the programme was compiled and run in debugger mode using Borland C++ Builder 6.0 on a laptop PC with a 2.1 GHz CPU, 4 GB RAM and a 32-bit OS (Windows Vista). For these cases, in both model systems, the implementation can only exploit Equations 11, 10 and 17. Exploiting this set of equations increases the time taken to simulate either model system ($K_a = 30.325$ ml/g or K_a undefined), as compared to the time that would be taken if Equations 33, 34 and 35 could be used to simulate

the corresponding model system. (See *Observations regarding the two model systems in case* 0*, for which* $X^s_{k,q\neq k} = 0$ *and* $X^D_{k,q\neq k} = 0$.)

Insofar as the time increment, Δt, remained at its upper limit of $\Delta t_{max} = 3$ s throughout the course of these simulations, the simulations showed evidence of being computationally stable. In regions from which the low-concentration solutes (all solutes except species *H*, *LH* and *L*) had been substantially depleted, however, the residual concentrations of those solutes took on a somewhat oscillatory character. This was particular true of the first model system ($K_a = 30.325$ ml/g) in cases 2 and -2a (Figures 29 to 32). Such results can be viewed as evidence of a gradually developing instability, a possible source of which might be the approximated derivatives, $\frac{\Delta c_k}{\Delta \xi}$ and $\frac{\Delta c_q}{\Delta \xi}$, in Equation 11, as an examination of $\frac{\Delta c_H}{\Delta \xi}$, $\frac{\Delta c_{LH}}{\Delta \xi}$ and $\frac{\Delta c_L}{\Delta \xi}$ reveals an abundance of regions in which these functions rapidly rise and fall with ξ. Despite the low magnitude by which these functions rise and fall in such regions, it could be supposed that the effects of such regions on D_k (Equation 11) would perhaps suffice to produce the observed oscillatory patterns. Such is not the case, however. Although increasing instability is observed with increasing $\left|X^D_{k,q\neq k}\right|$, setting all $X^D_{k,q\neq k}$ to 0, or setting all $X^D_{k,q\neq k}$ to -1E-12, makes little difference to the ocillatory patterns seen in $c_{k=7}$ or $c_{k=21}$ versus r with all $X^D_{k,q\neq k}$ = -1E-10 and all $X^s_{k,q\neq k}$ = -1E-4. The persistence of such patterns with all $X^D_{k,q\neq k}$ set to 0 suggests that these patterns either reflect genuine phenomena or are $\frac{\Delta c_q}{\Delta \xi}$-independent artefacts of the method of simulation.

While the $X^D_{k,q\neq k}$ values of $\pm$1E-10 used here (Table 2) are too low to destabilise the system to a noticeable extent, they are also too low to have more than a negligible effect on D_k values, relative to the D_k values that would be calculated if all $X^D_{k,q\neq k}$ were zero. Given the sometimes jagged appearance of $\frac{\Delta c_q}{\Delta \xi}$ (Equation 11), smoothing of each $\frac{\Delta c_q}{\Delta \xi}$ as a function of ξ would seem an obvious means to try to address the extremely low limits to which $X^D_{k,q\neq k}$ must otherwise be held in the interest of system stability. Such smoothing, however, has proven to be destabilising in systems for which $X^D_{k,q\neq k} = X^s_{k,q\neq k} = \pm$1E-4. Smoothing of D_k as a function of ξ has proven itself to be even more destabilising in such systems.

As the $X^D_{k,q\neq k}$ values of $\pm$1E-10 used here have only a minor effect on D_k values, it is the $X^s_{k,q\neq k}$ values of $\pm$1E-4 (Table 2) that account for most of the differences between the results for case 0

and the results for cases -2, -1, 1a and 2a (Table 2), regardless of the model system involved (K_a = 30.325 ml/g or K_a undefined). The minor effects of $X_{k,q\neq k}^D = \pm$1E-10 also render the results for cases -1 and 1a, in which $X_{k,q\neq k}^S$ = 1E-4, nearly identical. The minor effects of $X_{k,q\neq k}^D = \pm$1E-10 likewise render the results for cases -2 and 2a, in which $X_{k,q\neq k}^S$ = -1E-4, nearly identical. Furthermore, the effects of $X_{k,q\neq k}^S = \pm$1E-4 on the transport of the high-concentration species, *H*, *LH* and *L*, are practically inperceptable. That is so because, in Equation 10 or 17, for $k = 1$ (species *H*), $k = 14$ (species *LH*) or $k = 27$ (species *L*), the product of $\frac{c_k}{M_k}\sigma_k^0 D_k^0$ and $X_{k,k}^S = 1$ (Table 2) exceeds the sum of all products of $\frac{c_{q\neq k}}{M_{q\neq k}}\sigma_{q\neq k}^0 D_{q\neq k}^0$ and $X_{k,q\neq k}^S = \pm$1E-4 (Table 2) by an overwhelming amount, except in regions where c_k approaches zero and $c_{q\neq k}$ is high. In contrast, for each low-concentration species ($1 < k < 14$ or $14 < k < 27$), the product of $\frac{c_k}{M_k}\sigma_k^0 D_k^0$ and $X_{k,k}^S = 1$ usually exceeds the sum of all products of $\frac{c_{q\neq k}}{M_{q\neq k}}\sigma_{q\neq k}^0 D_{q\neq k}^0$ and $X_{k,q\neq k}^S = \pm$1E-4, but the latter sum of products often makes a significant contribution to σ_k. (As shown in Table 1, on average, each high-concentration species is present at approximately 792 times the concentration of each low-concentration species.)

Given the nearly imperceptible effects of both $X_{k,q\neq k}^D = \pm$1E-10 and $X_{k,q\neq k}^S = \pm$1E-4 on the transport of the high-concentration species (*H*, *LH* and *L*), Figures 3 to 5 suffice to show c_k versus r for these species in the first model system (K_a = 30.325 ml/g) for all cases (-2, -1, 1a and 2a) in which $\left|X_{k,q\neq k}^D\right| \leq$ 1E-10, and Figures 10 to 12 suffice to show c_k versus r for these species in the second model system (K_a undefined) for all cases (-2, -1, 1a and 2a) in which $\left|X_{k,q\neq k}^D\right| \leq$ 1E-10. (With respect to the high-concentration species, cases 1b and 2b show subtle differences from case 0 for K_a = 30.325 ml/g, but not for K_a undefined. See *The concentration gradients of H*, *L* and *LH for* K_a = 30.325 ml/g *and cases 1b and 2b*.) Given the nearly imperceptible effect of $X_{k,q\neq k}^D = \pm$1E-10 in general, the results from case -1 are nearly identical to the results from case 1a, and the results from case -2 are nearly identical to the results from case 2a. Thus, with respect to c_k versus r for species 7 and 21, only the results for cases -1 and -2 are shown below.

As will be shown later (*Results for case* 1b*, in which* $X_{k,q\neq k}^D = X_{k,q\neq k}^S$ = 1E-4*, and case* 2b*, in which* $X_{k,q\neq k}^D = X_{k,q\neq k}^S$ = -1E-4), the results for case 1b are similar to those for case 1a, and the results for case 2b are similar to those for case 2a. Other than raising the level of apparent instability,

setting $X^D_{k,q\neq k}$ to $\pm$1E-4 merely produces subtle effects by which the results can be distinguished from those seen when $X^D_{k,q\neq k}$ is set to $\pm$1E-10. Thus, the coupled-flow effects mediated by s_k (Equation 27) appear to be much more pronounced than those mediated by D_k (Equation 31), at least for the systems examined here. Where there is concern about the level of instabilty seen when $X^D_{k,q\neq k} = X^S_{k,q\neq k}$, that instability can be reduced by decreasing the time increment, Δt, and the spatial increment, $\Delta\xi$. (Figures 51 to 56 show comparison data obtained with decreased Δt and $\Delta\xi$ for case 1b, in which $K_a = 30.325$ ml/g and $X^D_{k,q\neq k} = X^S_{k,q\neq k} =$ 1E-4.)

Results for case 1a*, in which* $X^S_{k,q\neq k} =$ 1E-4 *and* $X^D_{k,q\neq k} =$ 1E-10*, and case* -1*, in which* $X^S_{k,q\neq k} =$ 1E-4 *and* $X^D_{k,q\neq k} =$ -1E-10

The results of AUC simulations for the two model systems ($K_a = 30.325$ ml/g and K_a undefined) are shown below for case 1a, in which $X^S_{k,q\neq k} =$ 1E-4 and $X^D_{k,q\neq k} =$ 1E-10, and case -1, in which $X^S_{k,q\neq k} =$ 1E-4 and $X^D_{k,q\neq k} =$ -1E-10.

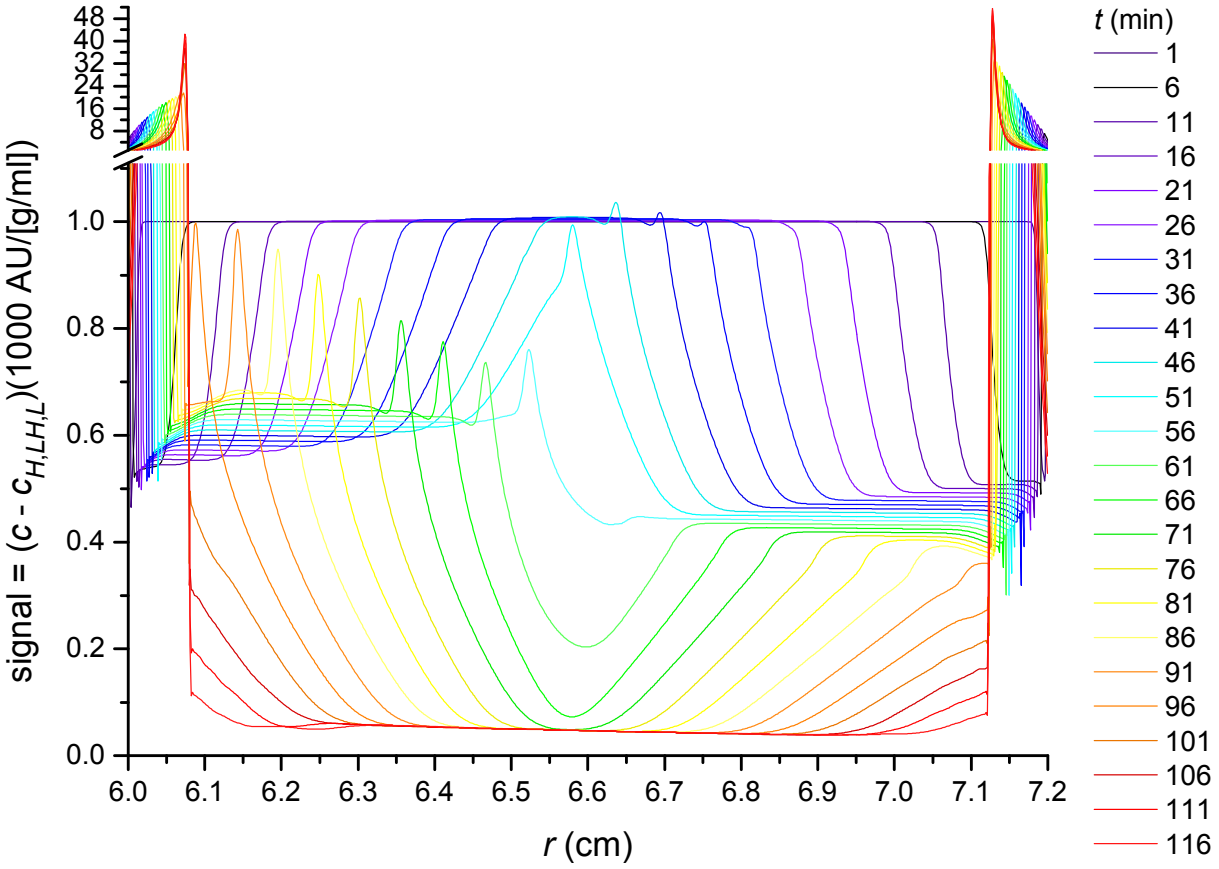

Figure 17, K_a undefined, case 1a (Table 2, $X^s_{k,q\neq k}$ = 1E-4 and $X^D_{k,q\neq k}$ = 1E-10). (Compare with Figure 8.) The sum of the signals from all species except species 1 (H), 14 (LH) and 27 (L), given by (c - $c_{H,LH,L}$)(1000 AU/[g/ml]), versus r (cm) for 1 min ≤ t ≤ 116 min.

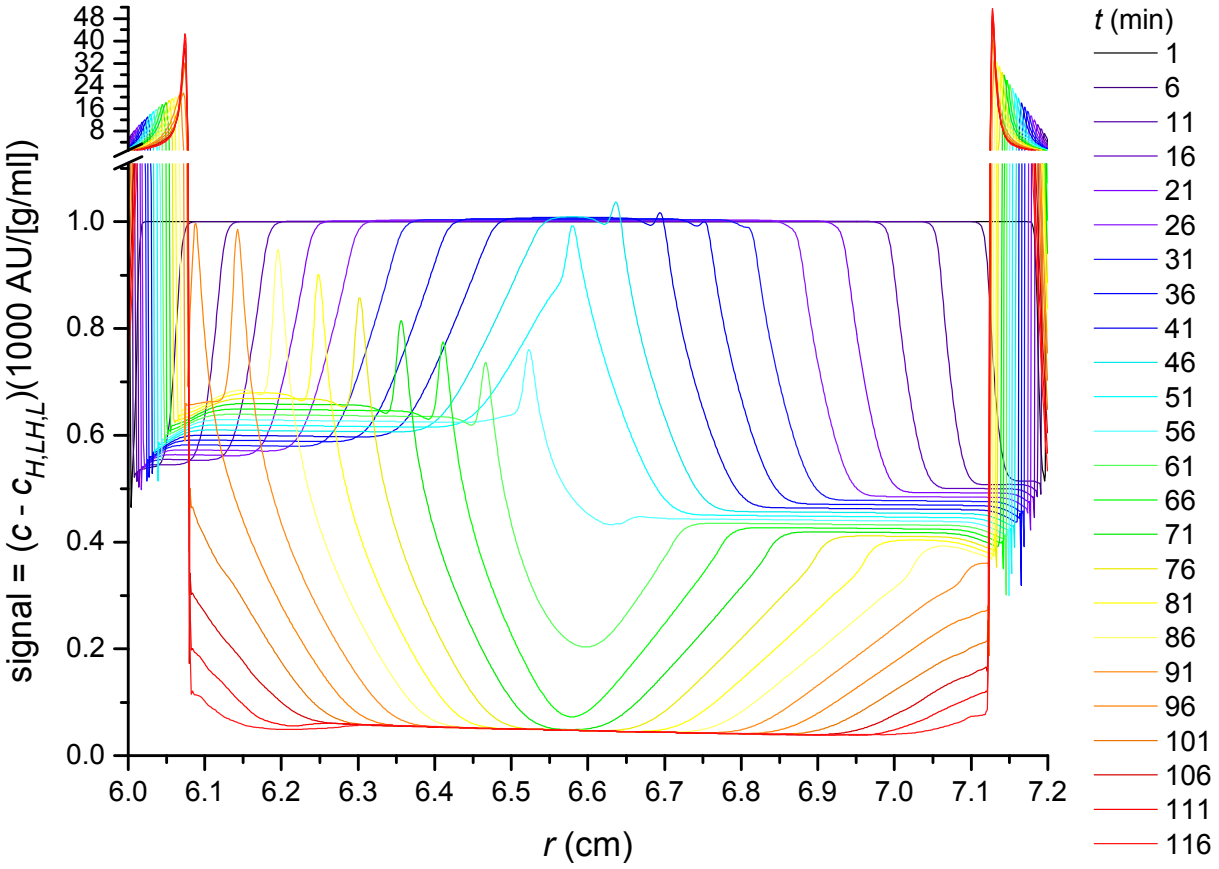

Figure 18, K_a undefined, case -1 (Table 2, $X^s_{k,q\neq k}$ = 1E-4 and $X^D_{k,q\neq k}$ = -1E-10). (Compare with Figure 8.) The sum of the signals from all species except species 1 (*H*), 14 (*LH*) and 27 (*L*), given by (c - $c_{H,LH,L}$)(1000 AU/[g/ml]), versus r (cm) for 1 min ≤ t ≤ 116 min.

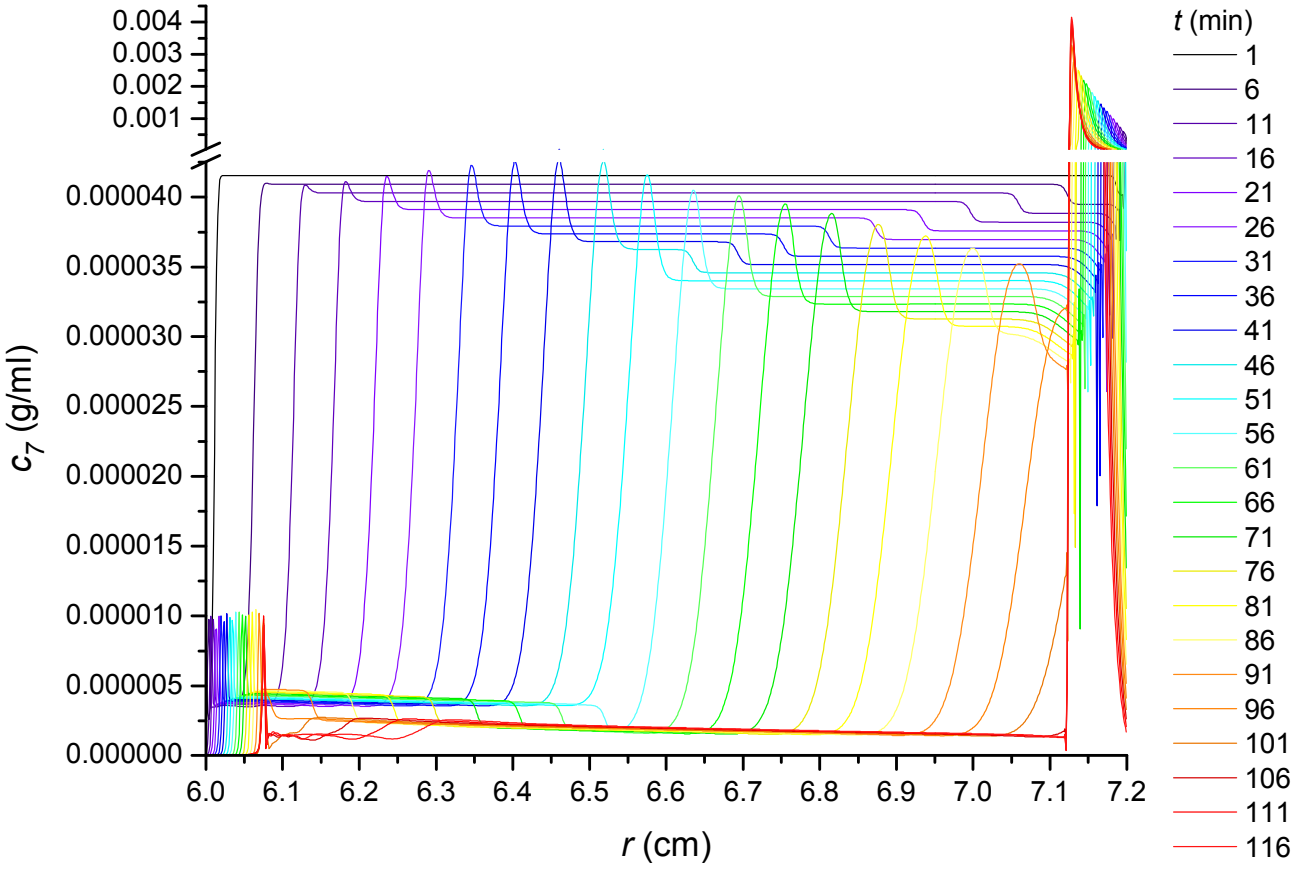

Figure 19, K_a undefined, case -1 (Table 2, $X^s_{k,q\neq k}$ = 1E-4 and $X^D_{k,q\neq k}$ = -1E-10). (Compare with Figure 13.) The concentration of species 7, c_7 (g/ml), versus r (cm) for 1 min ≤ t ≤ 116 min.

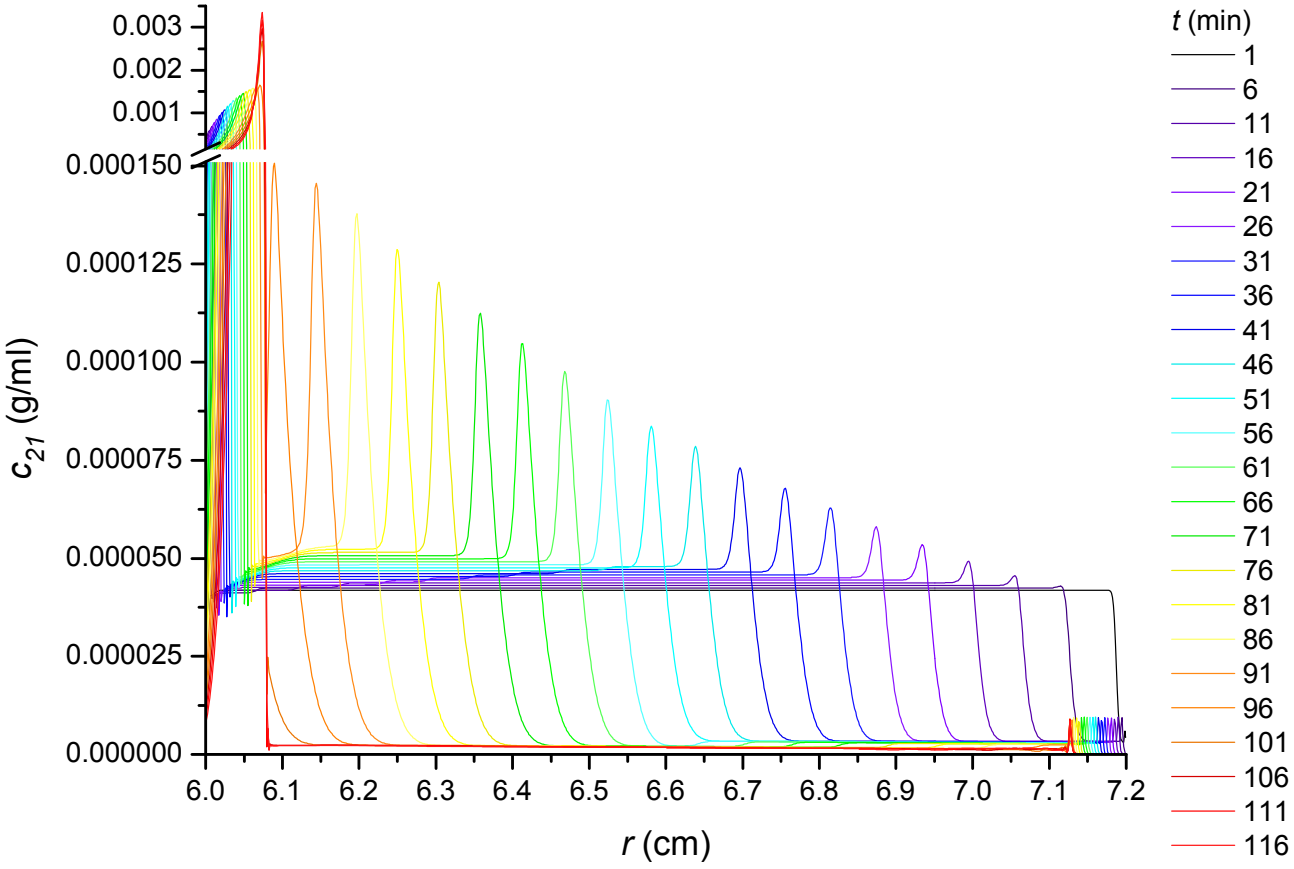

Figure 20, K_a undefined, case -1 (Table 2, $X^s_{k,q\neq k}$ = 1E-4 and $X^D_{k,q\neq k}$ = -1E-10). (Compare with Figure 14.) The concentration of species 21, c_{21} (g/ml), versus r (cm) for 1 min ≤ t ≤ 116 min.

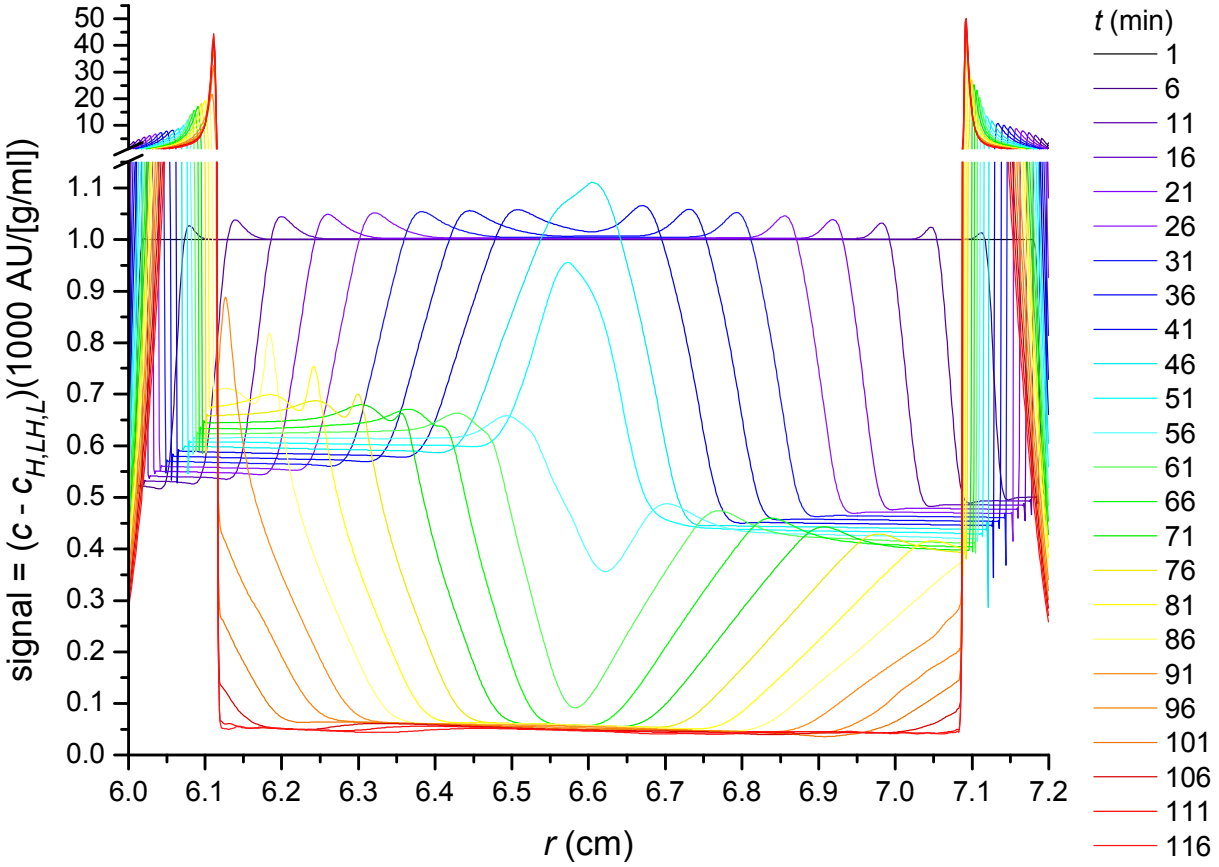

Figure 21, $K_a = 30.325$ ml/g, case 1a (Table 2, $X^s_{k,q\neq k} =$ 1E-4 and $X^D_{k,q\neq k} =$ 1E-10). (Compare with Figure 1.) The sum of the signals from all species except species 1 (H), 14 (LH) and 27 (L), given by $(c - c_{H,LH,L})$(1000 AU/[g/ml]), versus r (cm) for 1 min $\leq t \leq$ 116 min.

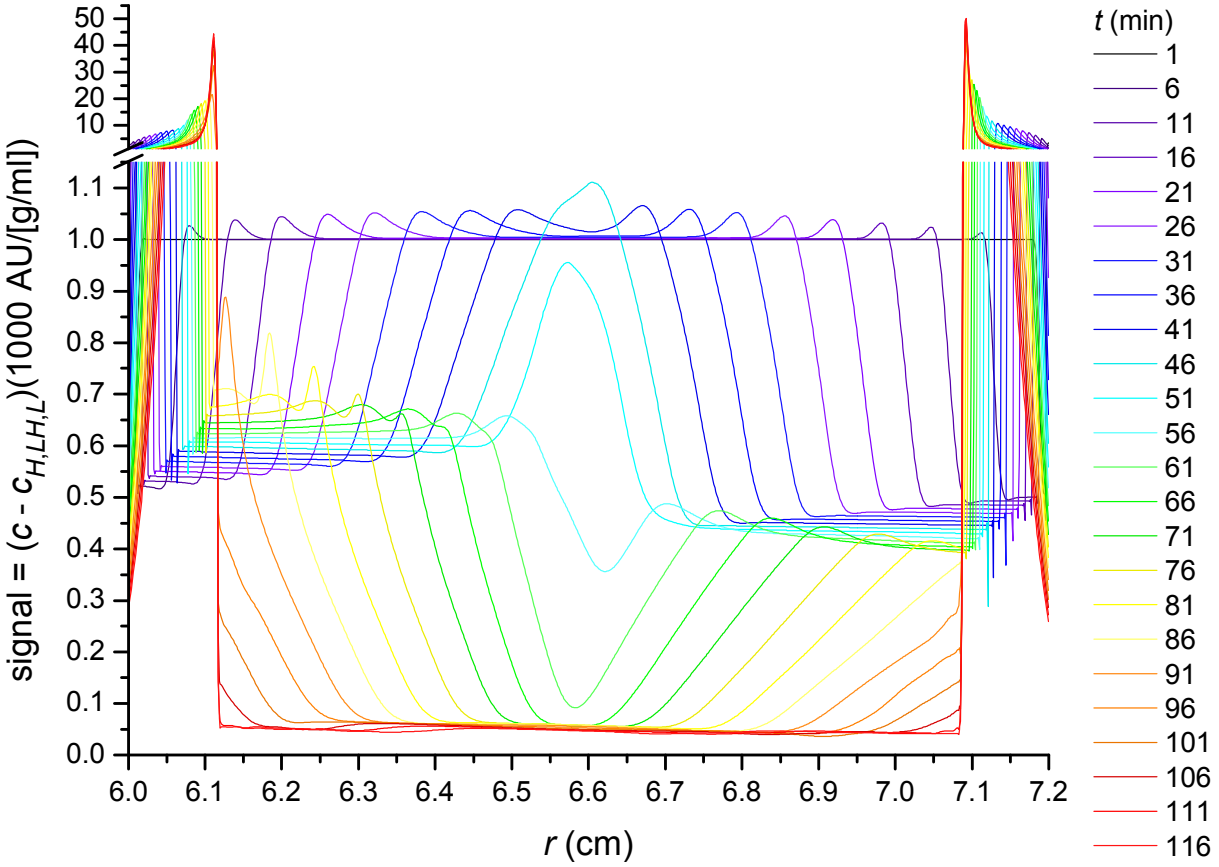

Figure 22, $K_a = 30.325$ ml/g, case -1 (Table 2, $X^s_{k,q\neq k}$ = 1E-4 and $X^D_{k,q\neq k}$ = -1E-10). (Compare with Figure 1.) The sum of the signals from all species except species 1 (H), 14 (LH) and 27 (L), given by $(c - c_{H,LH,L})$(1000 AU/[g/ml]), versus r (cm) for 1 min $\leq t \leq$ 116 min.

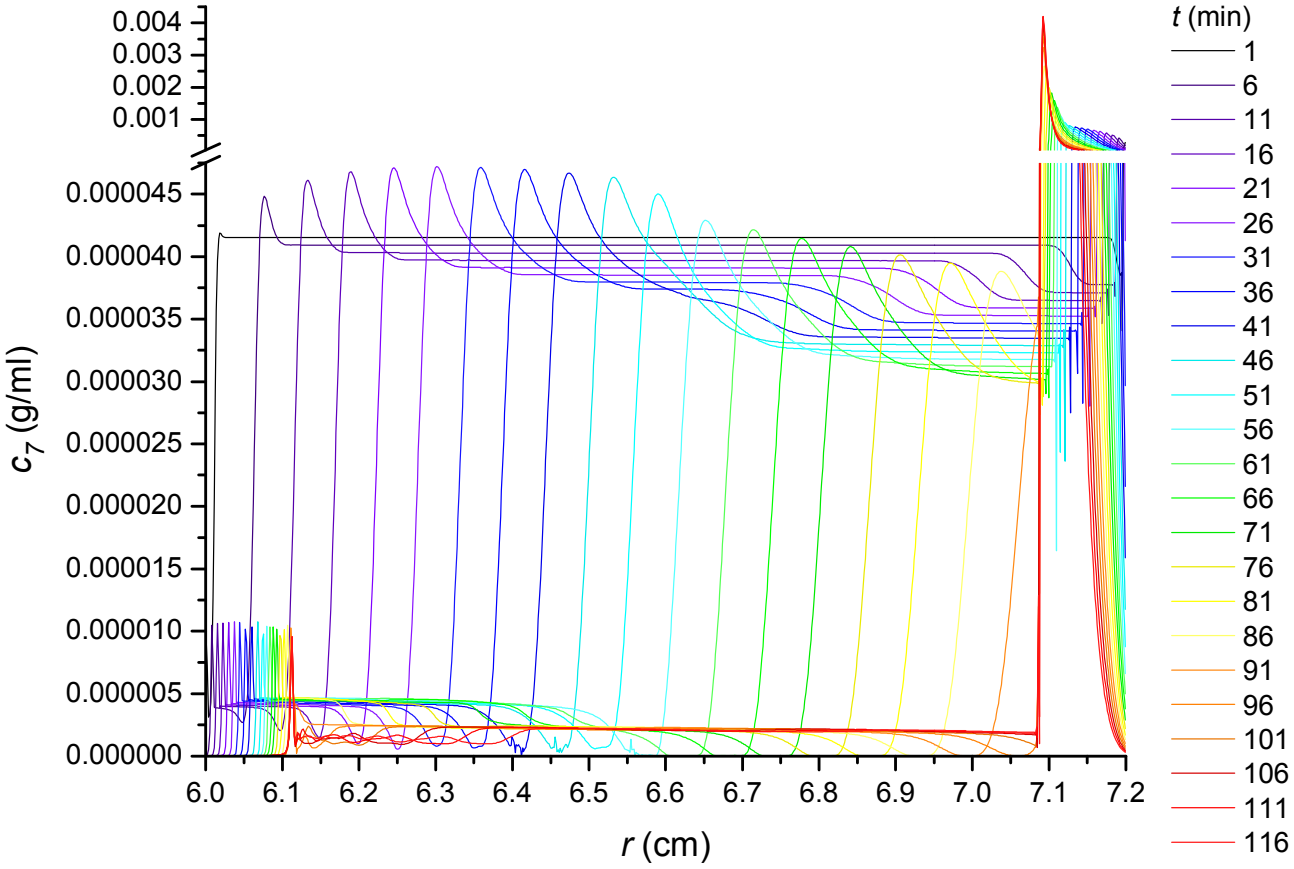

Figure 23, $K_a = 30.325$ ml/g, case -1 (Table 2, $X^S_{k,q\neq k}$ = 1E-4 and $X^D_{k,q\neq k}$ = -1E-10). (Compare with Figure 6.) The concentration of species 7, c_7 (g/ml), versus r (cm) for 1 min $\leq t \leq$ 116 min.

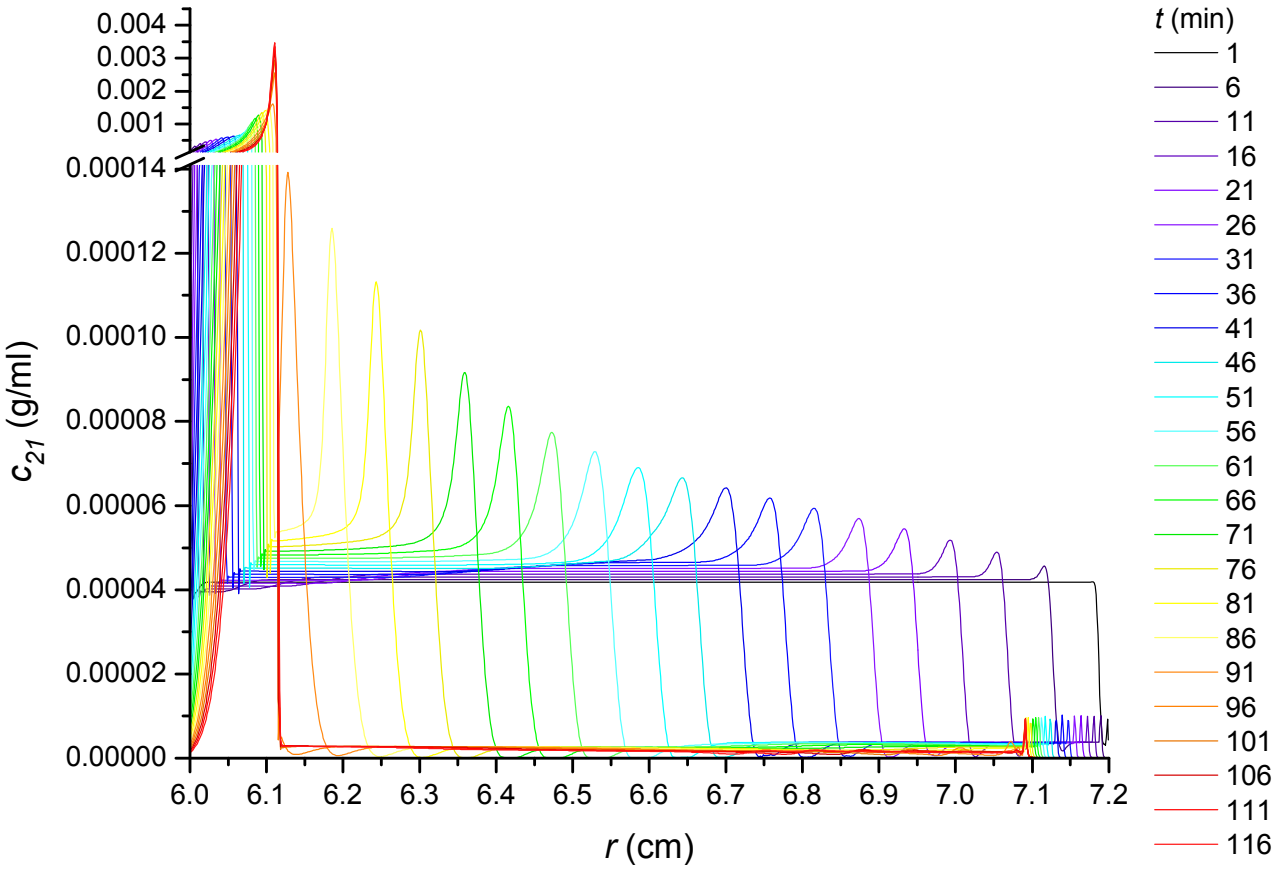

Figure 24, $K_a = 30.325$ ml/g, case -1 (Table 2, $X^s_{k,q\neq k}$ = 1E-4 and $X^D_{k,q\neq k}$ = -1E-10). (Compare with Figure 7.) The concentration of species 21, c_{21} (g/ml), versus r (cm) for 1 min $\leq t \leq$ 116 min.

Results for case 2a, *in which* $X^s_{k,q\neq k}$ = -1E-4 *and* $X^D_{k,q\neq k}$ = -1E-10, *and case* -2, *in which* $X^s_{k,q\neq k}$ = -1E-4 *and* $X^D_{k,q\neq k}$ = 1E-10

The results of AUC simulations for the two model systems ($K_a = 30.325$ ml/g and K_a undefined) are shown below for case 2a, in which $X^s_{k,q\neq k}$ = -1E-4 and $X^D_{k,q\neq k}$ = -1E-10, and case -2, in which $X^s_{k,q\neq k}$ = -1E-4 and $X^D_{k,q\neq k}$ = 1E-10.

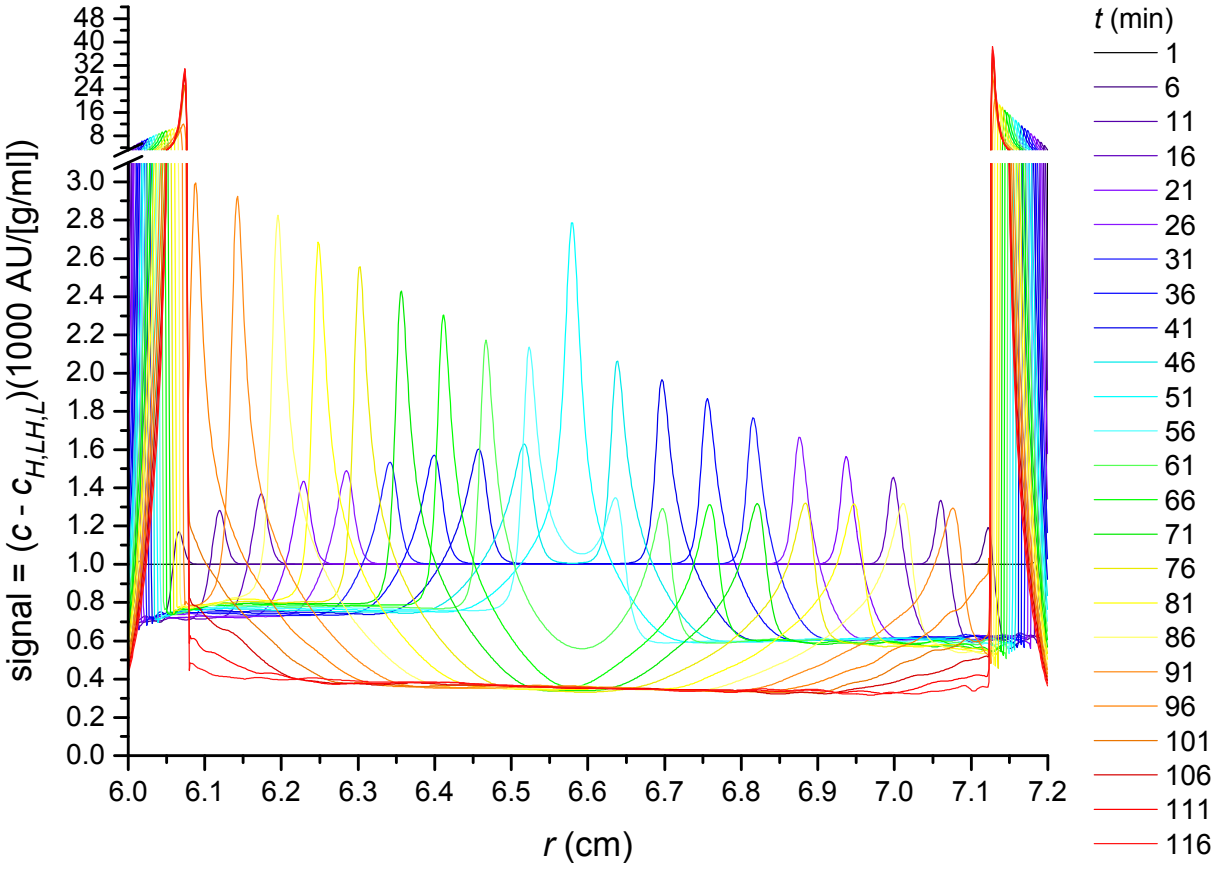

Figure 25, K_a undefined, case 2a (Table 2, $X^s_{k,q\neq k}$ = -1E-4 and $X^D_{k,q\neq k}$ = -1E-10). (Compare with Figure 8.) The sum of the signals from all species except species 1 (*H*), 14 (*LH*) and 27 (*L*), given by (c - $c_{H,LH,L}$)(1000 AU/[g/ml]), versus r (cm) for 1 min ≤ t ≤ 116 min.

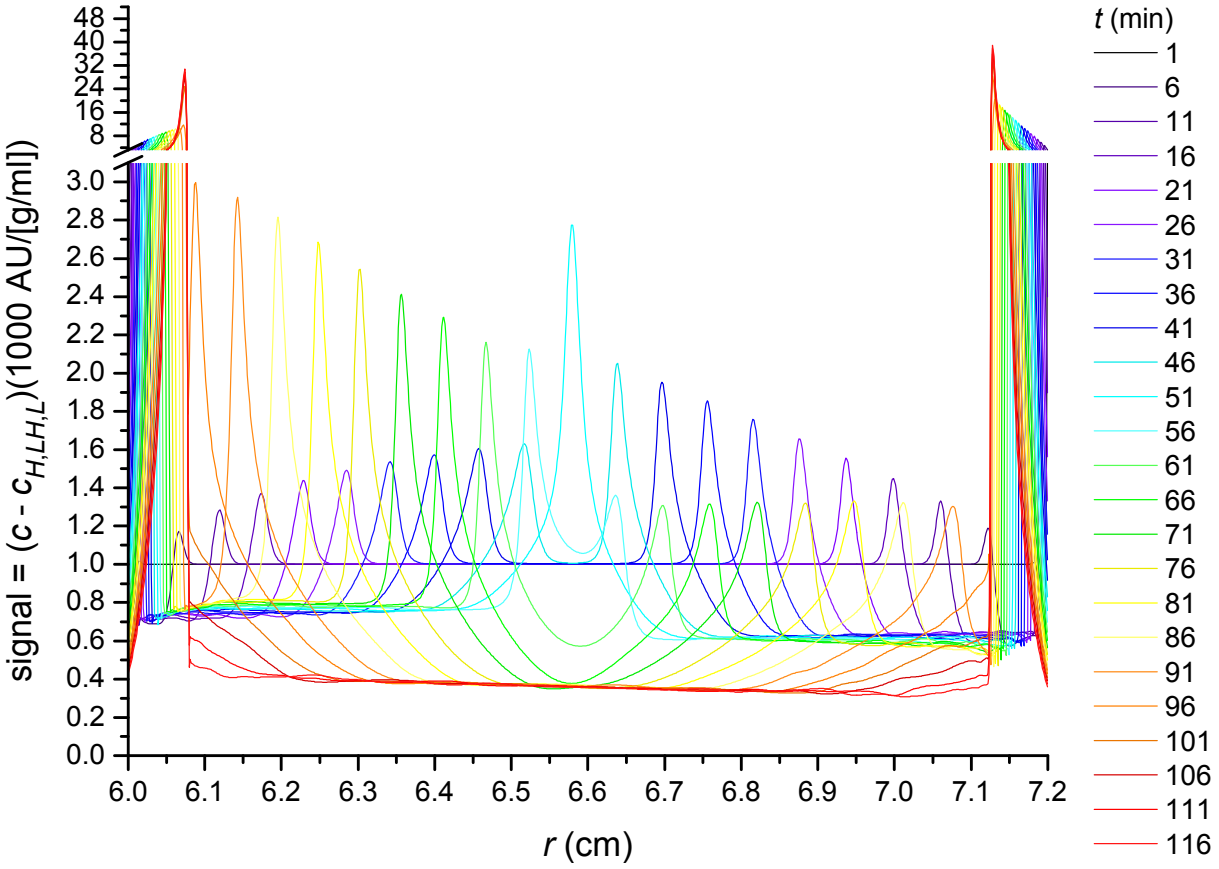

Figure 26, K_a undefined, case -2 (Table 2, $X^s_{k,q\neq k}$ = -1E-4 and $X^D_{k,q\neq k}$ = 1E-10). (Compare with Figure 8.) The sum of the signals from all species except species 1 (*H*), 14 (*LH*) and 27 (*L*), given by (c - $c_{H,LH,L}$)(1000 AU/[g/ml]), versus r (cm) for 1 min ≤ t ≤ 116 min.

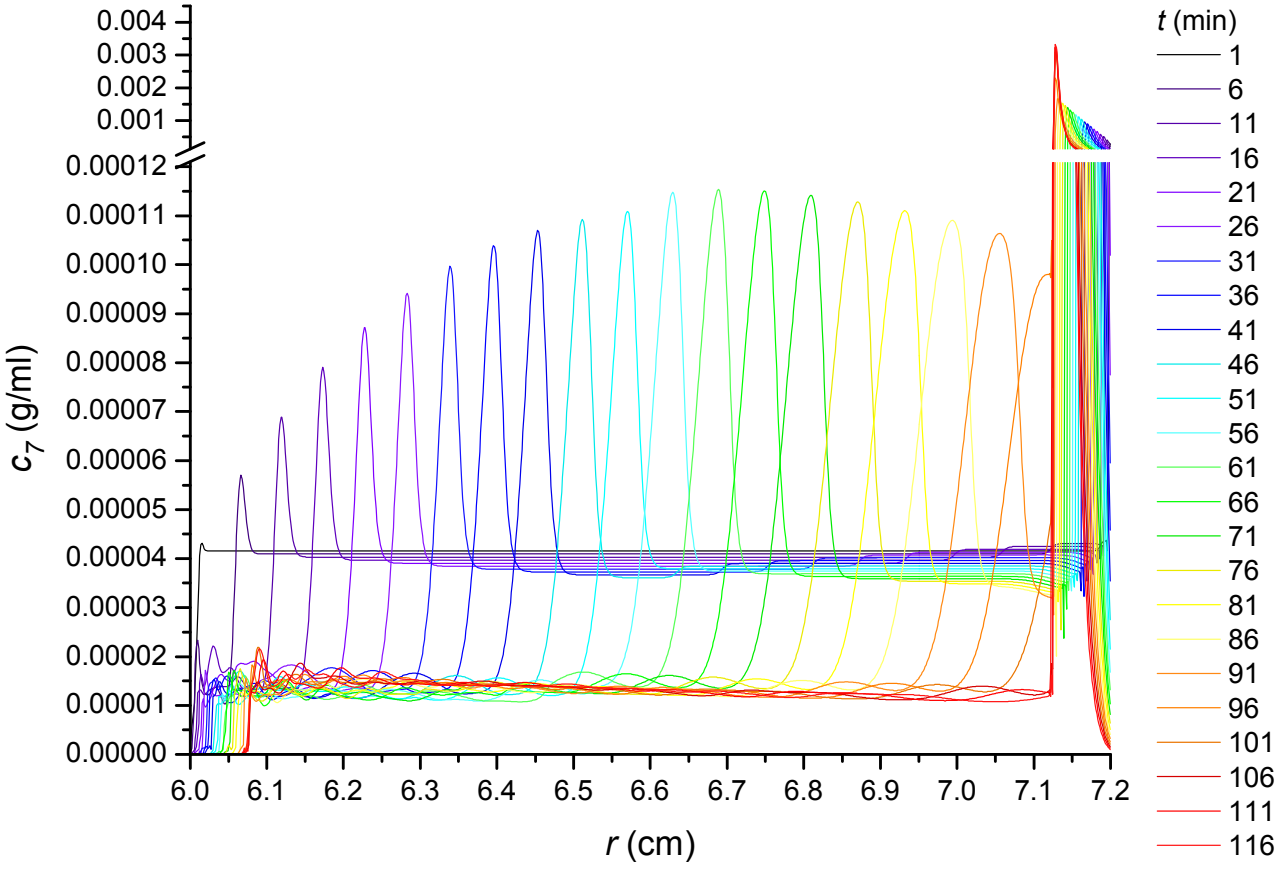

Figure 27, K_a undefined, case -2 (Table 2, $X^s_{k,q\neq k}$ = -1E-4 and $X^D_{k,q\neq k}$ = 1E-10). (Compare with Figure 13.) The concentration of species 7, c_7 (g/ml), versus r (cm) for 1 min ≤ t ≤ 116 min.

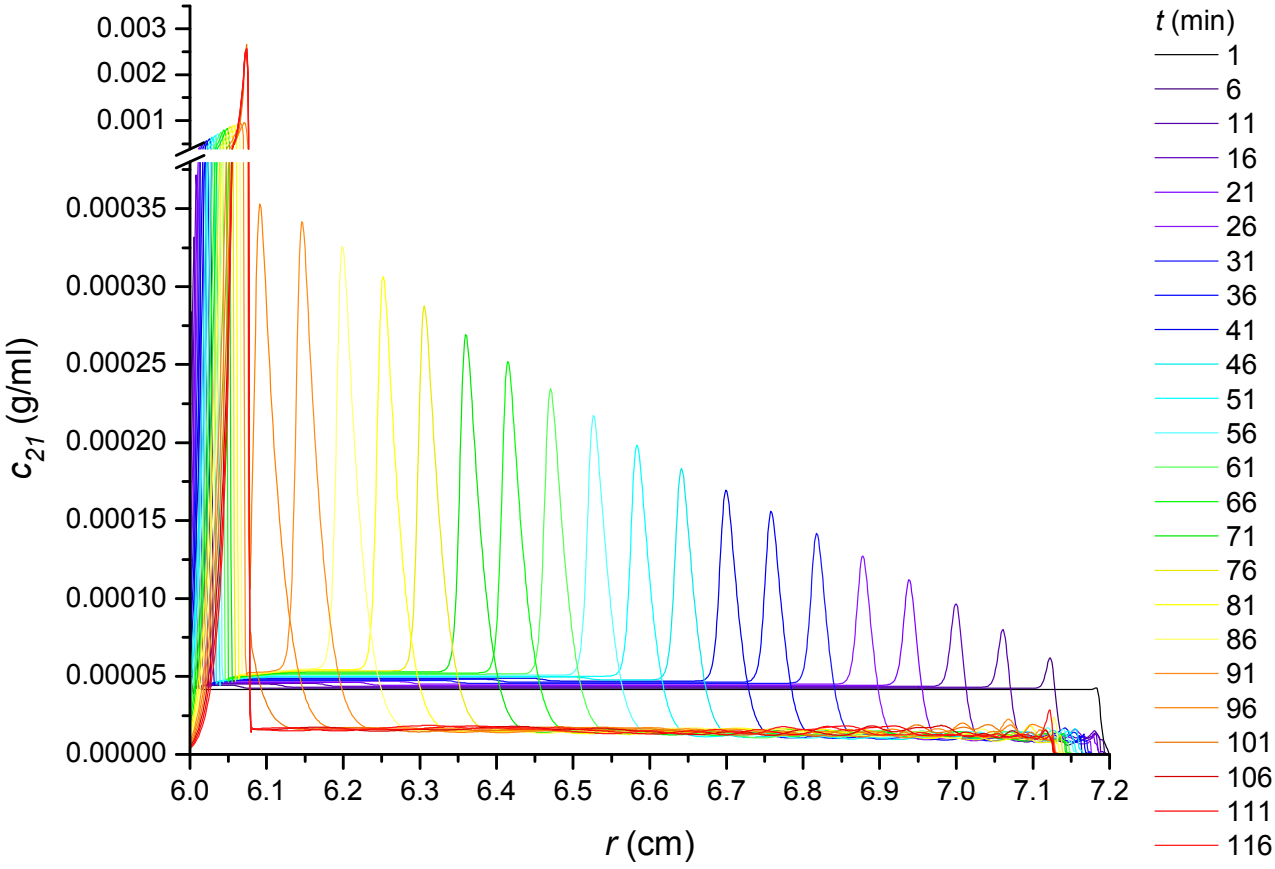

Figure 28, K_a undefined, case -2 (Table 2, $X^s_{k,q\neq k}$ = -1E-4 and $X^D_{k,q\neq k}$ = 1E-10). (Compare with Figure 14.) The concentration of species 21, c_{21} (g/ml), versus r (cm) for 1 min $\leq t \leq$ 116 min.

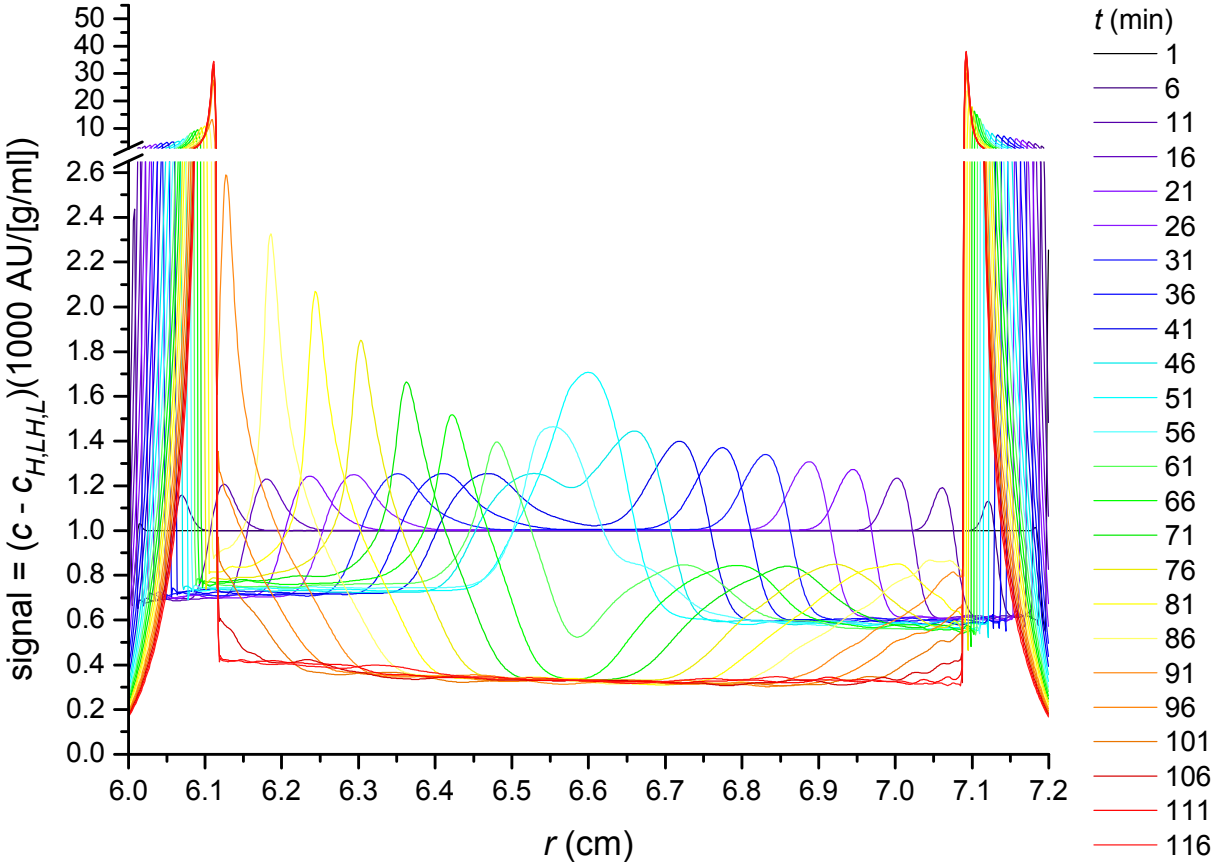

Figure 29, $K_a = 30.325$ ml/g, case 2a (Table 2, $X^s_{k,q\neq k}$ = -1E-4 and $X^D_{k,q\neq k}$ = -1E-10). (Compare with Figure 1.) The sum of the signals from all species except species 1 (H), 14 (LH) and 27 (L), given by (c - $c_{H,LH,L}$)(1000 AU/[g/ml]), versus r (cm) for 1 min ≤ t ≤ 116 min.

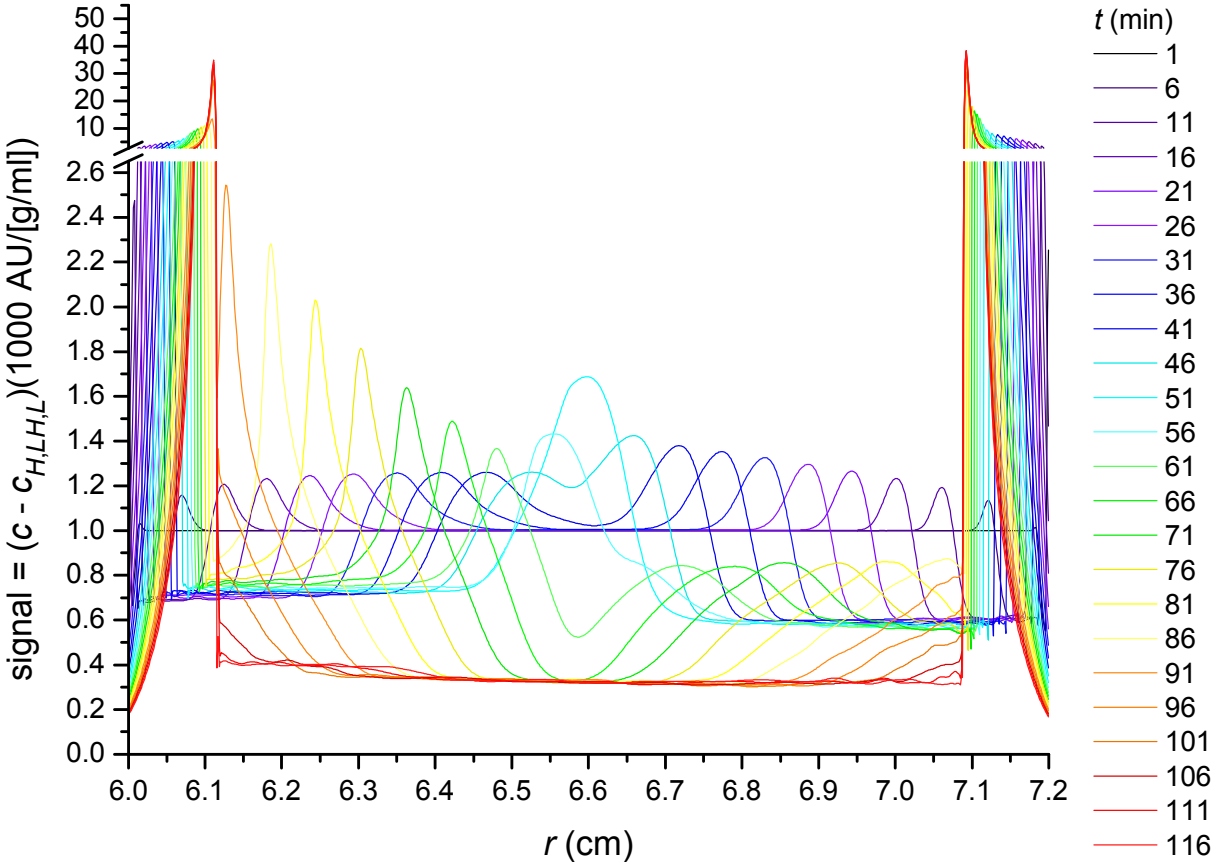

Figure 30, $K_a = 30.325$ ml/g, case -2 (Table 2, $X^s_{k,q\neq k}$ = -1E-4 and $X^D_{k,q\neq k}$ = 1E-10). (Compare with Figure 1.) The sum of the signals from all species except species 1 (H), 14 (LH) and 27 (L), given by $(c - c_{H,LH,L})$(1000 AU/[g/ml]), versus r (cm) for 1 min $\leq t \leq$ 116 min.

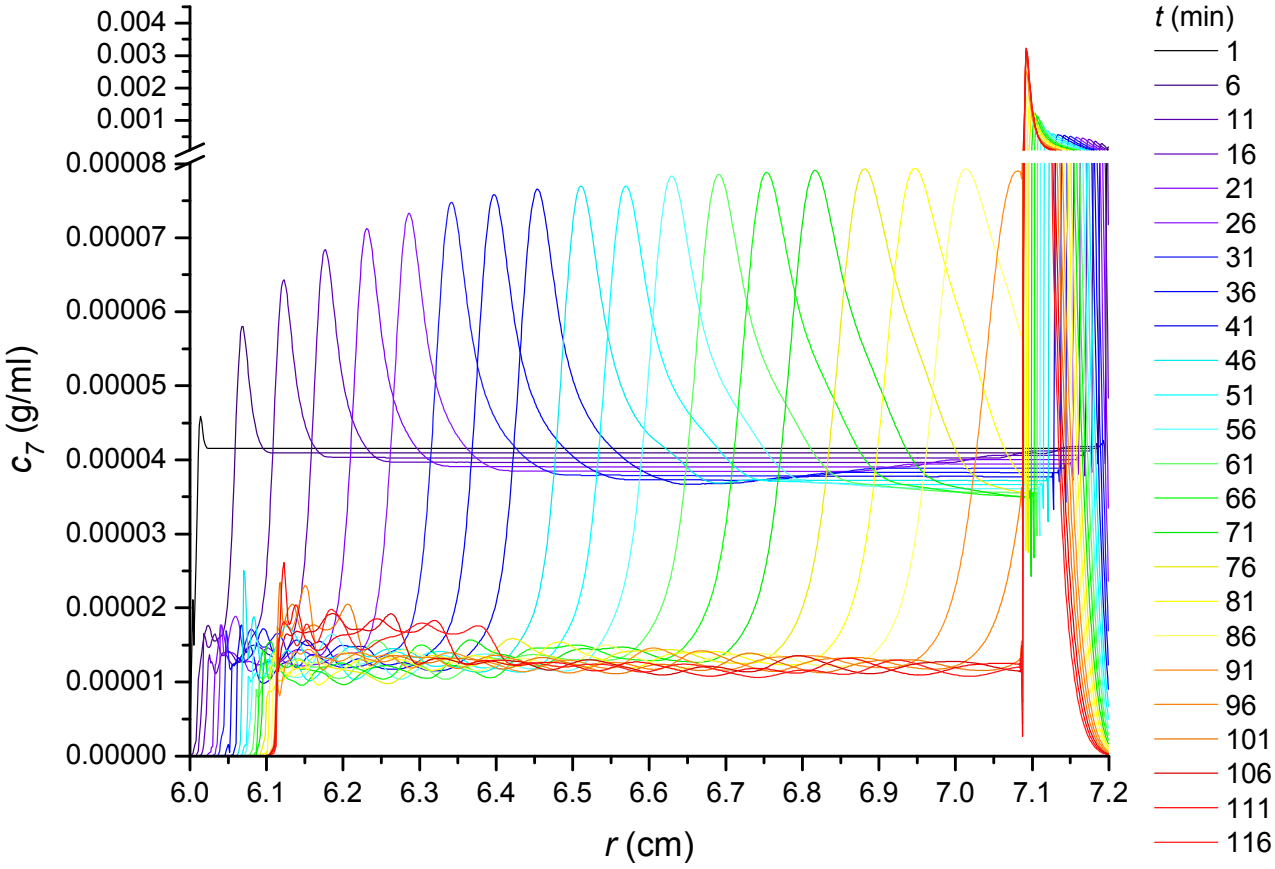

Figure 31, $K_a = 30.325$ ml/g, case -2 (Table 2, $X^S_{k,q\neq k}$ = -1E-4 and $X^D_{k,q\neq k}$ = 1E-10). (Compare with Figure 6.) The concentration of species 7, c_7 (g/ml), versus r (cm) for 1 min $\leq t \leq$ 116 min.

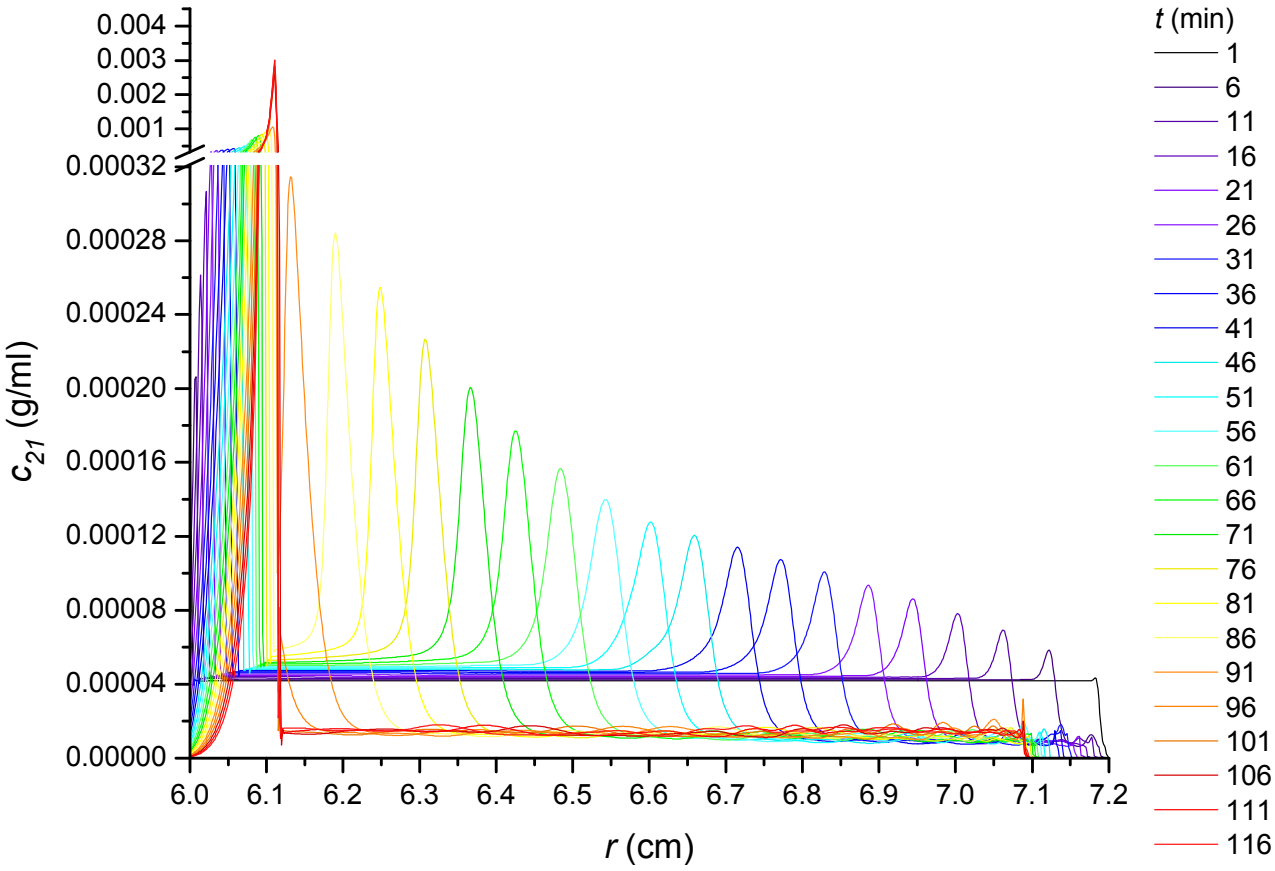

Figure 32, $K_a = 30.325$ ml/g, case -2 (Table 2, $X^s_{k,q\neq k}$ = -1E-4 and $X^D_{k,q\neq k}$ = 1E-10). (Compare with Figure 7.) The concentration of species 21, c_{21} (g/ml), versus r (cm) for 1 min $\leq t \leq$ 116 min.

Results for case 1b, *in which* $X^D_{k,q\neq k} = X^s_{k,q\neq k}$ = 1E-4, *and case* 2b, *in which* $X^D_{k,q\neq k} = X^s_{k,q\neq k}$ = -1E-4

The results of AUC simulations for the two model systems ($K_a = 30.325$ ml/g and K_a undefined) are shown below for case 1b, in which $X^D_{k,q\neq k} = X^s_{k,q\neq k}$ = 1E-4, and case 2b, in which $X^D_{k,q\neq k} = X^s_{k,q\neq k}$ = -1E-4.

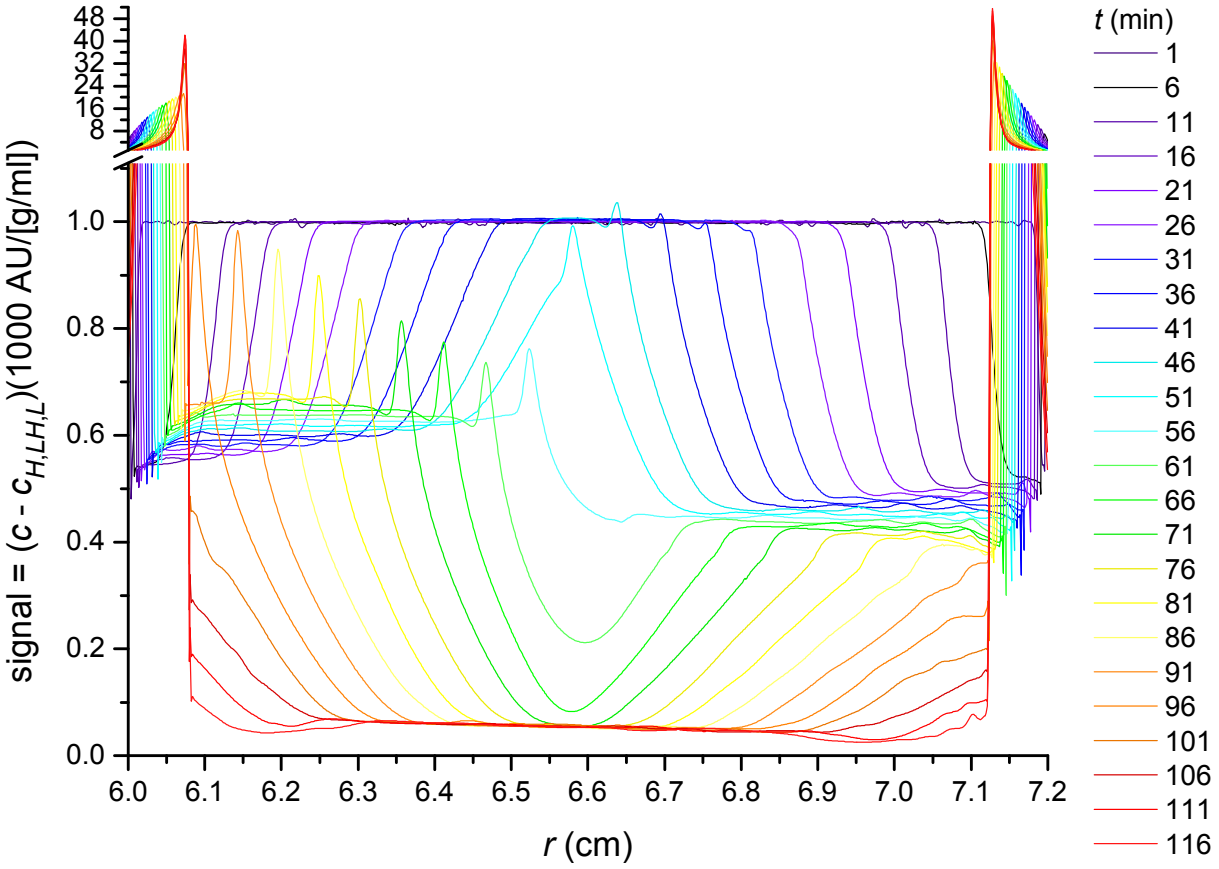

Figure 33, K_a undefined, case 1b (Table 2, $X^D_{k,q\neq k} = X^s_{k,q\neq k} =$ 1E-4). (Compare with Figures 8, 17 and 18.) The sum of the signals from all species except species 1 (*H*), 14 (*LH*) and 27 (*L*), given by (c - $c_{H,LH,L}$)(1000 AU/[g/ml]), versus r (cm) for 1 min $\leq t \leq$ 116 min.

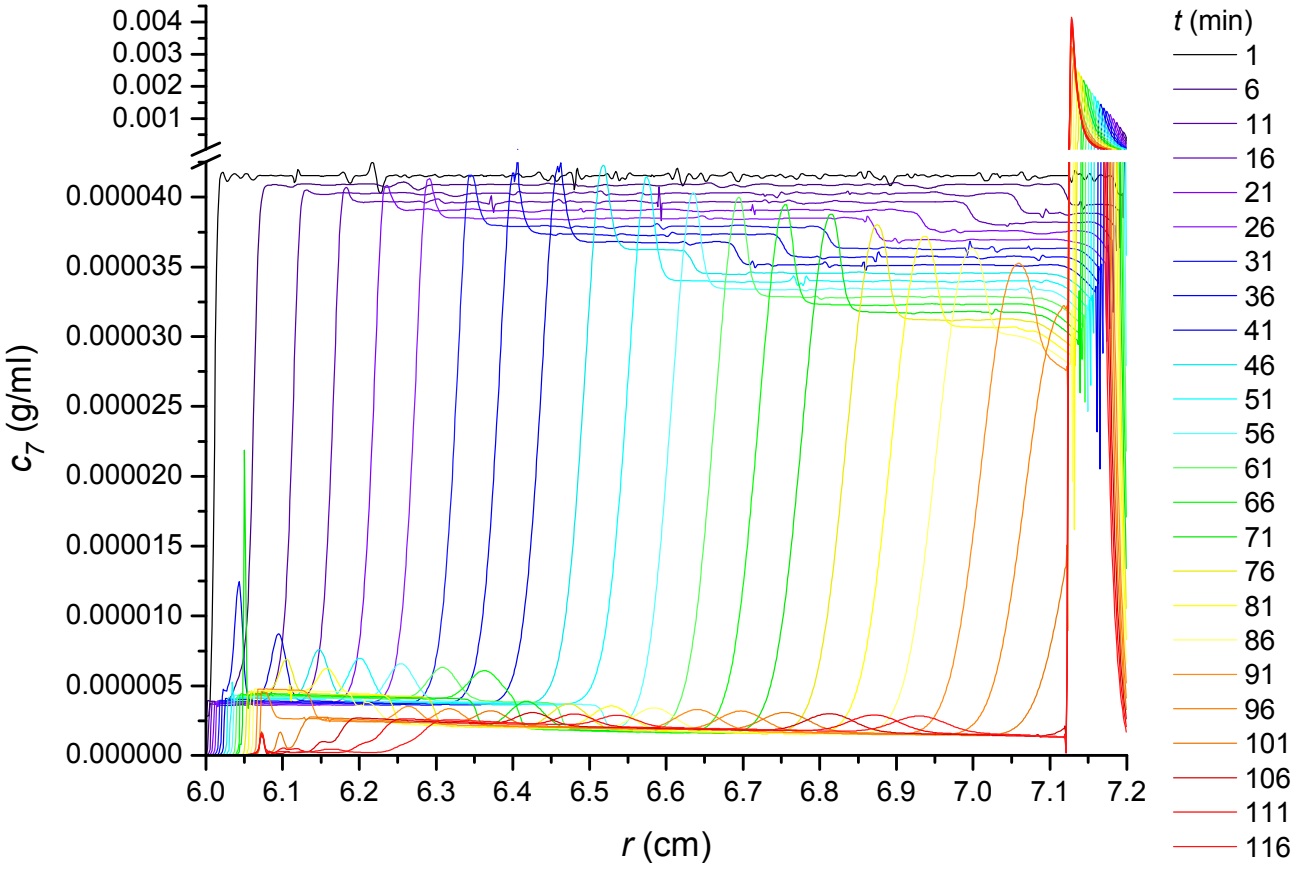

Figure 34, K_a undefined, case 1b (Table 2, $X^D_{k,q\neq k} = X^S_{k,q\neq k} =$ 1E-4). (Compare with Figures 13 and 19.) The concentration of species 7, c_7 (g/ml), versus r (cm) for 1 min $\leq t \leq$ 116 min.

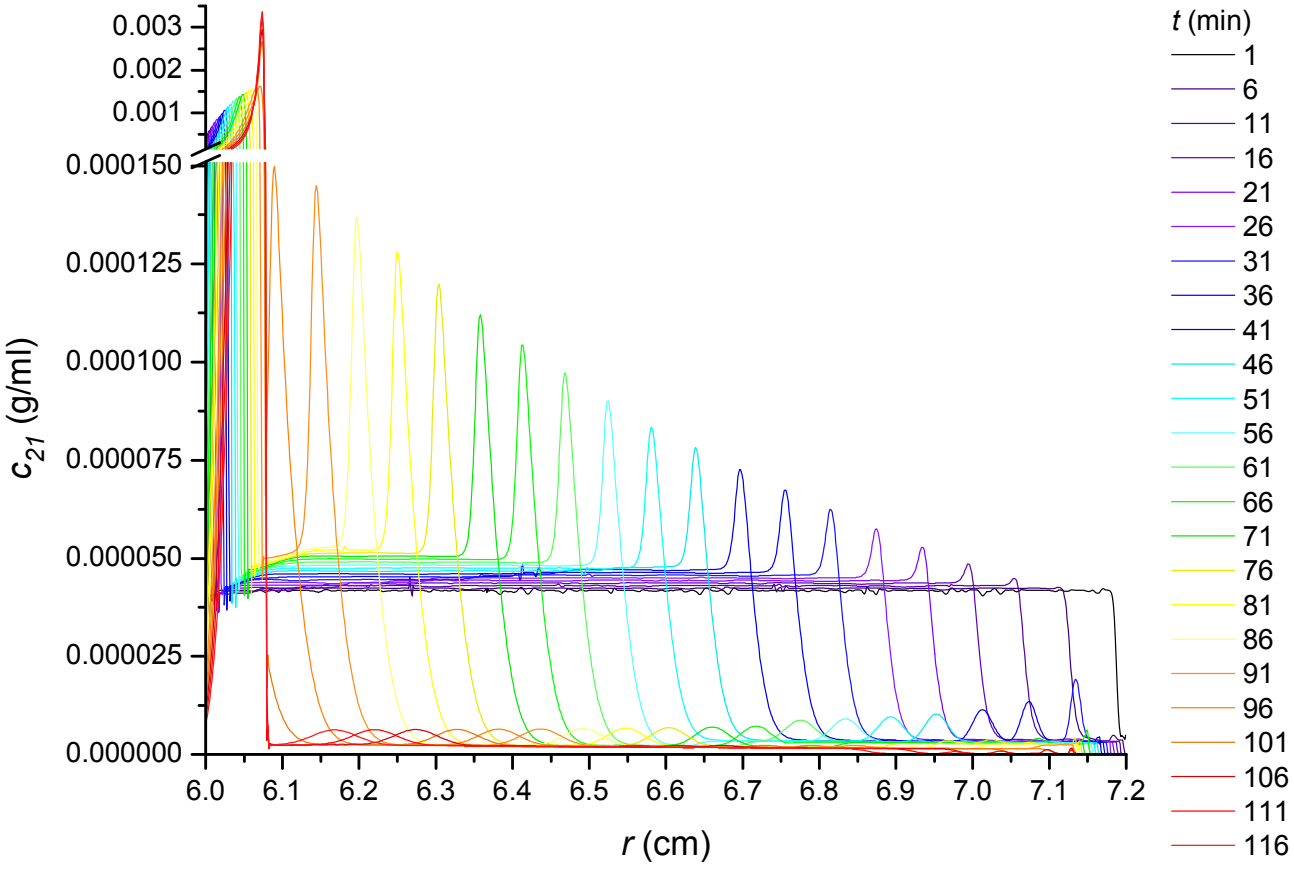

Figure 35, K_a undefined, case 1b (Table 2, $X^D_{k,q\neq k} = X^S_{k,q\neq k} =$ 1E-4). (Compare with Figures 14 and 20.) The concentration of species 21, c_{21} (g/ml), versus r (cm) for 1 min $\leq t \leq$ 116 min.

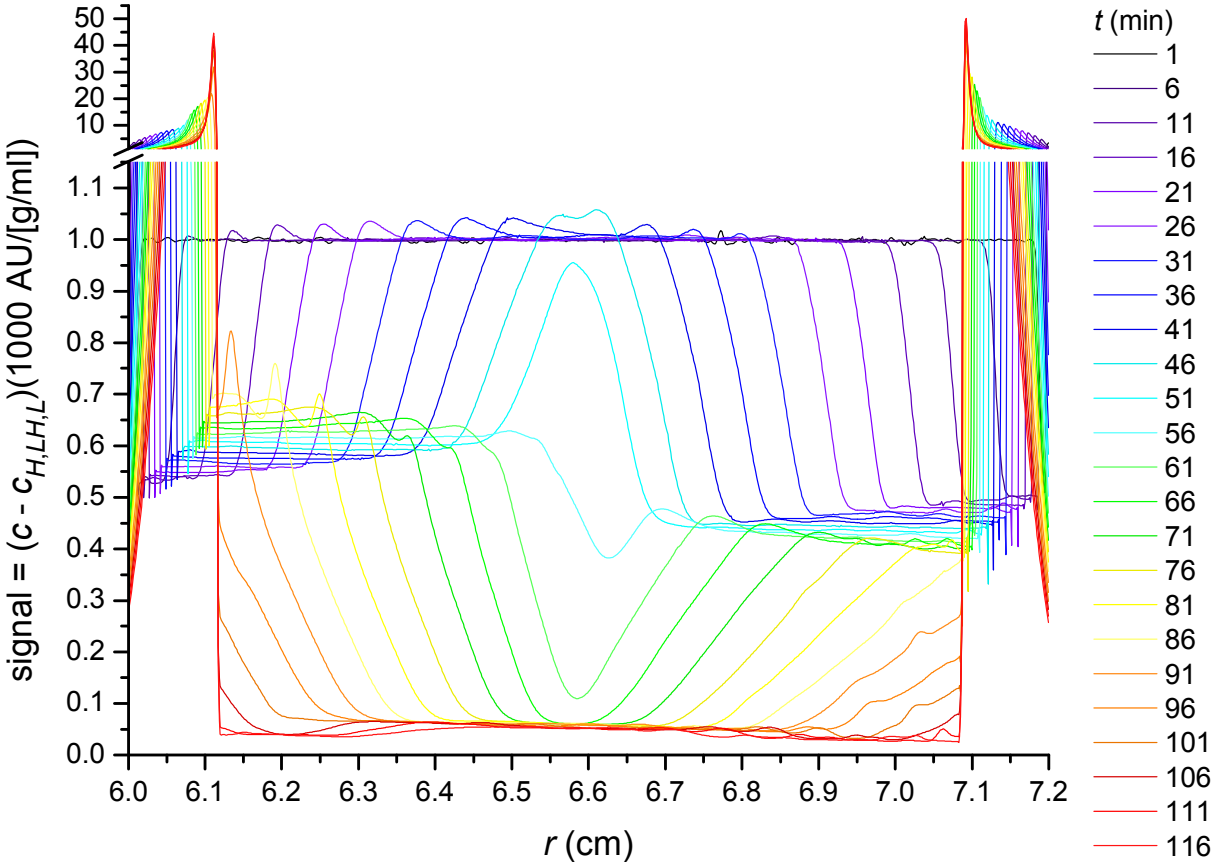

Figure 36, $K_a = 30.325$ ml/g, case 1b (Table 2, $X^D_{k,q\neq k} = X^s_{k,q\neq k} =$ 1E-4). (Compare with Figures 1, 21 and 22.) The sum of the signals from all species except species 1 (*H*), 14 (*LH*) and 27 (*L*), given by (c - $c_{H,LH,L}$)(1000 AU/[g/ml]), versus r (cm) for 1 min $\leq t \leq$ 116 min. (To obtain these results, a Δt of 3 s and a $\Delta\xi$ of 8.8E-3 cm^2 were used. Compare with Figure 51, for which the results were obtained using a Δt of 0.5 s and a $\Delta\xi =$ 6.6E-3 cm^2.)

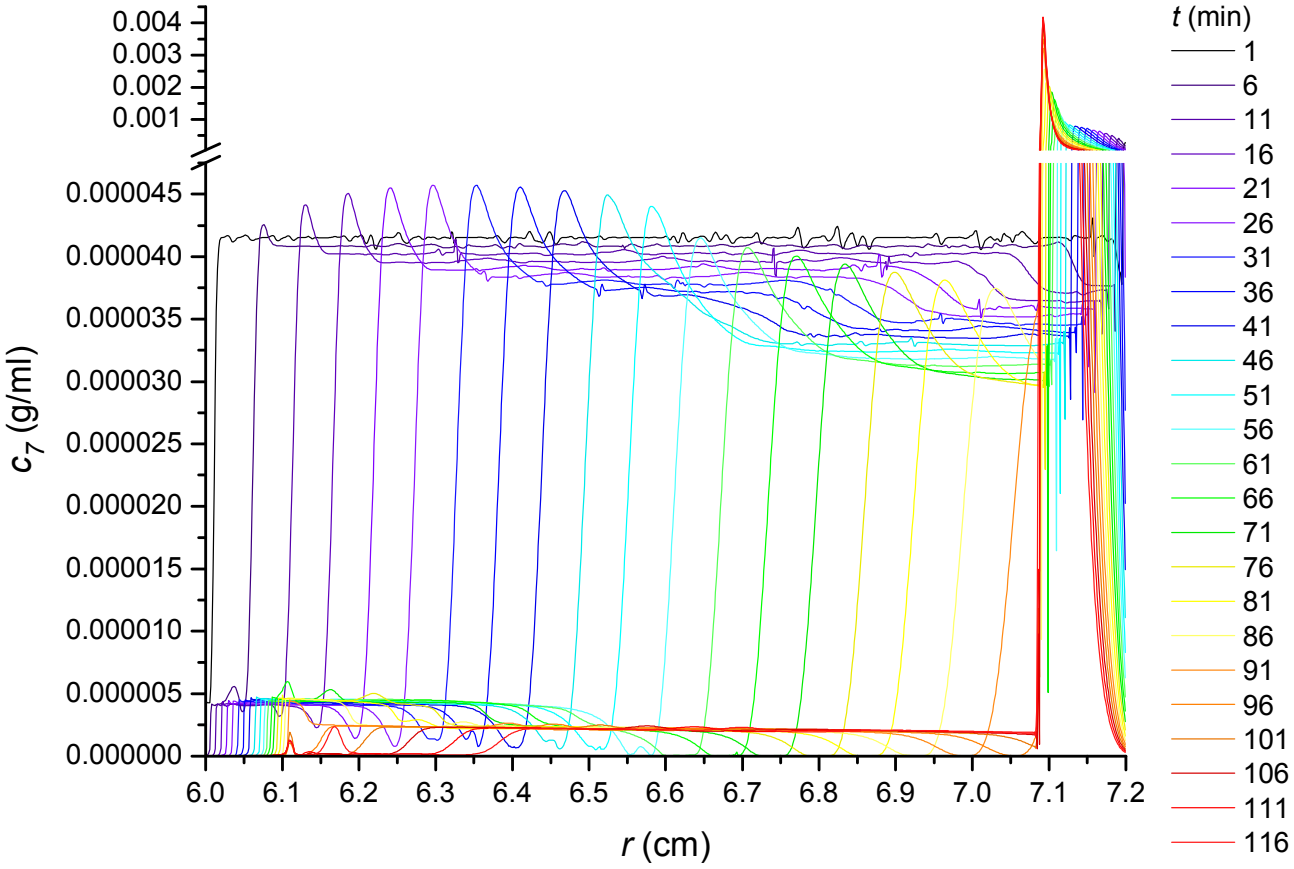

Figure 37, $K_a = 30.325$ ml/g, case 1b (Table 2, $X^D_{k,q\neq k} = X^s_{k,q\neq k} =$ 1E-4). (Compare with Figures 6 and 23.) The concentration of species 7, c_7 (g/ml), versus r (cm) for 1 min $\leq t \leq$ 116 min. (To obtain these results, a Δt of 3 s and a $\Delta\xi$ of 8.8E-3 cm^2 were used. Compare with Figure 52, for which the results were obtained using a Δt of 0.5 s and a $\Delta\xi =$ 6.6E-3 cm^2.)

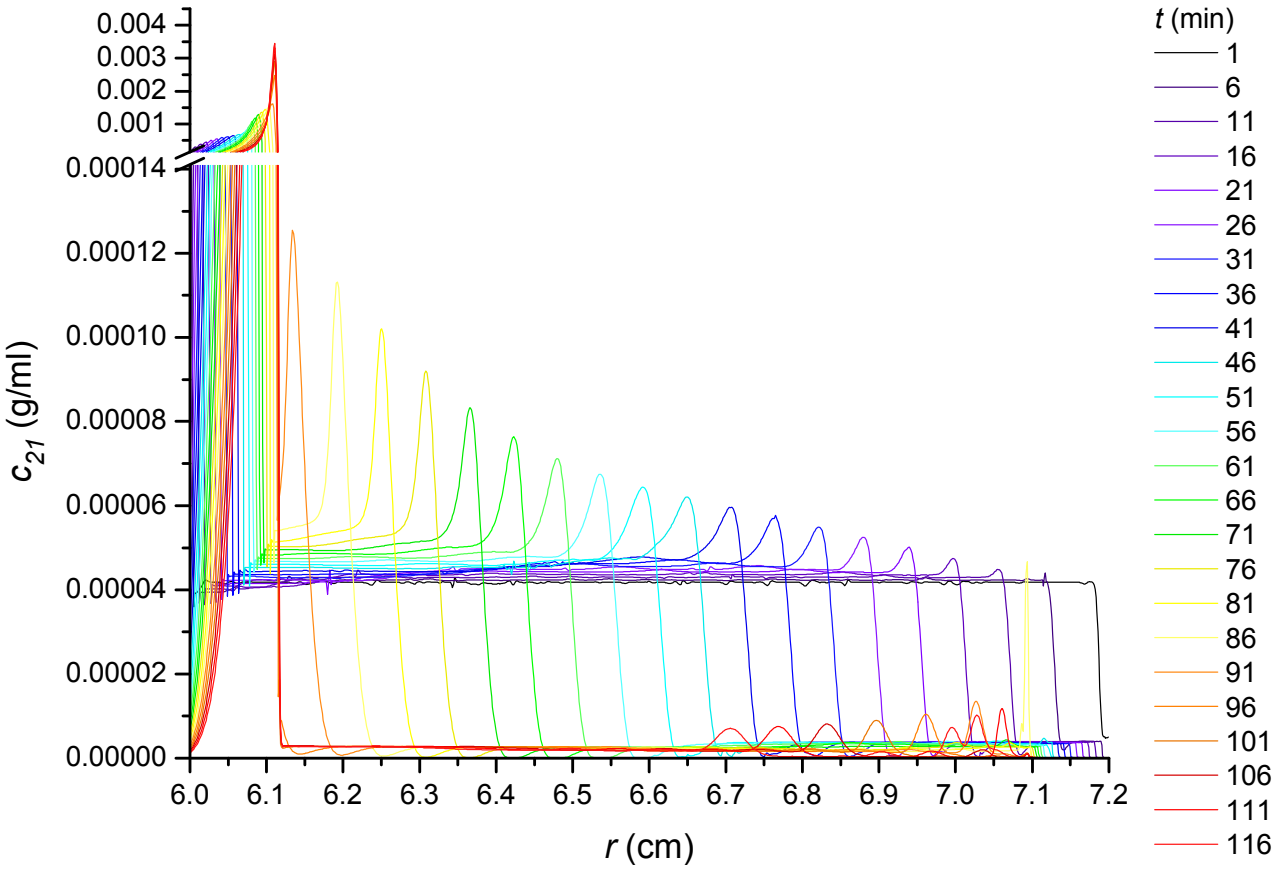

Figure 38, $K_a = 30.325$ ml/g, case 1b (Table 2, $X^D_{k,q\neq k} = X^s_{k,q\neq k} =$ 1E-4). (Compare with Figures 7 and 24.) The concentration of species 21, c_{21} (g/ml), versus r (cm) for 1 min $\leq t \leq$ 116 min. (To obtain these results, a Δt of 3 s and a $\Delta\xi$ of 8.8E-3 cm^2 were used. Compare with Figure 53, for which the results were obtained using a Δt of 0.5 s and a $\Delta\xi =$ 6.6E-3 cm^2.)

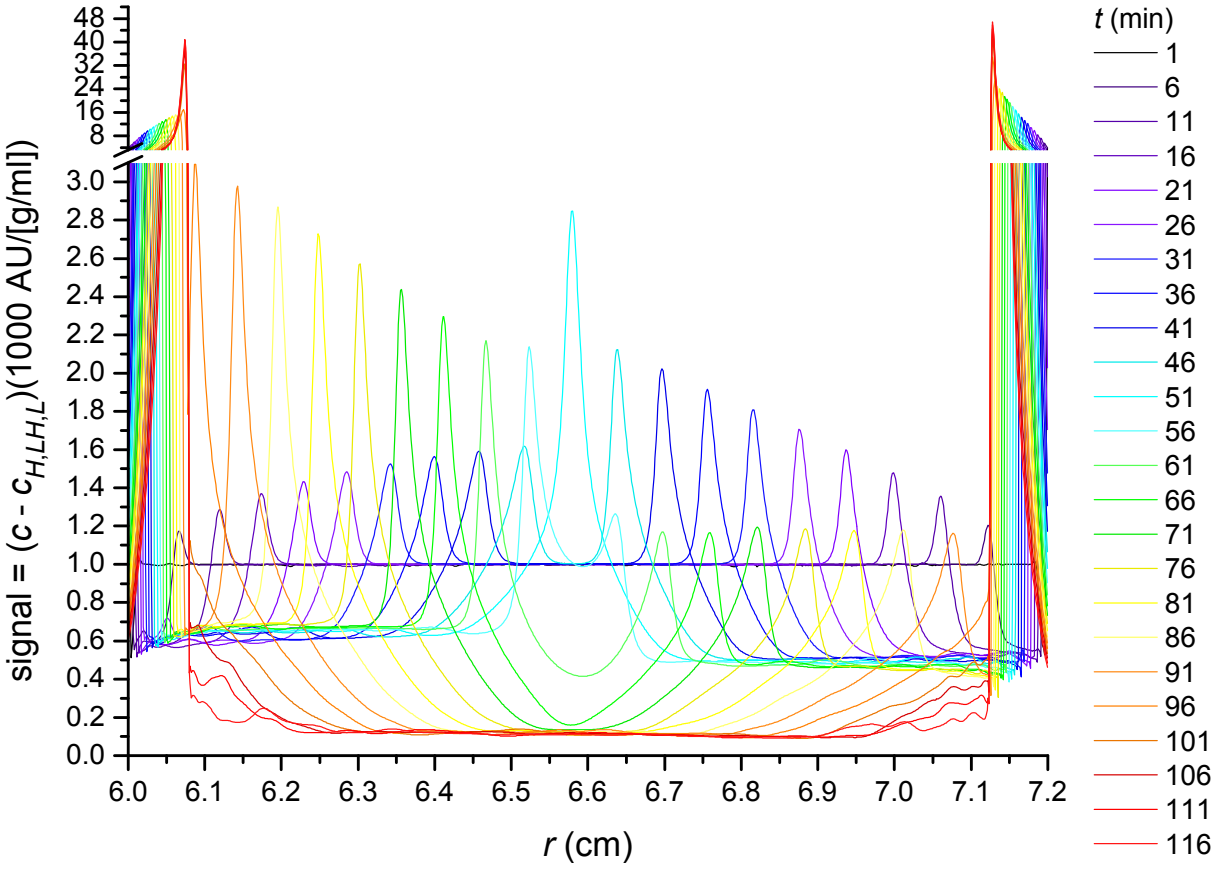

Figure 39, K_a undefined, case 2b (Table 2, $X^D_{k,q\neq k} = X^s_{k,q\neq k}$ = -1E-4). (Compare with Figures 8, 25 and 26.) The sum of the signals from all species except species 1 (*H*), 14 (*LH*) and 27 (*L*), given by (c - $c_{H,LH,L}$)(1000 AU/[g/ml]), versus r (cm) for 1 min ≤ t ≤ 116 min.

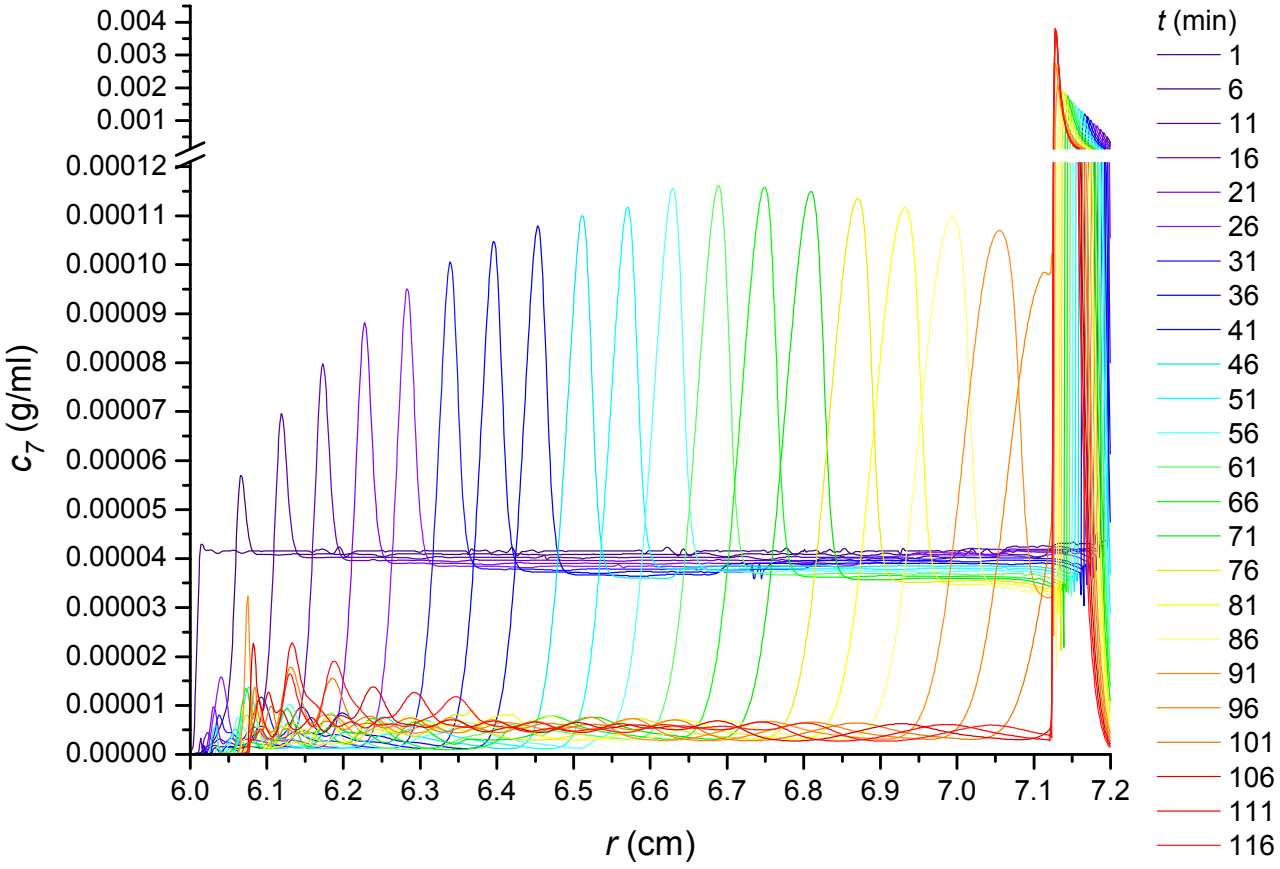

Figure 40, K_a undefined, case 2b (Table 2, $X^D_{k,q\neq k} = X^S_{k,q\neq k}$ = -1E-4). (Compare with Figures 13 and 27.) The concentration of species 7, c_7 (g/ml), versus r (cm) for 1 min $\leq t \leq$ 116 min.

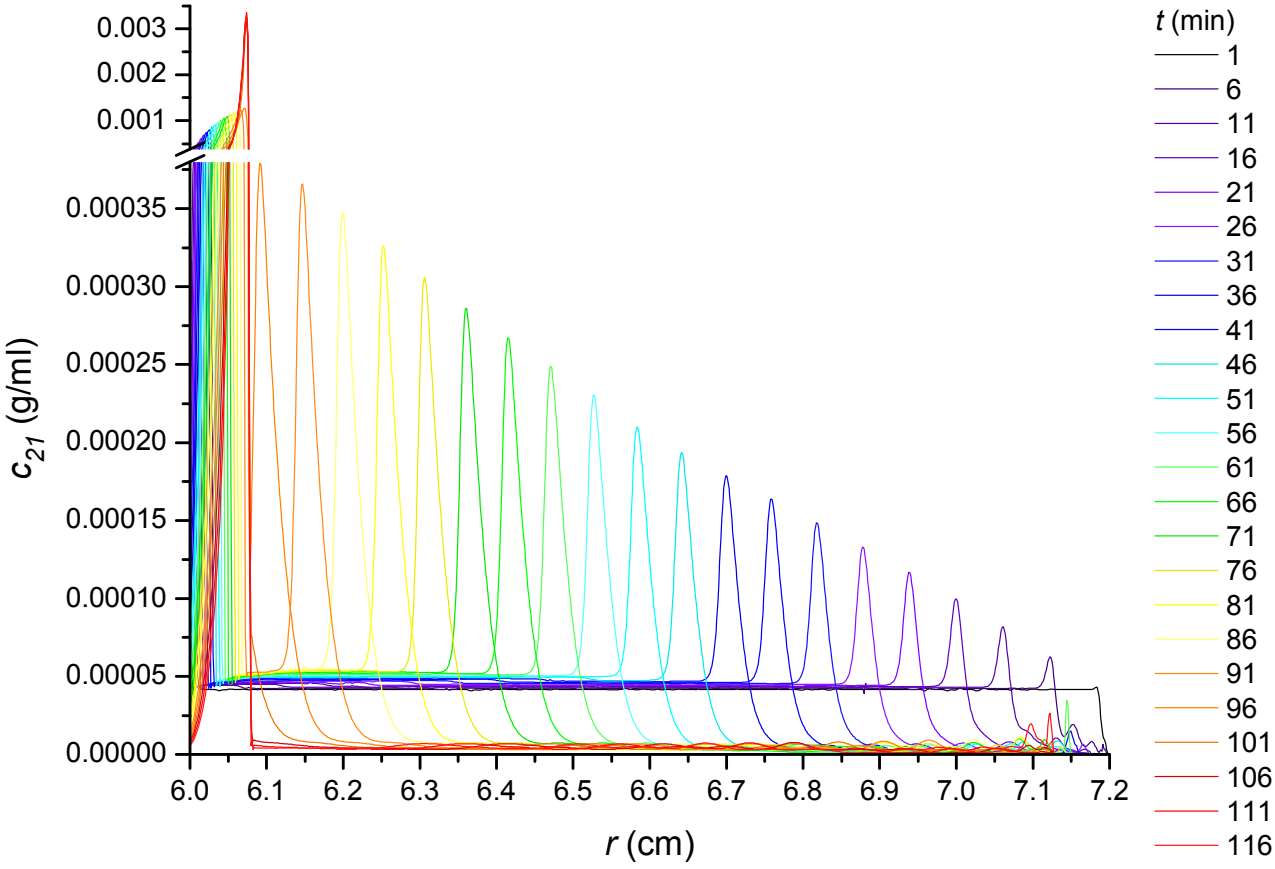

Figure 41, K_a undefined, case 2b (Table 2, $X^D_{k,q\neq k} = X^S_{k,q\neq k}$ = -1E-4). (Compare with Figures 14 and 28.) The concentration of species 21, c_{21} (g/ml), versus r (cm) for 1 min $\leq t \leq$ 116 min.

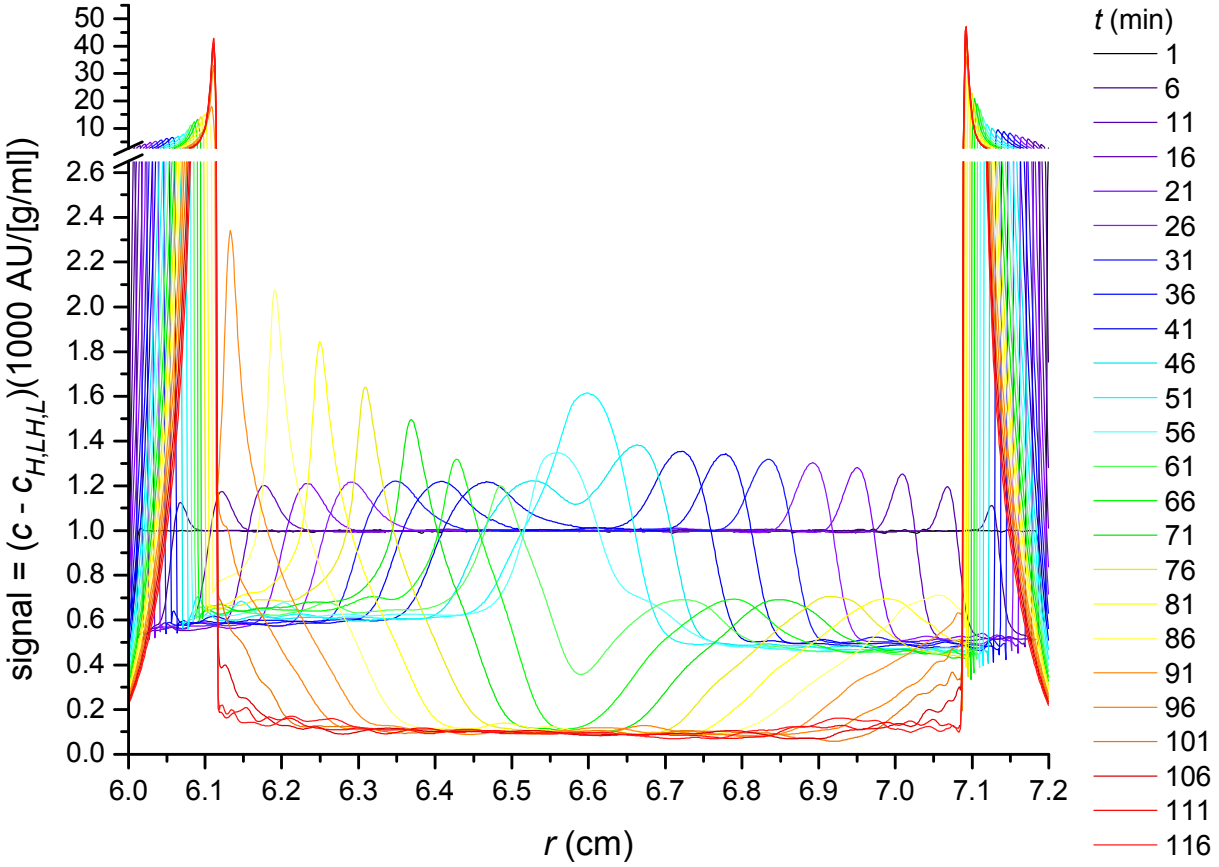

Figure 42, $K_a = 30.325$ ml/g, case 2b (Table 2, $X^D_{k,q\neq k} = X^s_{k,q\neq k}$ = -1E-4). (Compare with Figures 1, 29 and 30.) The sum of the signals from all species except species 1 (*H*), 14 (*LH*) and 27 (*L*), given by (c - $c_{H,LH,L}$)(1000 AU/[g/ml]), versus r (cm) for 1 min ≤ t ≤ 116 min.

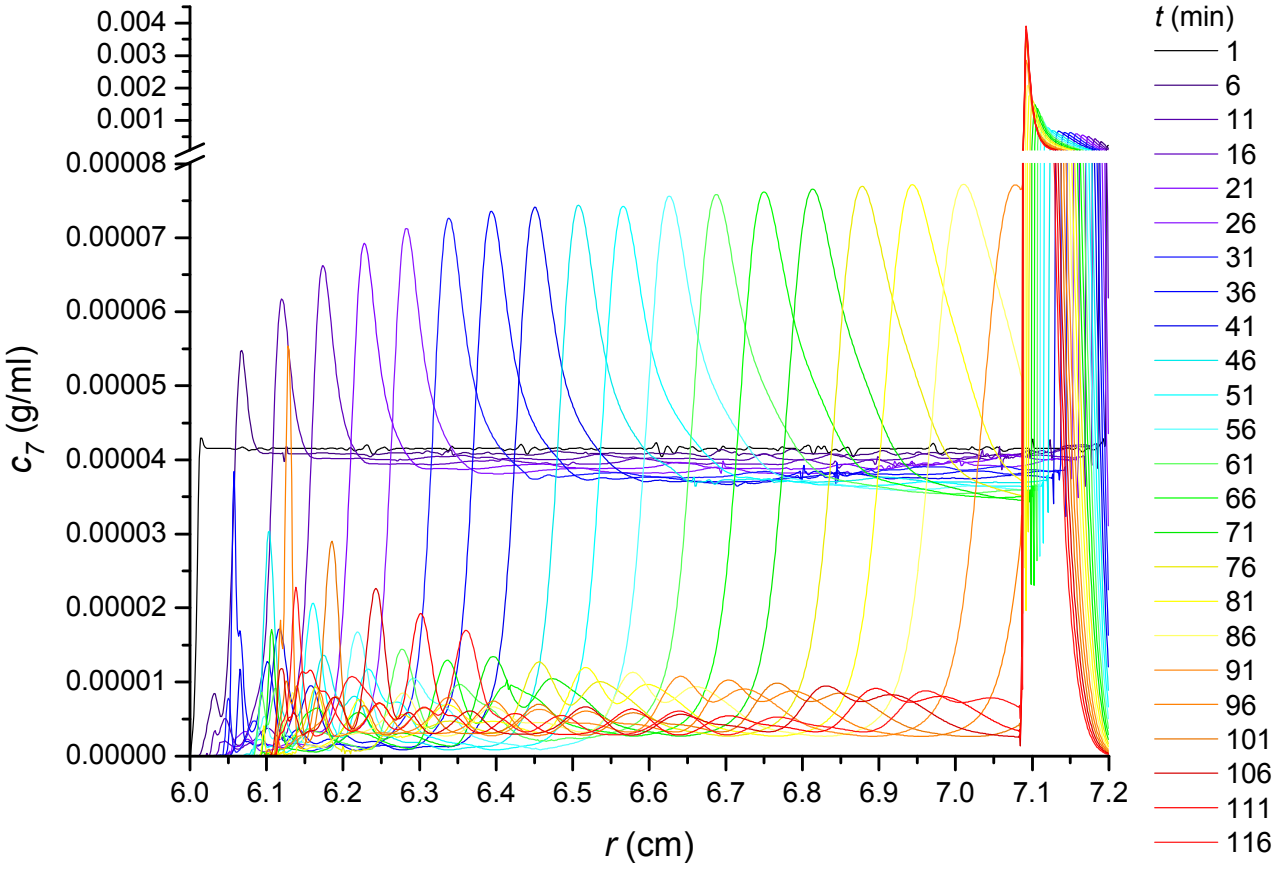

Figure 43, $K_a = 30.325$ ml/g, case 2b (Table 2, $X^D_{k,q\neq k} = X^S_{k,q\neq k}$ = -1E-4). (Compare with Figures 6 and 31.) The concentration of species 7, c_7 (g/ml), versus r (cm) for 1 min $\leq t \leq$ 116 min.

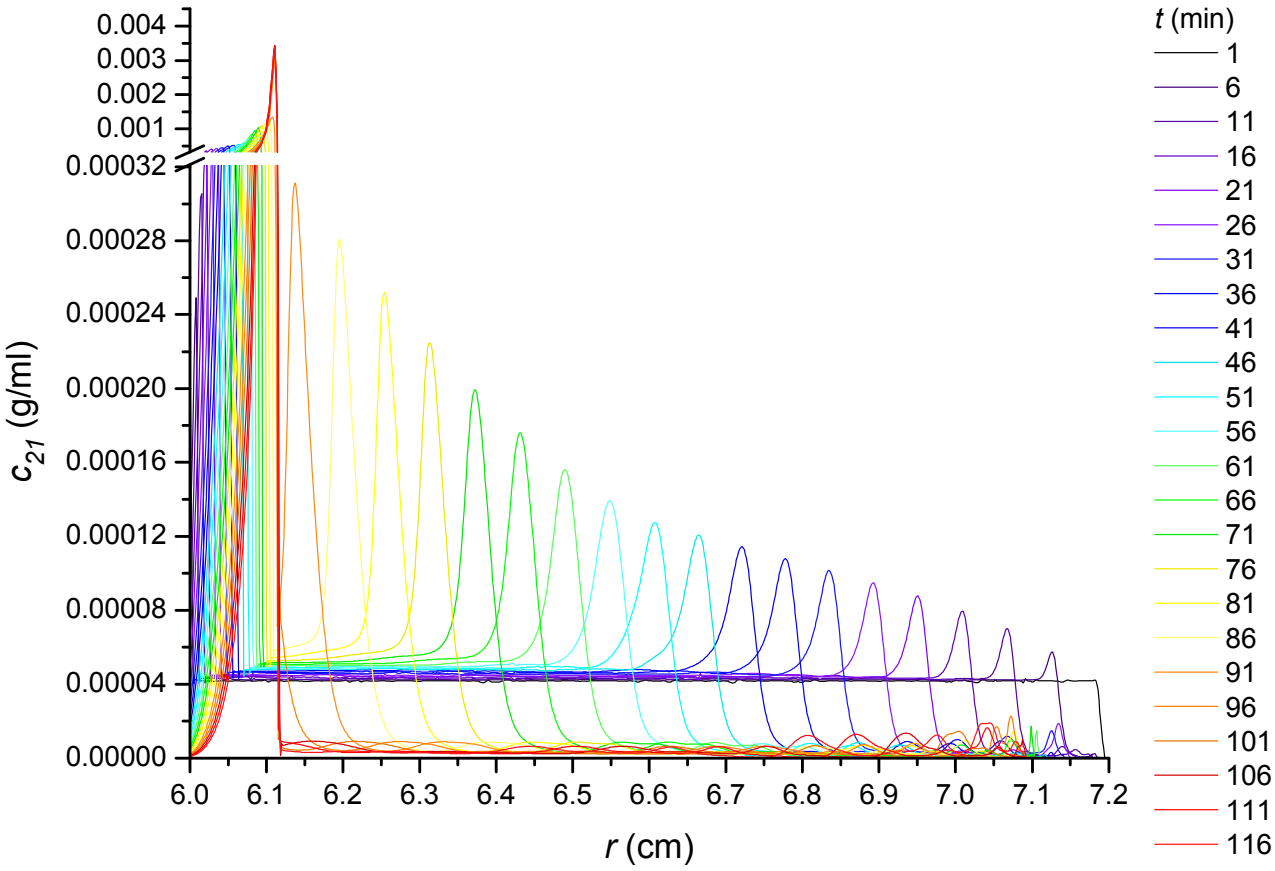

Figure 44, $K_a = 30.325$ ml/g, case 2b (Table 2, $X^D_{k,q\neq k} = X^s_{k,q\neq k}$ = -1E-4). (Compare with Figures 7 and 32.) The concentration of species 21, c_{21} (g/ml), versus r (cm) for 1 min $\leq t \leq$ 116 min.

The concentration gradients of H, L and *LH for* $K_a = 30.325$ ml/g *and cases 1b and 2b*

For K_a undefined, the concentration gradients (not shown) of *H*, *L* and *LH* of cases 1b ($X^D_{k,q\neq k} = X^s_{k,q\neq k}$ = 1E-4) and 2b ($X^D_{k,q\neq k} = X^s_{k,q\neq k}$ = -1E-4) would be indistinguishable from those of case 0 (Figures 10 to 12), were it not for the fairly mild signs of instability exhibited in cases 1b and 2b. For $K_a = 30.325$ ml/g, the concentration gradients of *H*, *L* and *LH* of cases 1b (Figures 45 to 47)

and 2b (Figures 48 to 50) would be subtly distinguishable from those of case 0 (Figures 3 to 5), even if the not-so-subtle signs of instability exhibited in cases 1b and 2b were absent.

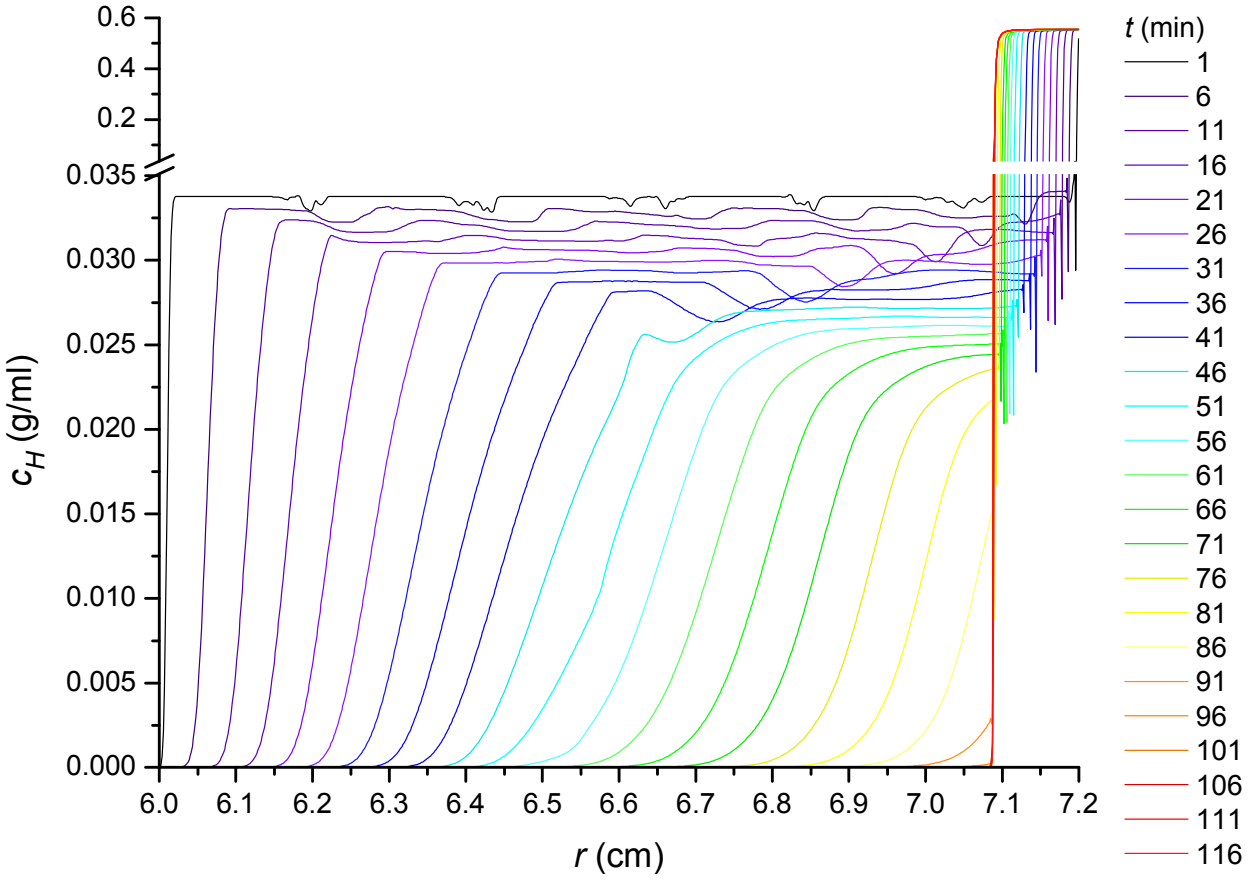

Figure 45, $K_a = 30.325$ ml/g, case 1b (Table 2, $X^D_{k,q\neq k} = X^s_{k,q\neq k} =$ 1E-4). The concentration of species 1 (H), c_H (g/ml), versus r (cm) for 1 min $\leq t \leq$ 116 min. Compare this figure with Figure 3. (To obtain these results, a Δt of 3 s and a $\Delta\xi$ of 8.8E-3 cm^2 were used. Compare with Figure 54, for which the results were obtained using a Δt of 0.5 s and a $\Delta\xi =$ 6.6E-3 cm^2.)

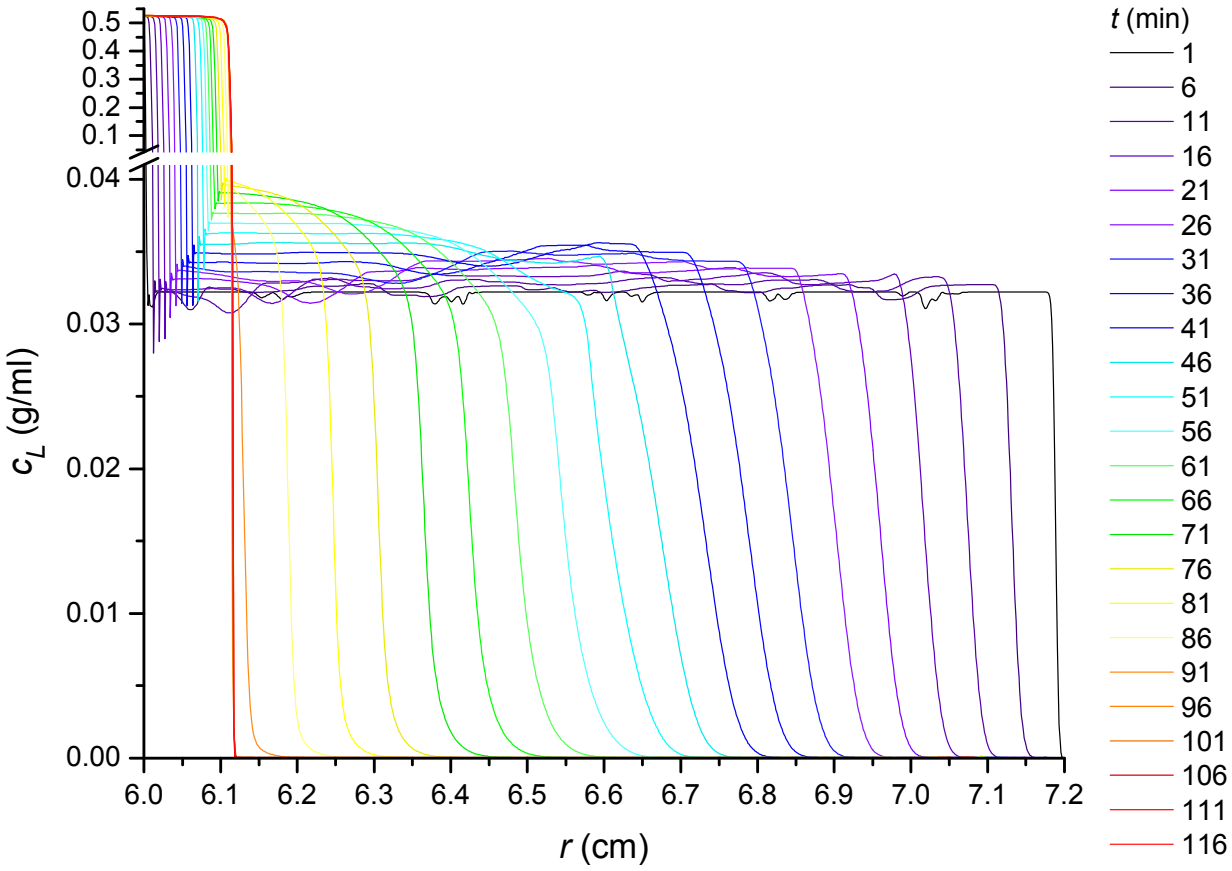

Figure 46, $K_a = 30.325$ ml/g, case 1b (Table 2, $X^D_{k,q\neq k} = X^S_{k,q\neq k} =$ 1E-4). The concentration of species 27 (L), c_L (g/ml), versus r (cm) for 1 min $\leq t \leq$ 116 min. Compare this figure with Figure 4. (To obtain these results, a Δt of 3 s and a $\Delta\xi$ of 8.8E-3 cm^2 were used. Compare with Figure 55, for which the results were obtained using a Δt of 0.5 s and a $\Delta\xi =$ 6.6E-3 cm^2.)

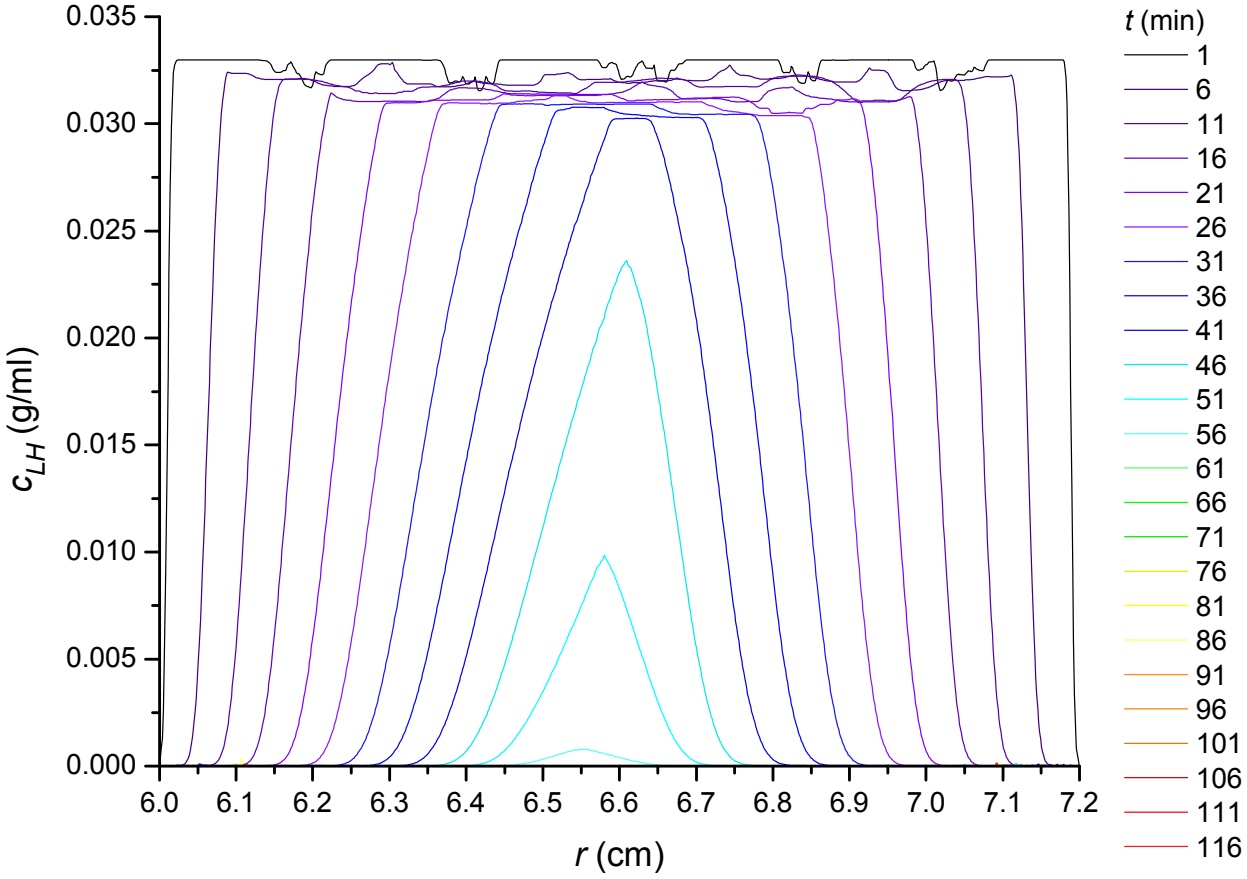

Figure 47, $K_a = 30.325$ ml/g, case 1b (Table 2, $X^D_{k,q\neq k} = X^s_{k,q\neq k} = 1\text{E-}4$). The concentration of species 14 (LH), c_{LH} (g/ml), versus r (cm) for 1 min $\leq t \leq$ 116 min. Compare this figure with Figure 5. (To obtain these results, a Δt of 3 s and a $\Delta\xi$ of 8.8E-3 cm^2 were used. Compare with Figure 56, for which the results were obtained using a Δt of 0.5 s and a $\Delta\xi = 6.6\text{E-}3$ cm^2.)

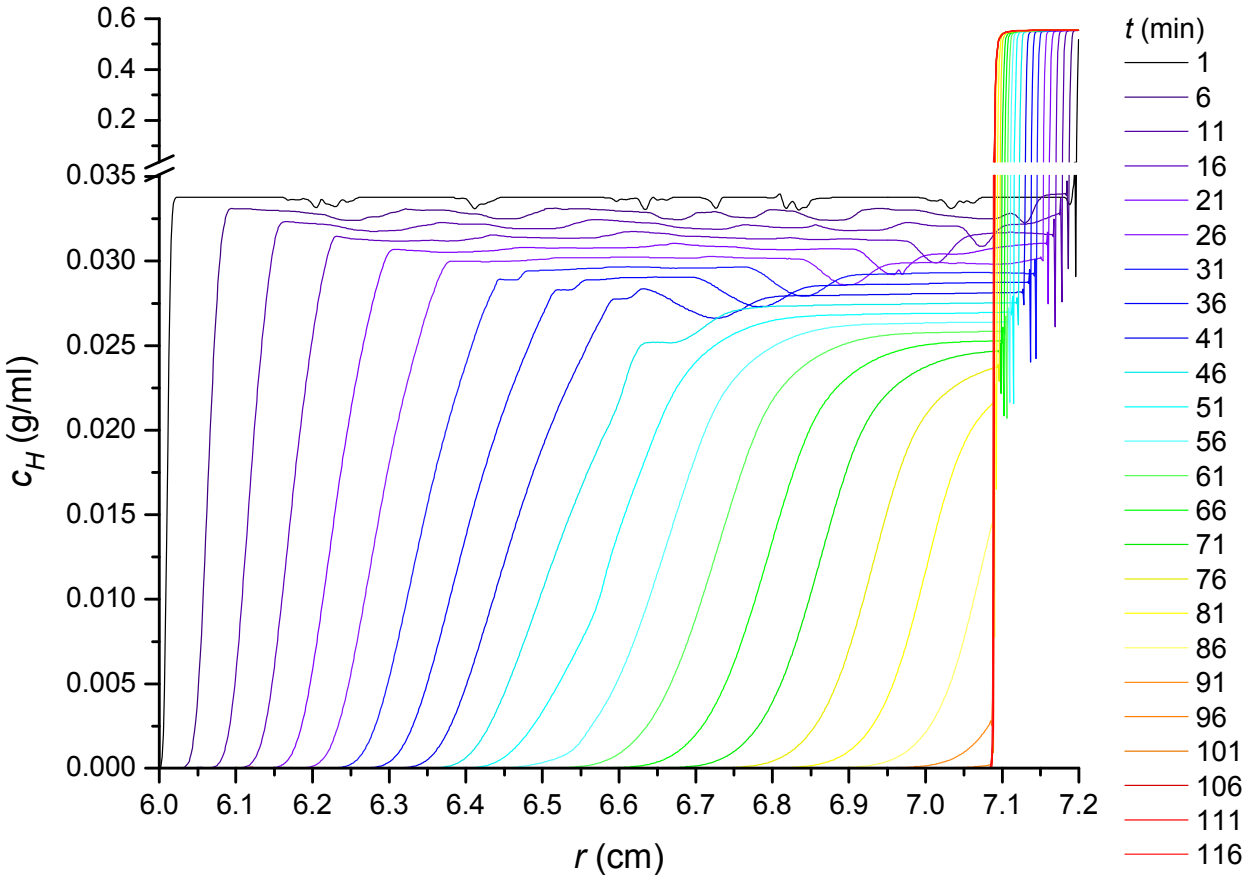

Figure 48, $K_a = 30.325$ ml/g, case 2b (Table 2, $X^D_{k,q\neq k} = X^s_{k,q\neq k}$ = -1E-4). The concentration of species 1 (H), c_H (g/ml), versus r (cm) for 1 min $\leq t \leq$ 116 min. Compare this figure with Figure 3.

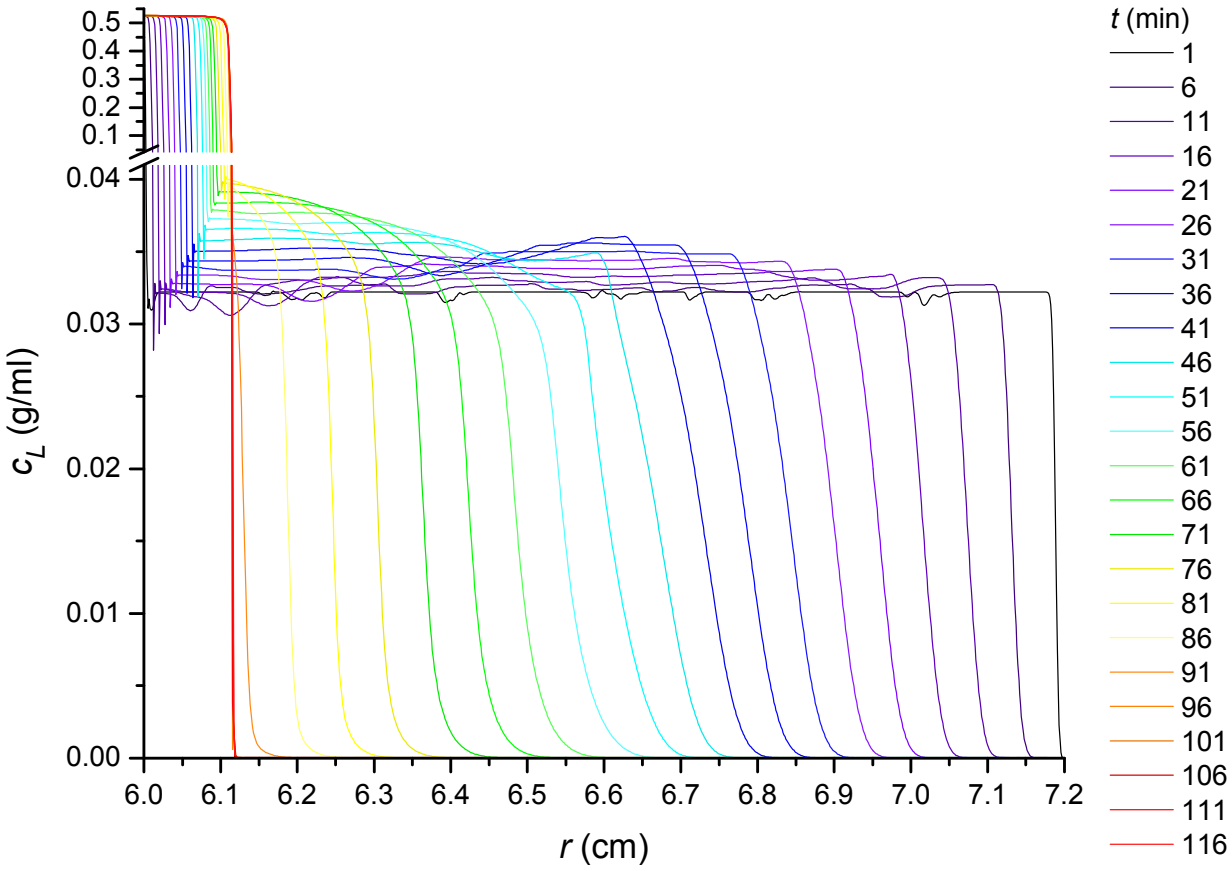

Figure 49, $K_a = 30.325$ ml/g, case 2b (Table 2, $X^D_{k,q\neq k} = X^S_{k,q\neq k}$ = -1E-4). The concentration of species 27 (L), c_L (g/ml), versus r (cm) for 1 min $\leq t \leq$ 116 min. Compare this figure with Figure 4.

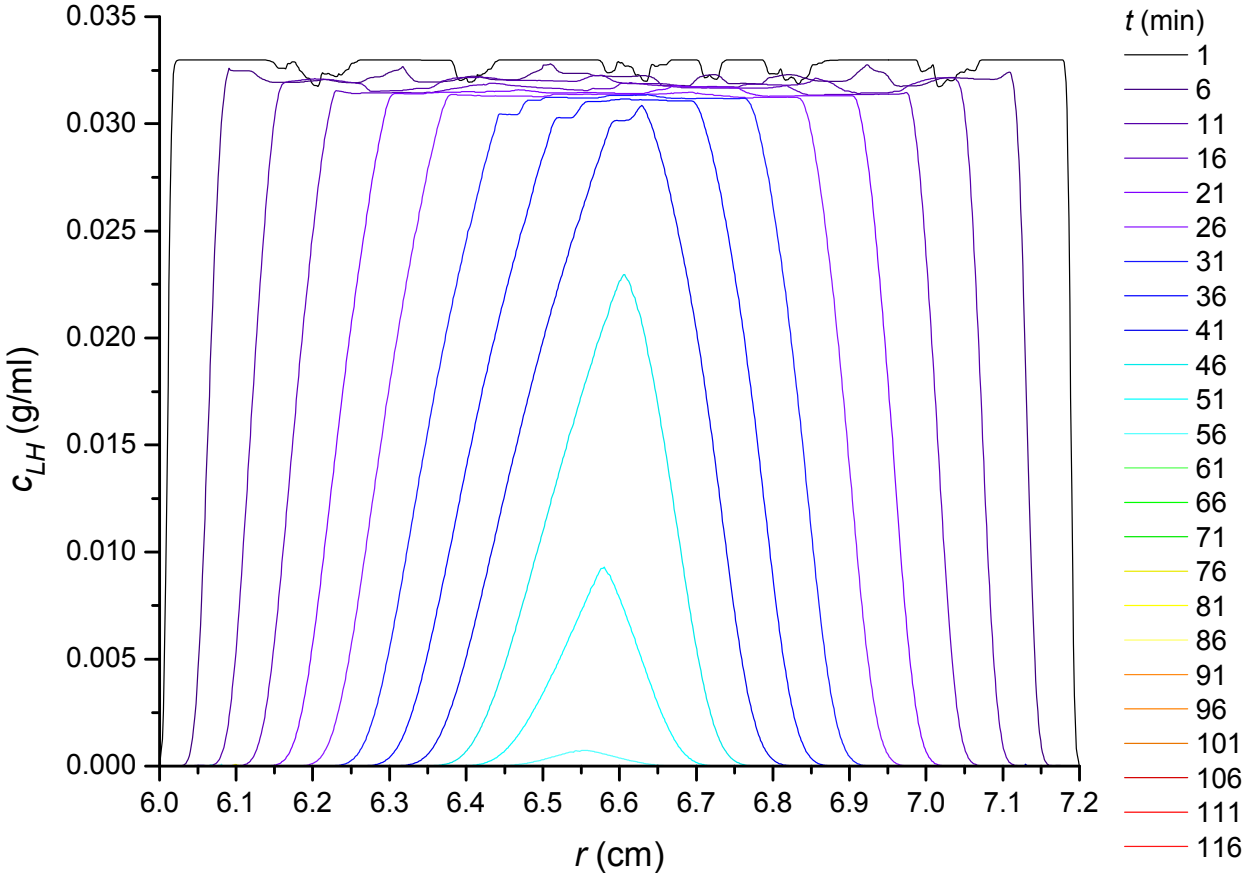

Figure 50, $K_a = 30.325$ ml/g, case 2b (Table 2, $X^D_{k,q\neq k} = X^s_{k,q\neq k}$ = -1E-4). The concentration of species 14 (LH), c_{LH} (g/ml), versus r (cm) for 1 min $\leq t \leq$ 116 min. Compare this figure with Figure 5.

Reduced Δt *and* $\Delta\xi$ *applied to case 1b:* $K_a = 30.325$ ml/g, $X^D_{k,q\neq k} = X^s_{k,q\neq k} = 1\text{E-}4$

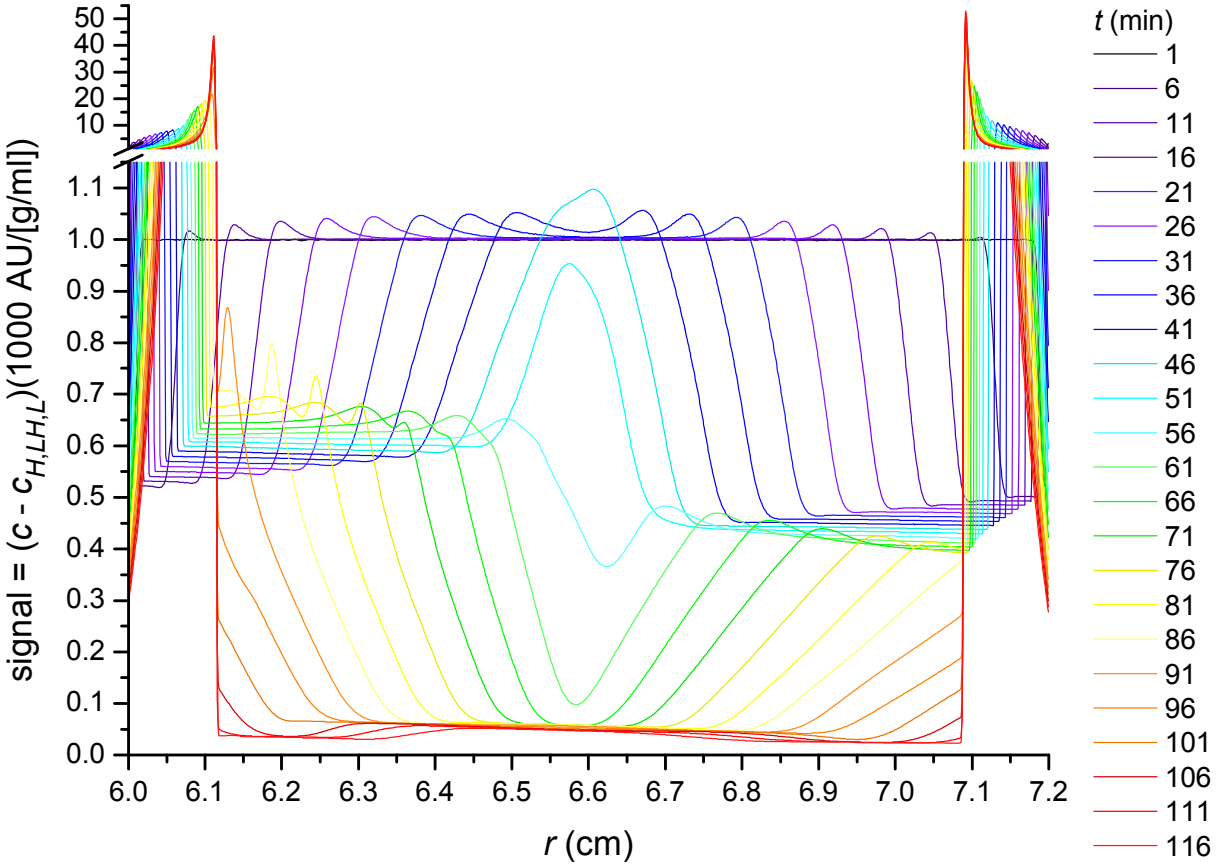

Figure 51, $K_a = 30.325$ ml/g, case 1b (Table 2, $X^D_{k,q\neq k} = X^s_{k,q\neq k} =$ 1E-4). The sum of the signals from all species except species 1 (H), 14 (LH) and 27 (L), given by (c - $c_{H,LH,L}$)(1000 AU/[g/ml]), versus r(cm) for 1 min $\leq t \leq$ 116 min. To obtain these results, a Δt of 0.5 s and a $\Delta\xi$ of 6.6E-3 cm^2 were used. Compare with Figure 36, for which the results were obtained using a Δt of 3 s and a $\Delta\xi$ = 8.8E-3 cm^2.

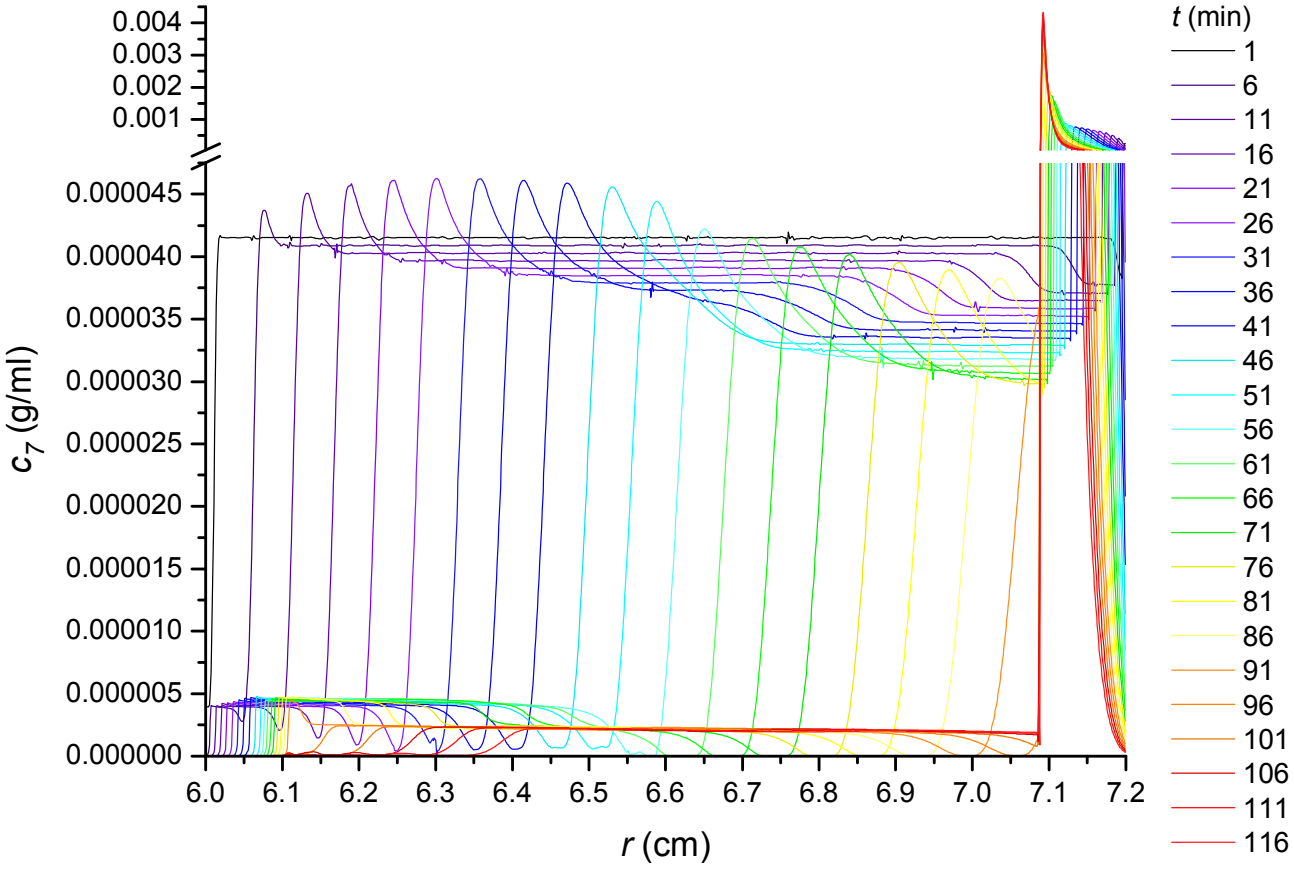

Figure 52, $K_a = 30.325$ ml/g, case 1b (Table 2, $X^D_{k,q\neq k} = X^S_{k,q\neq k} =$ 1E-4). The concentration of species 7, c_7 (g/ml), versus r (cm) for 1 min $\leq t \leq$ 116 min. To obtain these results, a Δt of 0.5 s and a $\Delta\xi$ of 6.6E-3 cm^2 were used. Compare with Figure 37, for which the results were obtained using a Δt of 3 s and a $\Delta\xi =$ 8.8E-3 cm^2.

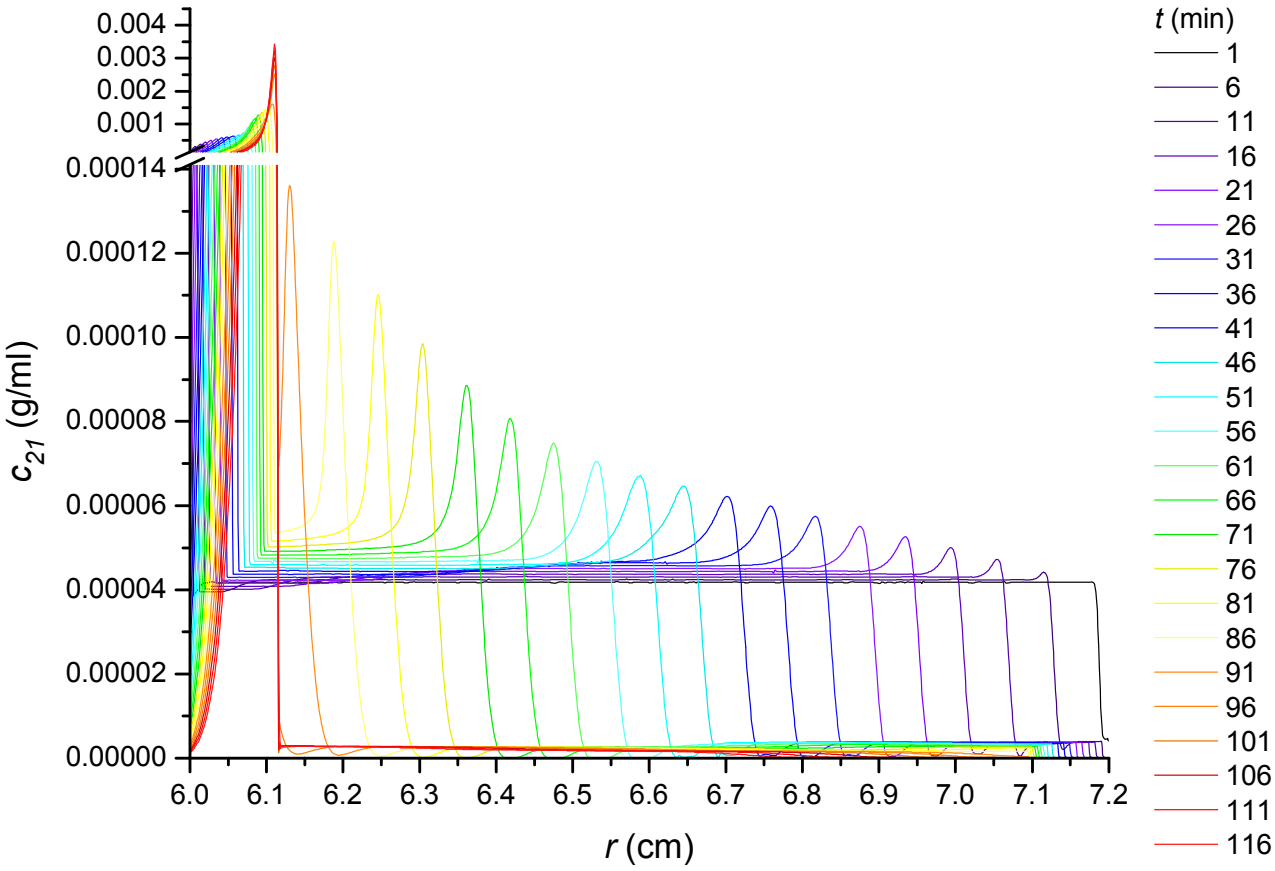

Figure 53, $K_a = 30.325$ ml/g, case 1b (Table 2, $X^D_{k,q\neq k} = X^S_{k,q\neq k} =$ 1E-4). The concentration of species 21, c_{21} (g/ml), versus r (cm) for 1 min $\leq t \leq$ 116 min. To obtain these results, a Δt of 0.5 s and a $\Delta\xi$ of 6.6E-3 cm^2 were used. Compare with Figure 38, for which the results were obtained using a Δt of 3 s and a $\Delta\xi =$ 8.8E-3 cm^2.

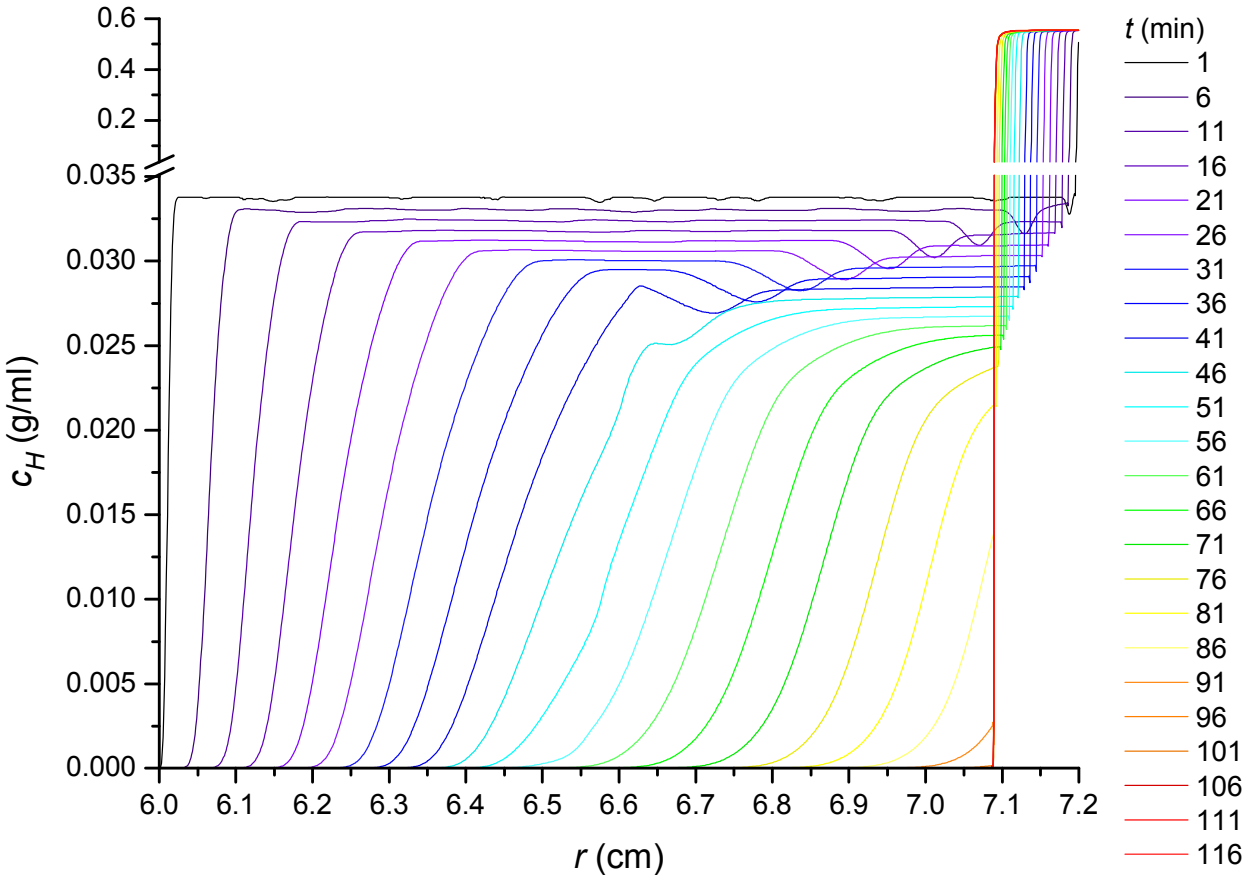

Figure 54, $K_a = 30.325$ ml/g, case 1b (Table 2, $X^D_{k,q\neq k} = X^s_{k,q\neq k} =$ 1E-4). The concentration of species 1 (H), c_H (g/ml), versus r (cm) for 1 min $\leq t \leq$ 116 min. To obtain these results, a Δt of 0.5 s and a $\Delta\xi$ of 6.6E-3 cm^2 were used. Compare with Figure 45, for which the results were obtained using a Δt of 3 s and a $\Delta\xi =$ 8.8E-3 cm^2.

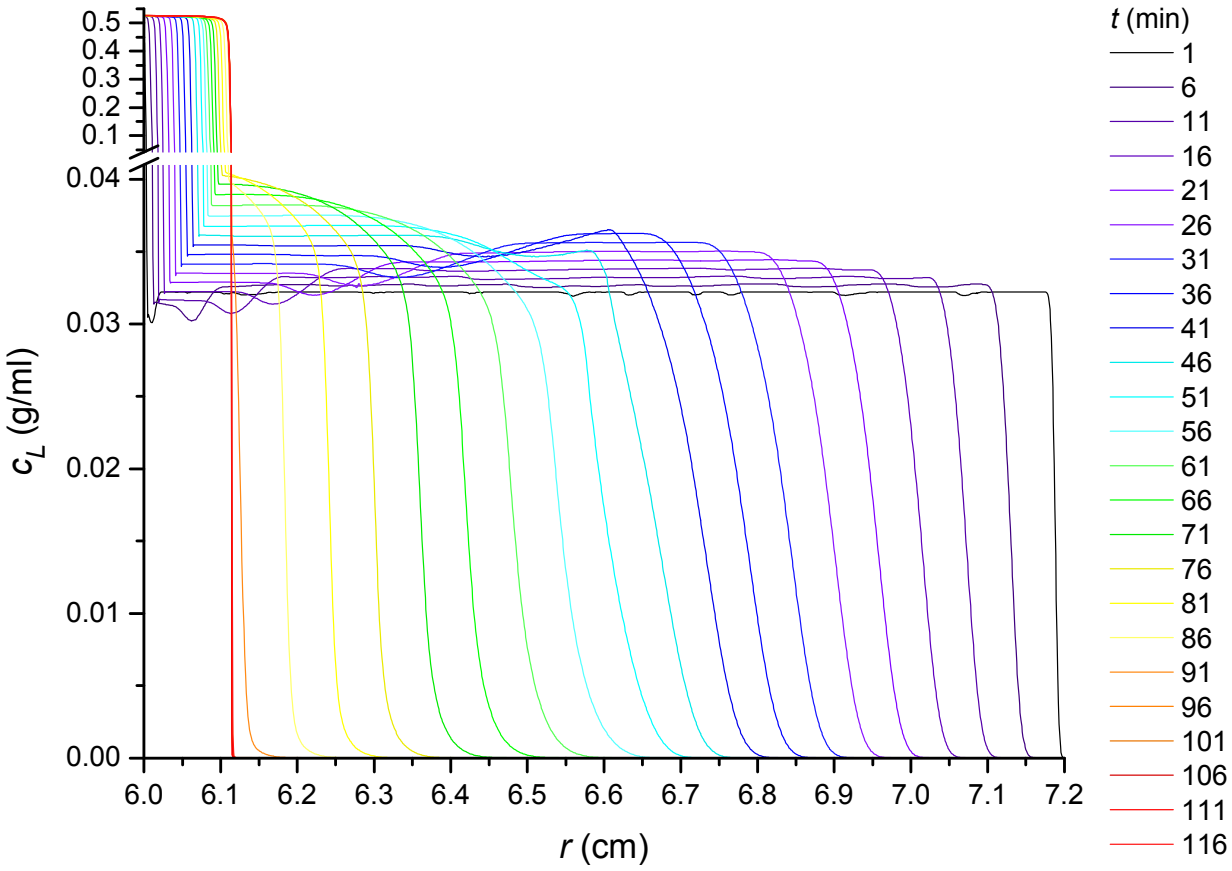

Figure 55, $K_a = 30.325$ ml/g, case 1b (Table 2, $X^D_{k,q\neq k} = X^S_{k,q\neq k} =$ 1E-4). The concentration of species 27 (L), c_L (g/ml), versus r (cm) for 1 min $\leq t \leq$ 116 min. To obtain these results, a Δt of 0.5 s and a $\Delta\xi$ of 6.6E-3 cm^2 were used. Compare with Figure 46, for which the results were obtained using a Δt of 3 s and a $\Delta\xi =$ 8.8E-3 cm^2.

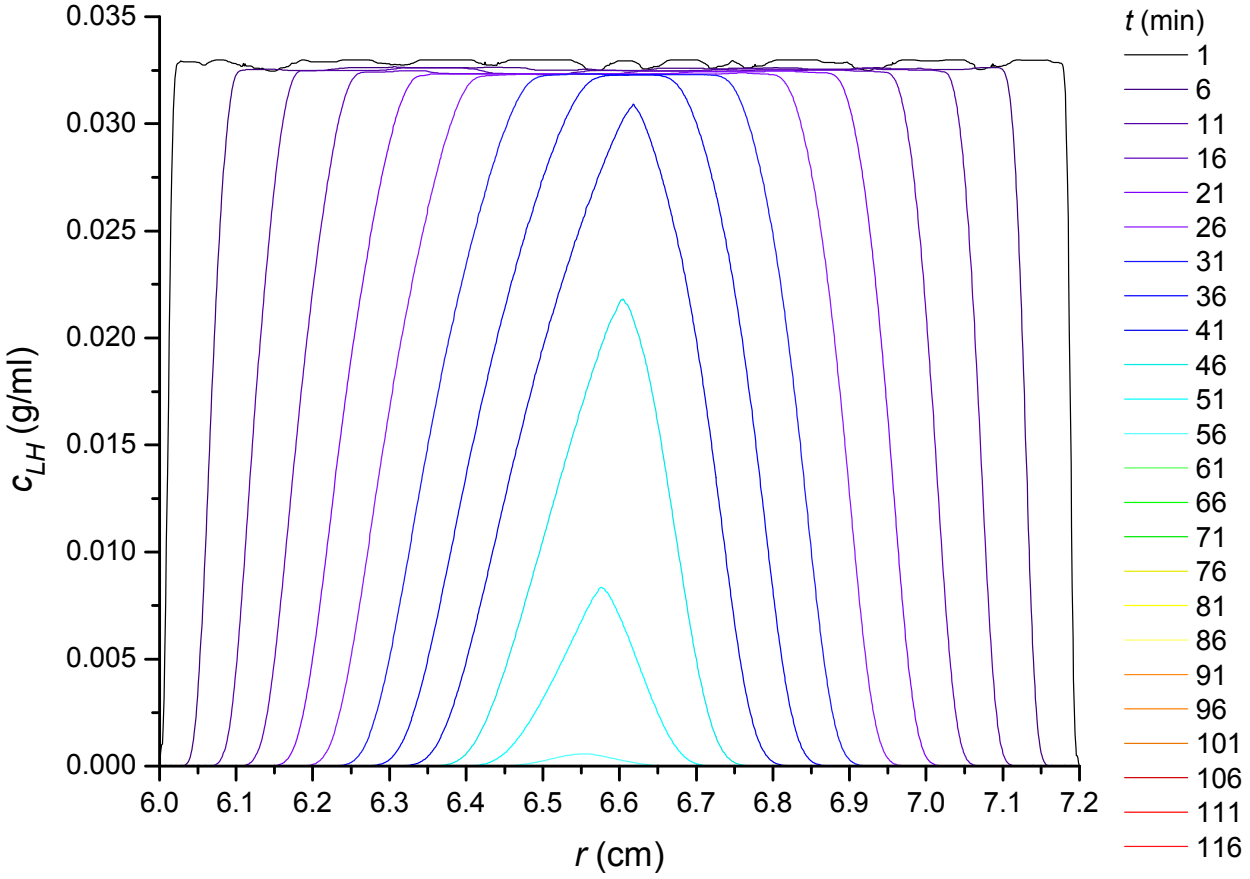

Figure 56, $K_a = 30.325$ ml/g, case 1b (Table 2, $X^D_{k,q\neq k} = X^s_{k,q\neq k} =$ 1E-4). The concentration of species 14 (LH), c_{LH} (g/ml), versus r (cm) for 1 min $\leq t \leq$ 116 min. To obtain these results, a Δt of 0.5 s and a $\Delta\xi$ of 6.6E-3 cm^2 were used. Compare with Figure 47, for which the results were obtained using a Δt of 3 s and a $\Delta\xi =$ 8.8E-3 cm^2.

References

Claverie, J.-M., Dreux, H., and Cohen, R. (1975). Sedimentation of generalized systems of interacting particles. I. Solution of systems of complete Lamm equations. *Biopolymers*. **14**, 1685-1700.

Moody, T. P. (2011). An irreversible thermodynamic description of analytical ultracentrifugation (AUC) applied to a solution of the time- and gravitational-potential-space-dependent Lamm equation. http://moodybiophysicalconsulting.blogspot.com/.

Moody, T. P. (2012b). The apparent sedimentation coefficient, s*, and its distribution function, g(s*), within $-\infty < s^* < \infty$. http://moodybiophysicalconsulting.blogspot.com/.

Moody, T. P. (2014). Distinguishing hypothetical systems of PS beads by $g(s^*)$ analysis of simulated AUC data to which noise has been added, and quantifying the statistical significance of any observed distinguishability. http://moodybiophysicalconsulting.blogspot.com/.

Sharp, D. G., and Beard, J. W. (1950). Size and density of polystyrene particles measured by ultracentrifugation. *J. Biol. Chem.* **185**, 247-253.

Laue, T. M., Shah, B. D., Ridgeway, T. M., and Pelletier, S. L. Computer Aided Interpretation of Analytical Sedimentation Data for Proteins. In *Analytical Ultracentrifugation in Biochemistry and Polymer Science*. S. E. Harding, A. J. Rowe, and J. C. Horton, editors. Royal Society of Chemistry, Cambridge, U.K., 1992, pp. 90-125.

Eisenberg, D. S., & Crothers, D. M. Transport Processes. In *Physical Chemistry with applications to the Life Sciences*. Benjamin/Cummings, Menlo Park, CA, 1979, pp. 700-745.

van Holde, K. E. Viscosity. In *Physical Biochemistry*, second edition. Prentice-Hall, Englewood Cliffs, NJ, 1985, pp. 164-181.

van Holde, K. E. Solutions of Macromolecules. In *Physical Biochemistry*, second edition. Prentice-Hall, Englewood Cliffs, NJ, 1985, pp. 24-50.